# On flow duration curve modelling in Alpine catchments

Thèse N° 9687

Présentée le 13 novembre 2019

À l'École Polytechnique Fédérale de Lausanne
à la Faculté de l'environnement naturel, architectural et construit
Laboratoire d'écohydrologie

et

À l'Instituto Superior Técnico (IST) da Universidade de Lisboa
Programme doctoral en en génie civil et environnement

et

Doutoramento em Engenharia civil

pour l'obtention du grade de Docteur ès Sciences (PhD)

par

Ana Clara PEREIRA BARBOSA SANTOS

Acceptée sur proposition du jury

Prof. A. Nussbaumer, président du jury
Prof. A. Rinaldo, Prof. M. M. Portela Correia dos Santos Ramos da Silva, directeurs de thèse
Dr D. Viviroli, rapporteur
Prof. M. Schirmer, rapporteur
Prof. A. J. Wüest, rapporteur

2019

TÉCNICO LISBOA

ÉCOLE POLYTECHNIQUE FÉDÉRALE DE LAUSANNE

Simplicity, simplicity, simplicity!
— Henry David Thoreau

To my family…

# Acknowledgements

First, I must thank my supervisors, Professor Maria Manuela Portela (IST), Professor Bettina Schaefli (Unil) and Professor Andrea Rinaldo (EPFL), who are not only great Hydrologists but also sources of inspiration for my personal life. Thank you for guiding me, sharing your knowledge, and providing the best working environment that you could.

I am also grateful to Professor Anton Schleiss for receiving me on his laboratory and sharing his vast knowledge and experience.

Many special thanks to Dulce, Anna, Bernard, Aldo, and Emma Sorrentino for being so helpful and patient! I don't know if I could survive all the bureaucracy of a double degree without your help!

I acknowledge the funding from the Portuguese Science and Technology Foundation (FCT).

At some moments I was very annoyed with them, but I know that the comments from editors and reviewers on the peer-review process contributed a lot to my work, so now that papers are accepted, I am also very grateful for them.

Many, many thanks to my colleagues at ECHO, LCH, and neighbor laboratories at EPFL and CERIS that made this journey not only more interesting but also funnier and more friendly. I feel fortunate to have had such great working environments and to have met so many supporting people with different ideas with whom I could share deep and not so deep conversations. Spending time in those multicultural environments was very enriching and changed the way I see the world.

Many thanks also to my friends, the old ones that kept supporting me from the other side of the world and having amazing conversations about everything and the new ones that became somehow a family.

Finally, I must thank my family, always present, even being away. Estar longe de vocês foi a parte mais difícil deste doutorado. Obrigada por tudo!

*Lisbon, 15 May 2019* A.C.S.

# Abstract

Mountain regions are considered to be the natural “water towers” of the world due to their importance as sources of many rivers. Reliable tools to estimate the availability and variability of streamflows in such regions are still rare. In this context, the present Thesis proposes to extend an existing Flow Duration Curve (FDC) modelling framework to Alpine environment. Such curves show the percentage of time a streamflow value is equaled or exceeded during a reference period and thereby give a representation of the probabilistic distribution of daily streamflows.

FDCs can be obtained empirically or based on models. Process-based FDC models have the advantage of incorporating hydrological process knowledge and thereby allowing the prediction of FDCs under changing conditions. This Thesis studies a simple process-based model that describes daily streamflow distributions as the result of subsurface flow pulses triggered by stochastic rainfall and censored by the soil moisture dynamics. The resulting streamflow distribution is characterized by only a few parameters: the mean rainfall depth and the frequency of rainfall events that produce streamflow and recession parameters.

The objective of this Thesis is the extension of the existing framework, originally developed by Botter et al. (2007c) for pluvial streamflow regimes to Alpine environments where the accumulation of water in the form of snow and ice influences the streamflow regime. The selected study region is Switzerland, a small Alpine country with a wide range of hydro-climatologic conditions.

The key of the extension of the model framework is a seasonal approach, i.e., a model set up for each of the up to three distinct seasons encountered in Alpine environments: i) pluvial season, ii) accumulation season (during winter), and iii) melting season (spring and summer). The pluvial season occurs between the end of the melting season and the beginning of a new accumulation season and the streamflows are rainfall driven. It can be modelled by the original model framework, but required the definition of more robust parameter estimation methods in the context of this Thesis, particularly for the linear and nonlinear recession parameters. The extension to the melting season is newly developed in this Thesis, incorporating the earlier extension to the snow accumulation season by Schaefli et al. (2013).

A key result of all completed parameter estimation tests for pluvial regimes is the very good performance of an inverse approach based on maximum likelihood estimation (MLE). MLE shows outstanding results even for short series of observations and can be retained as the recommended method to be used for the model framework studied in this Thesis.

The extension to the ablation (melt) season is achieved by the incorporation of the melting contribution as equivalent precipitation (sum of rainfall and snowmelt) and an ensuing increase of the streamflow producing frequency as compared to the one resulting from rainfall input alone. The amount of equivalent precipitation is calculated based on the snow accumulation from the existing model extension to winter low flows, combined with a process-based definition of seasons rather than calendar dates. A detailed analysis for all seasons for 10 selected case studies shows that the new seasonal approach yields good results for Alpine streamflow distributions, including for glacier-influenced catchments.

The improved parameter estimation methods developed in this thesis for all dominant hydrologic seasons establish a new reference approach for regionalization, opening new perspectives for flow duration curve estimation in ungauged catchments. Other promising results are the consistency of estimated model parameters with underlying physical processes and namely the observed correlation between model parameters and mean catchment elevation. This will allow the study of land use and climate changes in future model applications.

# Resumo

Montanhas são consideradas as "caixas d'água" naturais do mundo por serem o local onde diversos rios nascem. Ferramentas confiáveis que nos permitam avaliar a disponibilidade e a variabilidade destes recursos ainda são raras. Neste contexto, esta Tese busca estender um modelo existente para o cálculo de curvas de permanência para ambientes Alpinos. Estas curvas mostram a porcentagem de tempo em que um valor de vazão é igualado ou excedido durante um período, tratando-se de uma representação probabilística da distribuição de escoamentos diários.

Curvas de permanência podem ser obtidas empiricamente ou com base em modelos. As curvas obtidas por meio de modelos de base física têm a vantagem de permitir uma boa compreensão de processos hidrológicos e a predição de comportamentos de variáveis sujeitas a alterações. Esta Tese estuda um modelo simples, baseado em processos físicos que descreve a distribuição probabilística de escoamentos diários como sendo o resultado de pulsos subsuperficiais de água gerados por eventos de precipitação estocástica e limitados pela dinâmica da umidade no solo. A distribuição resultante é caracterizada por poucos parâmetros: a altura média de precipitação, a frequência média de eventos de precipitação que geram escoamento e parâmetros de recessão.

O objetivo desta Tese é estender o modelo existente, desenvolvido originalmente por Botter et al. (2007c) para regimes hidrológicos pluviais para ambientes Alpinos onde a acumulação de água na forma de neve e gelo influencia o regime hidrológico. A região selecionada para o estudo foi a Suíça, um pequeno país Alpino com uma grande variedade de condições hidro-climáticas.

A chave para a extensão do modelo é uma abordagem sazonal, ou seja, uma configuração diferente para cada uma das até três estações distintas encontradas em ambientes Alpinos: i) estação pluvial, ii) estação de acumulação (durante o inverno), iii) e estação de desgelo (primavera e verão). A estação pluvial acontece entre o fim do desgelo e o início de uma nova acumulação e o escoamento é gerado por eventos de chuva. Ela pode ser tratada pelo modelo original, mas demandava métodos mais robustos para a estimativa de parâmetros no contexto da Tese, em particular para os parâmetros de recessão lineares ou não lineares. No contexto desta Tese, foi desenvolvida uma nova extensão para a estação de desgelo, incorporando a extensão existente para o acúmulo de neve proposta por Schaefli et al. (2013).

Outro resultado fundamental de todos os testes desenvolvidos para regimes pluviais envolvendo a estimativa de parâmetros é a ótima performance de uma abordagem inversa baseada no método da máxima verossimilhança (MMV). O MMV apresentou resultados excepcionais

inclusive para séries de observações curtas e pode ser considerado o método recomendado para ser usado com o modelo estudado nesta Tese.
A extensão para o período de ablação (desgelo) foi feita baseada na incorporação da contribuição do desgelo para o escoamento como precipitação equivalente (que soma a chuva e o desgelo) e pela consideração de um aumento na frequência de geração de escoamento em comparação com a frequência dos eventos de chuva. A precipitação equivalente é calculada com base na estimativa da neve acumulada obtida pela aplicação do modelo para baixas vazões no inverno, combinado a uma nova definição de estações, fundamentada em processos hidrológicos ao invés de datas padronizadas. Foi feita uma análise detalhada de cada estação para 10 estudos de caso e esta abordagem sazonal levou a bons resultados para as curvas de permanência Alpinas, inclusive em bacias com regime glaciar.
A melhoria dos métodos de estimativa de parâmetros desenvolvida nesta tese para todas as estações hidrológicas dominantes estabelece novas referências para a regionalização, e abre perspectivas para a estimativa de curvas de permanência em bacias não monitoradas. Outros resultados promissores são relacionados à consistência dos resultados com processos físicos, mais especificamente à correlação observada entre os parâmetros do modelo e a altura média das bacias. Estas observações vão permitir estudos sobre alterações no uso de solo e no clima em aplicações futuras do modelo.

# Résumé

Les montagnes sont considérées comme les « châteaux d'eau » naturelles du monde en raison de leur importance en tant que source de plusieurs rivières. Des outils fiables permettant d'évaluer la disponibilité et la variabilité de ces fonctionnalités sont encore rares. Dans ce contexte, cette Thèse vise à étendre un modèle existant pour le calcul de courbes de débits classés pour des milieux Alpins. Ces courbes montrent le pourcentage de temps pendant lequel un débit est égalisé ou dépassé sur une période donnée, ce qui constitue une représentation de la distribution probabiliste des débits journaliers.

Les courbes de débits classés peuvent être obtenues de manière empirique ou à partir de modèles. Les courbes obtenues à l'aide de modèles de base physiques présentent l'avantage de permettre une bonne compréhension des processus hydrologiques et la prédiction du comportement de variables sujettes à des changements. Cette Thèse étudie un modèle simple, basé sur des processus physiques, décrivant la distribution probabiliste des écoulements journaliers comme étant le résultat de pulses d'eau souterraine générées par les précipitations stochastiques et limitées par la dynamique de l'humidité du sol. La distribution résultante est caractérisée par quelques paramètres : hauteur moyenne des précipitations, fréquence moyenne des événements de précipitation qui génèrent des écoulements et des paramètres de récession.

L'objectif de cette Thèse est d'étendre le modèle existant, développé originalement par Botter et al. (2007c) pour des régimes pluviaux, aux les environnements Alpins où l'accumulation d'eau sous forme de neige et de glace influence le régime hydrologique. La région choisie pour l'étude est la Suisse, un petit pays alpin avec une grande variété de conditions hydro-climatiques.

L'extension du modèle est basé sur une approche saisonnière, c'est-à-dire une configuration différente pour chacune des jusqu'à trois saisons distinctes que on trouve dans des milieux Alpins : (i) saison de pluie, (ii) saison d'accumulation (en hiver), (iii) et saison de fonte (printemps et été). La saison des pluies se produit entre la fin de la fonte et le début d'une nouvelle accumulation et le ruissellement est généré par les événements pluvieux. Elle peut être traité selon le modèle original, mais il demandait des méthodes plus robustes pour l'estimation des paramètres dans le contexte de cette Thèse, en particulier pour les paramètres de récession linéaire ou non linéaire. Dans le cadre de cette Thèse, une nouvelle extension a été développée pour la saison de fonte, incorporant l'extension existante pour l'accumulation de neige proposée par Schaefli et al. (2013).

Un autre résultat clé de tous les tests développés pour les régimes pluviaux sur l'estimation de

paramètres est la bonne performance d'une approche inverse basée sur la méthode du maximum de vraisemblance (MMV). La MMV a présenté des résultats exceptionnels même pour des séries d'observations courtes et peut être considéré comme la méthode recommandée pour être utilisé avec le modèle étudié dans cette Thèse.
L'extension pour la période d'ablation est basée sur l'incorporation de la contribution de la fonte de neige pour l'écoulement en tant que précipitation équivalente (la somme des précipitations et de la fonte de neige) et à la prise en compte d'une augmentation de la fréquence de génération d'écoulement par rapport à fréquence des pluies. Les précipitations équivalentes sont calculées en fonction de la quantité de neige accumulée estimée par l'application du modèle pour les débits d'hiver, combinée à une nouvelle définition des saisons, basée sur des processus hydrologiques plutôt que sur des dates standard. Une analyse détaillée de chaque saison a été réalisée pour 10 cas d'études et cette approche saisonnière a donné de bons résultats pour les courbes de débits classés Alpines, y compris dans les bassins glaciaires.
L'amélioration des méthodes d'estimation de paramètres développée dans cette Thèse pour toutes les saisons hydrologiques dominantes établit de nouvelles références pour la régionalisation et ouvre des perspectives pour l'estimation des courbes de débits classés dans des bassins non surveillés. D'autres résultats prometteurs sont liés à la cohérence des résultats avec les processus physiques, plus spécifiquement à la corrélation observée entre les paramètres du modèle et la hauteur moyenne des bassins. Ces observations permettront d'étudier le changement de l'usage des sols et du climat dans les applications futures du modèle.

# Contents

# List of Figures

# List of Tables

# List of symbols and acronyms

## Roman capitals

| | |
|---|---|
| $A$ | Catchment area |
| $A^*$ | Non-responsive area of the catchment |
| $CV$ | Coefficient of variation |
| $CV_{a^{(1)}}$ | Coefficient of variation of $a$ for a 1 year length scenario |
| $CV_{a^{(2)}}$ | Coefficient of variation of $a$ for a 2 years length scenario |
| $CV_{a^{(5)}}$ | Coefficient of variation of $a$ for a 5 years length scenario |
| $CV_{k_n^{(1)}}$ | Coefficient of variation of $k_n$ for a 1 year length scenario |
| $CV_{k_n^{(2)}}$ | Coefficient of variation of $k_n$ for a 2 years length scenario |
| $CV_{k_n^{(5)}}$ | Coefficient of variation of $k_n$ for a 5 years length scenario |
| $E$ | Maximum evapotranspiration rate |
| E1 | Permissive recession extraction |
| E2 | Intermediate recession extraction |
| E3 | Recession extraction with concavity criteria |
| $F(.)$ | Empirical cumulative distribution function |
| $I$ | Interception |
| $\overline{I_y}$ | Mean annual interception |
| $\mathscr{L}(.)$ | Likelihood function |
| $\overline{L_y}$ | Mean annual losses |
| $N$ | Size of a sample |
| $P$ | Mean total precipitation during an application time interval |
| $P_{eq}$ | Equivalent precipitation |
| $P_Q^{(a)}(.)$ | Probability density function during the accumulation season |
| $P_Q^{(m)}(.)$ | Probability density function during the melting season |
| $P_Q^{(p)}(.)$ | Probability density function during the pluvial season |
| $P_s$ | Mean total precipitation during the meteorological summer |
| $\overline{P_y}$ | Mean annual precipitation |
| $P_Y(.)$ | Annual probability density function |
| P1 | Nonlinear parameter estimation method based on master equation |
| P2 | Per event linear least square nonlinear parameter estimation method |
| P3 | Decorrelation nonlinear parameter estimation per event |

| | |
|---|---|
| PL1 | Linear parameter estimation method based on master equation |
| PL2 | Per event linear parameter estimation method |
| PN1 | Nonlinear parameter estimation method based on master equation |
| PN2 | Per event linear least square nonlinear parameter estimation method |
| PN3 | Decorrelation nonlinear parameter estimation per event |
| $Q$ | Daily streamflow |
| $\overline{Q}$ | Mean daily streamflow during a given time interval |
| $\tilde{Q}$ | Observed streamflows |
| $\overline{\tilde{Q}}$ | Mean observed streamflow |
| $\overline{Q_y}$ | Mean annual streamflow |
| $\overline{Q^{(m)}}$ | Mean daily streamflow during the melting season |
| $\overline{Q_a^{(m)}}$ | Mean daily streamflow during the melting season originated from melting |
| $\overline{Q_p^{(m)}}$ | Mean daily streamflow during the melting season originated from precipitation |
| $Q^{(w)}$ | Daily streamflow during winter |
| $Q(t)$ | Streamflow at the time $t$ |
| $Q_{95}$ | Upper 95% quantile of $c^{KS}$ |
| $Q_{95\%}$ | Streamflow flow rate exceeded during 95% of the time |
| $Q_{95}^{(1)}$ | Upper 95% quantile of $c^{KS}$ for a 1 year length scenario |
| $Q_{95}^{(2)}$ | Upper 95% quantile of $c^{KS}$ for a 2 years length scenario |
| $Q_{95}^{(5)}$ | Upper 95% quantile of $c^{KS}$ for a 2 years length scenario |
| $Q_{347}$ | Streamflow flow rate exceeded during 347 days per year |
| $R^{(1)}$ | Range of values obtained with MLE for 1 year length scenarios |
| $R^2$ | Coefficient of determination |
| $S^{(a)}$ | Specific accumulated water volume |
| $\overline{T}$ | Mean air temperature during a given time interval |
| $\overline{T}_s$ | Mean air temperature during the meteorological summer |
| $Z_r$ | Effective soil depth |

# Roman lower cases

| | |
|---|---|
| $a$ | Nonlinear recession exponent |
| $a^{(p)}$ | Nonlinear recession exponent for the pluvial season |
| $\overline{a^d}$ | Mean of the set of fitted recession exponents obtained without linearization |
| $\overline{a_i^{(1)}}$ | Mean $a$ for a 1 year length scenario |
| $\overline{a_i^{(2)}}$ | Mean $a$ for a 2 years length scenario |
| $\overline{a_i^{(5)}}$ | Mean $a$ for a 5 years length scenario |
| $a_f$ | Nonlinear recession exponent for forward estimation |
| $a_i$ | Nonlinear recession exponent for inverse estimation |
| $a_j$ | Set of fitted recession exponents |
| $a_j^d$ | Set of fitted recession exponents obtained without linearization |
| $c^{AIC}$ | Akaike information criterion |

| | |
|---|---|
| $c_l^{AIC}$ | Akaike information criterion for the linear model |
| $c_{li}^{AIC}$ | Akaike information criterion for the nonlinear model and inverse estimation |
| $c_n^{AIC}$ | Akaike information criterion for the nonlinear model |
| $c_{ni}^{AIC}$ | Akaike information criterion for the linear model and inverse estimation |
| $c^{KS}$ | Kolmogorov-Smirnov distance |
| $c_{lf}^{KS}$ | Kolmogorov-Smirnov distance for linear model and forward estimation |
| $c_{li}^{KS}$ | Kolmogorov-Smirnov distance for linear model and inverse estimation |
| $c_{nf}^{KS}$ | Kolmogorov-Smirnov distance for nonlinear model and forward estimation |
| $c_{ni}^{KS}$ | Kolmogorov-Smirnov distance for nonlinear model and inverse estimation |
| $c^{KS,a}$ | Kolmogorov-Smirnov distance for the accumulation season |
| $c^{KS,m}$ | Kolmogorov-Smirnov distance for the melting season |
| $c^{KS,p}$ | Kolmogorov-Smirnov distance for the pluvial season |
| $d$ | Duration of the seasonal cycle |
| $f$ | Empirical frequency |
| $j$ | Index for individual recessions |
| $k$ | Linear recession coefficient |
| $k^{(m)}$ | Linear recession coefficient for the melting season |
| $k^{(w)}$ | Linear recession coefficient for winter |
| $k_f$ | Linear recession coefficient for forward estimation |
| $k_i$ | Linear recession coefficient for inverse estimation |
| $k_n$ | Nonlinear recession coefficient |
| $\overline{k_n^{(1)}}$ | Mean $k_n$ for a 1 year length scenario |
| $\overline{k_n^{(2)}}$ | Mean $k_n$ for a 2 years length scenario |
| $\overline{k_n^{(5)}}$ | Mean $k_n$ for a 5 years length scenario |
| $k_n^{(p)}$ | Nonlinear recession coefficient for the pluvial season |
| $k_{nf}$ | Nonlinear recession coefficient for forward estimation |
| $k_{ni}$ | Nonlinear recession coefficient for inverse estimation |
| $k_{nj}$ | Set of fitted recession coefficients |
| $k_{nj}^d$ | Set of fitted recession coefficients obtained without linearization |
| $l$ | Length of an application time interval (or season) |
| $l^{(a)}$ | Length of the accumulation season |
| $l^{(m)}$ | Length of the melting season |
| $l^{(p)}$ | Length of the pluvial season |
| $n$ | Soil porosity |
| $n_m$ | Number of model parameters |
| $p(.)$ | Probability density function |
| $q_0$ | Streamflow rescaling constant |
| $r^{AIC}$ | Relative Akaike information criterion |
| $s_l$ | Soil retention capacity |
| $s_T$ | Phase shift |
| $s_w$ | Permanent wilting point |

| | |
|---|---|
| $s(t)$ | Soil moisture at the time $t$ |
| $\sup(.)$ | Supremum function |
| $t$ | Time step |

## Greek symbols

| | |
|---|---|
| $\alpha$ | Average rainfall on raindays |
| $\alpha^{(a)}$ | Average precipitation on days with precipitation during the accumulation season |
| $\alpha^{(m)}$ | Average rainfall on raindays during the melting season |
| $\alpha^{(p)}$ | Average rainfall on raindays during the pluvial season |
| $\alpha^{(w)}$ | Average rainfall on raindays during the winter |
| $\gamma$ | Inverse of mean streamflow increment due to incoming rainfall |
| $\gamma_P$ | Inverse of average rainfall on raindays |
| $\Gamma(a,b)$ | Incomplete gamma function |
| $\Delta$ | Mass balance difference |
| $\Delta_T$ | Dimensionless seasonal amplitude |
| $\eta$ | normalized maximum evapotranspiration rate |
| $\lambda$ | Streamflow-producing frequency |
| $\lambda^{(m)}$ | Streamflow producing frequency during the melting season |
| $\lambda^{(m,t)}$ | Streamflow producing frequency during the melting season obtained theoretically |
| $\lambda^{(m,o)}$ | Streamflow producing frequency during the melting season obtained empirically |
| $\lambda^{(p,o)}$ | Observed streamflow producing frequency during the pluvial season |
| $\lambda_P$ | Precipitation frequency |
| $\lambda_P^{(a)}$ | Precipitation frequency during the accumulation season |
| $\lambda_P^{(m)}$ | Precipitation frequency during the melting season |
| $\lambda_P^{(p)}$ | Precipitation frequency during the pluvial season |
| $\lambda_P^{(w)}$ | Precipitation frequency during winter |
| $\xi_t$ | Rainfall stochastic process |
| $\xi_t''$ | Streamflow production stochastic process |
| $-\rho[s(t)]$ | Water loss function |
| $\tau$ | Residence time of water in a catchment in periods without snow influence |
| $\tau^{(m)}$ | Inverse of linear recession coefficient during the melting season |
| $\tau^{(w)}$ | Inverse of linear recession coefficient during winter |
| $\tau_D$ | Delay caused by the presence of snow |
| $\tau_k$ | Residence time of water in a catchment |

## Acronyms

| | |
|---|---|
| ANETZ | Swiss Automatic Measurement Network |
| APB | Alpbach catchment |
| DIS | Dischmabach catchment |

| | |
|---|---|
| FDC | Flow duration curve |
| FOEN | Swiss Federal Office for the Environment |
| GOL | Goldach catchment |
| GPM | Global Precipitation Measurement |
| GRO | Grosstalbach catchment |
| GUR | Gürbe catchment |
| ID | Identification code |
| KS | Kolmogorov-Smirnov |
| LS | Least squares |
| MAS | Massa catchment |
| MLE | Maximum likelihood estimation |
| MUW | Murg at Wängi catchment |
| NEC | Necker catchment |
| OVA | Ova da Cluozza catchment |
| POS | Poschiavino catchment |
| RAM | Recession analysis method |
| RDC | Riale di Calnegia catchment |
| RHG | Rhône - Gletsch catchment |
| RhiresD | Swiss gridded daily precipitation database |
| ROT | Rotenbach catchment |
| SEN | Sense catchment |
| SIT | Sitter catchment |

# Introduction Part I

# 1 Introduction

Flow duration curves (FDCs) show the percentage of time a streamflow value is equaled or exceeded during a period and provide information about the availability and variability of water resources (Foster, 1934; Searcy, 1959; Vogel and Fennessey, 1994). Their many uses include, for example, the design of water supply systems and run-of-river hydropower plants and ecological studies (Ceola et al., 2010; Vogel and Fennessey, 1995; Wagner and Mathur, 2011).

Besides being a tool for managing water resources management, FDCs are also used in more theoretical studies about catchments. Because they result from the complex interactions between the climate and geomorphological characteristics of a catchment (Vogel and Fennessey, 1995), they are sensitive to changes in these conditions, and can be used to investigate impacts on water resources (Botter et al., 2010; Mejía et al., 2014). Furthermore, FDCs can provide insights on the hydrological resilience of river regimes (Botter et al., 2013), low flows (Smakhtin, 2001) and the ecological integrity of a stream (Poff et al., 1997).

Switzerland is an Alpine country well-supplied by surface waters. Its mountains are the source to some of the most important rivers of Europe, such as the The Rhine and the Rhône (Spreafico and Weingartner, 2005; Viviroli and Weingartner, 2004). Despite its small size, with only around $41 \cdot 10^3\ km^2$, it shows diverse hydrological conditions. The hydrological regimes in Switzerland range from exclusively pluvial, to glacier, passing by snow-dominated. This variability happens as a consequence of the elevation gradient (Weingartner and Aschwanden, 1992). The country relies strongly on hydropower production – it currently accounts for around 50% of its electricity supply – and is expected to increase this dependence as a result of the Energy Strategy 2050 (FOEN, 2018), in which one of the goals is to increase hydropower production (Schaefli et al., 2019). In the Swiss context, FDCs are an essential tool for hydropower design and to establish environmental flows. This importance motivates the search for better methods to obtain FDCs for Alpine catchments.

There are empirical or model-based methods to calculate FDCs (Blöschl and Sivapalan, 2013). One of the latter is the model proposed by Botter et al. (2007c), who derived a process-based analytical description of streamflow distributions as the result of subsurface flow pulses triggered by stochastic rainfall and censored by the soil moisture dynamics. The resulting streamflow distribution, analogous to a FDC, is characterized by only a few parameters: the mean rainfall depth and the frequency of rainfall events that produce streamflow and recession parameters. According to Müller and Thompson (2016), this model has advantages when compared to purely statistical or empirical methods: i) it provides an explicit link between the FDC shape, rainfall characteristics, and catchment recession characteristics rather than an empirical or statistical link to regional FDC shapes; and ii) it is applicable to periods characterized by different meteorological conditions, thanks due to the explicit treatment of rainfall and evapotranspiration characteristics. This model has been successfully applied to different regions with some adaptations for different hydrological conditions but has not yet been extended to fully describing Alpine streamflow regimes influenced by snow accumulation and melt.

## 1.1 Objectives

Motivated by the advantages of the analytical streamflow distribution model derived by Botter et al. (2007c), by the hydrological variety in Switzerland and by the importance of assessing the availability and variability of water resources in this country and mountainous regions, the objectives of this Thesis are:

- The adaptation of the model framework proposed by Schaefli et al. (2013) to the different Alpine hydrological regimes, namely: pluvial, snow-dominated, and glacier. Originally, the analytical model for streamflow distributions developed by Botter et al. (2007c) assumed that only rainfall events drive streamflow production. Later, Schaefli et al. (2013) extended the framework to consider periods of snow accumulation, but there was no previous development related to snow and glacier melt, typical in mountain areas.
- The definition of the most suitable methods to calculate model parameters (particularly of the recession parameters) based on a detailed analysis of Swiss case studies as a reference. There is a wide variety of recession analysis methods that yield different results, and specific methods can be more or less suitable for particular applications.

These objectives emerged from the needs identified in the state-of-the-art presented in Chapter 2.

## 1.2 Organization of the Thesis

This document is structured in three parts: Introduction, Scientific developments, and Conclusion. It is a thesis by publications, so each of the scientific developments, presented in Chapters 3 to 6, correspond to four articles that have been prepared for publication in international peer-reviewed scientific journals.

The scientific developments are organized as follows:

- **Chapter 3**: This Chapter studies the behavior of the analytical streamflow distribution model in 25 Swiss catchments with different regimes, including catchments with snow-dominated and glacier regimes. Since the original model assumes a pluvial regime, it was applied to the meteorological summer, when snow-melt is supposed to be finished in the snow-driven catchments, but there is still glacier melting. The pluvial model was tested with assumptions of linear and nonlinear recessions. Recession parameters were obtained by a conventional recession analysis method (Brutsaert and Nieber, 1977) and by an inverse method, the maximum likelihood estimation (MLE). The application of the model raised two main issues: i) the need of better recession parameters estimation methods, and ii) the need of an extension of the model to make it suitable also for periods when streamflow production is affected by snow or glacier melt. Accordingly, the study showed that this increase in the streamflow can be incorporated into the model by an increase in the streamflow producing frequency.
- **Chapter 4**: The use of MLE to calculate recession parameters in Chapter 3 yield outstanding model performances and this Chapter investigates the possibility of applying it to the nonlinear model to obtain recession parameters systematically. The MLE and a selection of recession analysis methods (RAM) were applied to five case studies with a pluvial regime for a civil year considering different lengths of streamflow time series (1 year, 2 years, 5 years and 40 years). The selection of RAMs included combinations of diverse recession extraction and parameter estimation methods. The key findings of this study were: i) the combination of a strict recession selection method with a parameter estimation per event leads to recession parameters that suit the model and ii) the best RAM combination and MLE work well even for short series of data.
- **Chapter 5**: The study about recession parameters estimation was complemented by the examination of conventional RAMs applied to linear and nonlinear, seasonal and annual recession parameters for pluvial Swiss catchments. Again, different recession extraction and parameter estimation methods were tested, and the results obtained were evaluated in terms of parameters values and model performances. Parameters obtained by MLE were adopted as a reference for the comparisons. Different RAMs yield different parameters and model performances, and no RAM systematically reaches the model performances obtained with MLE, particularly for the linear model.
- **Chapter 6**: The second point raised in the first study was the need of an extension of the model to make it suitable for periods of snow and glacier melt, allowing the description of annual streamflow distributions for glacier and snow-dominated catchments. The Chapter builds on the idea of incorporating the additional water source as an increase in the frequency of streamflow production. To allow this, the seasons of application of the model were redefined by the identification of periods of snow accumulation

and melt and a pluvial period, if it exists. Then, the volume of stored water (and the additional glacier melting contribution, when it exists) is estimated, and the frequency of streamflow producing events is recalculated based on a water balance.

# 2 State-of-the-art

This chapter presents the state-of-the-art relevant to this Thesis. It begins with a presentation of concepts related to flow duration curves (Sec. 2.1) and their modelling (Sec. 2.2). Section 2.4 presents the analytic streamflow distribution model that was variously extended in this Thesis. Section 2.5 is about mountain hydrology, particularly relevant in Switzerland, where the case studies used in comparative analysis were selected. Finally, Section 2.6 summarizes the main research gaps found in the literature review.

## 2.1 Flow duration curves

Flow duration curves (FDCs) are a basic tool for water resources management. They represent graphically the percentage of time (that can also be understood as the frequency) a given streamflow is equaled or exceeded in a given stream (Foster, 1934; Searcy, 1959; Vogel and Fennessey, 1994).

If the sample of daily streamflow observations is large enough, a FDC can be interpreted as a probabilistic representation of this variable and carries the same information as a probability density function (pdf) and the cumulative distribution function (cdf), as shown in Figure 2.1.

Vogel and Fennessey (1995) listed many uses for FDCs, such as in hydropower engineering, in water management in terms of quantity and quality (e.g. Von Sperling, 2007), in studies about water allocation (e.g. Petts, 1996) and sediment transport (e.g. Basso et al., 2015a), in ecohydrological studies (e.g. Botter et al., 2008) and even as an input to hydrological modelling (e.g. Archfield and Vogel, 2010).

In hydropower design, FDCs are adopted for many purposes, for example, as a tool to evaluate the water availability for run-of-river schemes (Mays, 2010; Penche, 1998; Wagner and Mathur, 2011) or, coupled with the available head, for turbine selection (Montanari, 2003; Basso and Botter, 2012; Santolin et al., 2011).

There exist a general agreement that FDCs are an excellent tool to study low flows (Smakhtin, 2001; Vogel and Fennessey, 1995; Westerberg et al., 2011). Because of that, an essential use of FDCs in water management is as a tool to assess the minimum

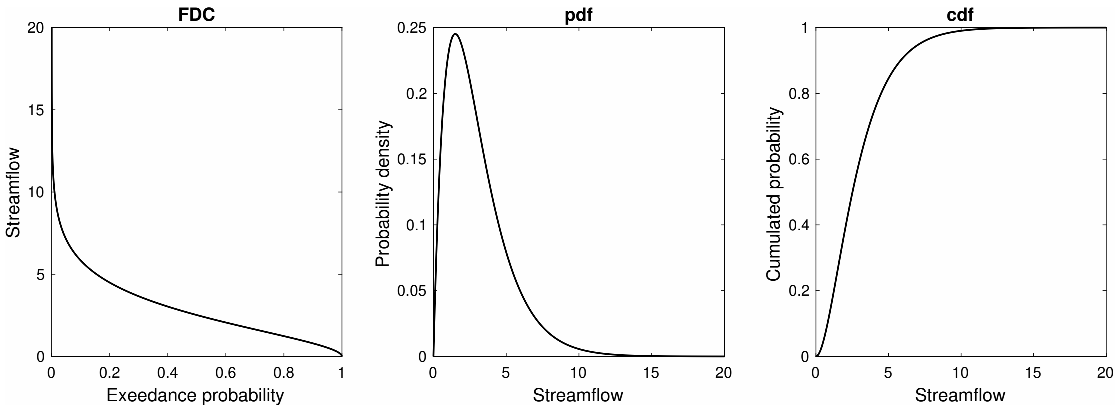


Figure 2.1 – Representation of a probabilistic distribution of daily streamflows in terms of FDC, pdf and cdf

streamflow environmentally viable, which is the flow rate that must remain in a stream after one or several water withdrawals. In Switzerland, for example, it is a function of the $Q_{347}$ (or $Q_{95\%}$, if the FDC's abscissa is presented as frequency), "the flow rate which, averaged over ten years, is reached or exceeded on an average of 347 days per year" (LEaux, 1991). Estoppey et al. (2000) provide guidelines on how to estimate those streamflow values for gauged and ungauged sites in Switzerland.

The streamflow regime is fundamental to sustain the ecological integrity of rivers (Poff et al., 1997) and FDCs are also useful to evaluate regimes in this sense. Some previous applications on FDCs regarding ecological studies are the one by Ceola et al. (2013), who showed that altering the streamflow distribution changes the nature of the stream ecosystem using FDCs to asses those changes and Fabris et al. (2018) who studies the effect of regime variability on fish habitat.

The most straightforward method to calculate an FDC is empirical, based on a series of observed daily streamflows. This is done by assigning empirical frequencies, $f$, to sorted observed data. Then, the values of streamflows are plotted against the values of probabilities of exceedance, $1-f$. Based on this, they can be considered a complement of a cumulative relative frequency diagram.

There are two essential approaches to construct empirical FDCs. The first one is the long-term FDC, based on a single curve for all the available data. The other is the annually based FDC, for which one classifies yearly data individually, and obtains a final curve by averaging the individual yearly curves. Both approaches are useful in water resources management, but long-term FDCs incorporate more information, especially about extremes, and annual FDCs have the advantage of allowing the study of variabilities in the streamflows and are less sensitive to the data acquisition period, despite losing some information in the averaging step (Vogel and Fennessey, 1994).

## 2.2 Flow duration curves modelling

Flow duration curve models can be used to asses the values of unknown variables, to better understand hydrological processes and to predict the values of variables in a changing environment. If FDCs are to be used to make predictions, a major preoccupation is to understand the underlying hydrological processes that drive streamflow production.

FDCs result from many processes and agents that include climatic forcing, catchments characteristics, and environmental factors. To be able to model FDCs it is necessary to understand and describe the relationships between the attributes of the FDCs and appropriate climatic and landscape characteristics.

An FDC can be divided into three zones: high flows, intermediate flows, and low flows. In pluvial regimes, the dominant driver for high flows is precipitation, and rainfall and streamflow statistics should be similar. For intermediate flows, the dominant controls are the soil water storage and the evapotranspiration processes and finally, for low flows, the competition between deep groundwater and riparian evaporation drive streamflow generation (Blöschl and Sivapalan, 2013). In glacier and snow dominated catchments there are additional storage and streamflow release processes, as snow accumulation and melting that should be considered.

Blöschl and Sivapalan (2013) reviewed statistical methods and physically based models for FDC modelling in ungauged catchments. Statistical methods generate FDCs based on FDCs in neighbouring catchments and catchment or climate characteristics. They can be categorized in:

- Regression methods: estimate each flow quantile separately from the catchment and climate characteristics (e.g. Nag and Biswal, 2019; Nathan and McMahon, 1992; Swain, 2017) ;
- Index methods: i) parametric methods, which regionalize the parameters of a distribution function that represent an FDC (e.g. Castellarin et al., 2004b) or ii) index flow methods, which scale FDCs with an index flow of all catchments in a region having the same shape. The index flow is frequently the annual runoff or the medium daily runoff (e.g. Ganora et al., 2009);
- Geostatistical: methods that apply geostatistical criteria, mostly some type of spatial interpolation, to the regionalization of hydrological information (e.g. Castiglioni et al., 2009);
- Methods that use streamflow records: short series of data (with less than five years) can be used to improve the quality of FDCs calculated with other techniques (e.g. Castellarin et al., 2004a).

Physically based models or process-based models are the ones that try to understand and describe the effects of climate processes and catchment characteristics on the shape of the FDCs, linking drivers of processes to the conditions of a system and its responses. There are two main types of physically based models: i) Continuous models and ii) Derived distribution models (Blöschl and Sivapalan, 2013).

Continuous models are the ones that use long-term simulations of the water balance coupled with routing models to reproduce the movement of water in soil and streams (e.g. Biswal, 2016; Nag and Biswal, 2019; Wagener and Wheater, 2006). They provide a detailed description of the system and driving processes, but they tend to be complex, with a large number of parameters and costly in terms of simulation time. The increased complexity can constrain the transferability of the model to other catchments (i.e., prevent reliable regionalization).

In the derived distribution models, FDCs are derived from precipitation analytically, considering some simplifications. An example of this type of model is the one proposed by Botter et al. (2007c), in which a probability density function (pdf) for seasonal daily streamflows is described as being triggered by subsurface flow induced by subsurface forcings. This model and its extensions will be described in more detail in section 2.4.

According to Blöschl and Sivapalan (2013), process-based methods are not widely used for predicting FDCs in ungauged basins but have good potential because they provide a good understanding of processes. Besides, the derived distribution models have the advantage of possessing a reduced number of parameters, that avoids an overcomplexity. The authors also mention that treating the curves seasonally could bring an additional understanding of the underlying processes.

Few methods exist for FDC estimation at ungauged sites specifically in Switzerland. A simple approach to obtain FDCs was proposed by Weingartner and Aschwanden (1994) and is a case of what Booker and Snelder (2012) would classify as "parametrization of curves and then regionalization". The parametrization is done using Pardé coefficients for some characteristic catchments, and they can be regionalized and used for ungauged sites. However, the reliability of the method is not reported for average flow. For low flows, errors are reported to be high.

## 2.3 Representation of flow duration curve models

Besides FDCs, there are other graphical representations of the distribution of daily streamflows along with the range of values contained in a sample. A typical representation is a histogram, that is a bar chart with class intervals on the horizontal axis and the frequencies of values in each class in the vertical axis. Frequency polygons have the same basis; they are formed by joining the midpoints of the topsides of the histogram bars, after adding one bin on both sides of the diagram. There are simple rules to obtain the number of interval classes that allow good visualization of the sample distribution without too many fluctuations in the shape of the distribution. A common approximation of this number is by $\sqrt{N}$, being N the size of the sample and the number of classes between 5 and 25 (Kottegoda and Rosso, 1997). Sturges (1926) also proposed a rule that the number of classes should be approximated by $1 + 3.3\log_{10}(N)$.

Both histograms and frequency polygons are comparable to pdfs, but both depend on the choice of class intervals that can vary and bias the visualization of results. Cumulative relative frequency diagrams, on the other hand, can be obtained by ranking the data and assigning frequencies to each value, which eliminates the uncertainties related to the choice of classes (Naghettini, 2016). Since neither, FDCs and cdfs, depend on classes selection, it is preferable to represent empiric data using one of them.

## 2.4 Analytical streamflow distribution model

### 2.4.1 Model framework

A stochastic model for rainfall can be combined with a deterministic recession to get an analytical modelling framework for probabilistic characterization of rainfall-driven daily streamflows. Botter et al. (2007c) proposed this framework based in a point-scale soil moisture model originally proposed by Rodriguez-Iturbe et al. (1999). It represents the dynamics of soil moisture as the result of a deterministic, state-dependent loss function, combined with stochastic increments triggered by rainfall events. Rodriguez-Iturbe et al. (1999) showed that the corresponding spatially averaged soil moisture $s(t)$ can be obtained from the water balance equation as follows:

$$\frac{ds(t)}{dt} = -\rho[s(t)] + \xi_t, \tag{2.1}$$

where $-\rho[s(t)]$ is the loss function, due to evapotranspiration, surface runoff and deep percolation, and where $\xi_t$ represents the stochastic instantaneous increments due to infiltration from rainfall.

Botter et al. (2007c) described the dynamics of daily streamflow with a similar stochastic differential equation, supposing that rainfall acts as a stochastic forcing for streamflow production and that, at the catchment-scale, the water is released following a linear decay:

$$\frac{dQ(t)}{dt} = -kQ(t) + \xi_t", \tag{2.2}$$

where $Q$ is the daily streamflow, $k$ is the inverse of the time constant associated with the loss function (i.e., the linear recession coefficient) and $\xi_t"$ is the stochastic process associated to streamflow-producing precipitation events (i.e. the sequence of events that trigger a flow response in the river).

The streamflow $Q$ is assumed to be the result of a series of rainfall inputs that deliver enough water to fill the water deficit in the soil ($\xi_t"$), i.e. that deliver enough water to raise the soil moisture level above its retention capacity, which is valid for pluvial regimes. The excess of water is removed from the soil as subsurface run-off and becomes streamflow. This implies in a dunnian mechanism of streamflow production, for which streamflows are produced as a consequence of soil saturation and not by infiltration capacity exceedance as in a hortonian flow.

The rainfall forcing $\xi_t$ is modelled as a marked Poisson process with frequency $\lambda_p$ and exponentially distributed rainfall depths with average $\alpha$ (average rainfall on raindays). Not all the rainfall events trigger a streamflow response, i.e. the frequency of streamflow-producing events corresponds to $\lambda < \lambda_p$, where $\lambda$ is influenced by the soil storage capacity and soil drying time and can be written as (Botter et al., 2007a; Cox and Miller, 1987):

$$\lambda = \eta \frac{\exp(-\gamma)\gamma^{\frac{\lambda_p}{\eta}}}{\Gamma(\lambda_p/\eta, \gamma)}, \tag{2.3}$$

where $\Gamma(a,b)$ is a lower incomplete Gamma function with parameters $a$ and $b$, $\eta = E/(nZ_r(s_1 - s_w))$, $\gamma = \gamma_p nZ_r(s_1 - s_w)$ and $\gamma_p = 1/\alpha$. $E$ is the maximum evapotranspiration rate and $nZ_r(s_1 - s_w)$ synthesizes the soil volume liable to be filled by water before drainage starts; $n$ is the porosity of the soil, $Z_r$ is the effective soil depth, $s_1$ is the retention capacity and $s_w$ the permanent wilting point.

As discussed in detail by Botter et al. (2007c), this framework results in the following probability distribution of daily streamflows at the catchment-scale:

$$p(Q, t \to \infty) = \frac{1}{\Gamma\left(\frac{\lambda}{k}\right)} \frac{1}{Q} \left(\frac{Q}{\alpha k A}\right)^{\frac{\lambda}{k}} \exp\left(-\frac{Q}{\alpha k A}\right), \tag{2.4}$$

where $A$ is the catchment area. This corresponds to a Gamma distribution with shape parameter $\lambda/k$ and a scale parameter $\alpha k A$. The corresponding expected mean streamflow equals $\overline{Q} = \lambda\alpha$. The model is suitable for steady state conditions, at the annual or seasonal scale, depending on the temporal variability of the model parameters (Botter et al., 2007a).

Nonlinear storage-streamflow relations at the catchment-scale are commonly observed (Botter et al., 2009; Brutsaert and Nieber, 1977; Mutzner et al., 2013). Accordingly, Botter et al. (2009) proposed an extension of the above modelling framework assuming that:

$$\frac{dQ(t)}{dt} = -k_n Q(t)^a + \xi_t", \tag{2.5}$$

where $k_n$ and $a$ are the constants of the nonlinear recession. As for the linear model, it is possible to obtain an equation for the pdf of the daily streamflows:

$$p(Q, t \to \infty) = C\left\{\frac{1}{Q^a} \exp\left[-\frac{Q^{2-a}}{\alpha k_n(2-a)} + \frac{Q^{1-a}\lambda}{k_n(1-a)}\right]\right\}, \tag{2.6}$$

where $C$ is a normalizing constant (Botter et al., 2009).

In practice, the assumptions necessary to the validity of the model framework are:

- The study catchment is smaller than the correlation scale of rainfall events.
- The study timescale is greater than the characteristic duration of single rainfall events (e.g., daily timescale).
- Inter-arrival times between streamflow producing events can be considered independent and exponentially distributed.
- Conditions to streamflow production can be considered steady.
- Any direct surface flow is neglected.

Figure 2.2 summarizes the evolution of the key model developments. The most relevant to this thesis are the incorporation of nonlinear storage-discharge relations (Botter et al., 2009), the extension to winter in snow dominated regimes, proposed by Schaefli et al. (2013) and the extension of model to seasonally dry climates (Müller et al., 2014), that considered the carry-over effect between seasons.

The different forms of the model were tested in different hydrological contexts and with different assumptions. Table 2.1 summarizes characteristics of the previous applications of the model.

- 2007 Development of the analytical model framework (Botter et al., 2007c)
- 2007 Study of cases with complex geomorphologies and heterogeneous soil and vegetation properties (Botter et al., 2007b)
- 2007 First observational validation (Botter et al., 2007a)
- 2008 Extension to annual timescale to derive annual minima (Botter et al., 2008)
- 2009 Incorporation of nonlinear storage-streamflow relations (Botter et al., 2009)
- 2010 Incorporation of variability in storage streamflow relations as a noise (Suweis et al., 2010)
- 2010 Consideration the catchment response as a gamma pulse and incorporation of high-flows (Muneepeerakul et al., 2010)
- 2010 Link between the variability of stream stage ($h$) and the stochasticity in daily streamflows and link to the nutrient loss rate ($k_e$) (Botter, 2010)
- 2010 Incorporation of random recession rates (Botter, 2010)
- 2013 Extension to winter flow in snow dominated regimes (Schaefli et al., 2013)
- 2013 Use to classify river regimes (erratic or persistent) (Botter et al., 2013)
- 2014 Extension to urbanized basins (Mejía et al., 2014)
- 2014 Extension to seasonally dry climates (Müller et al., 2014)
- 2014 Extension to describe the dynamics of inundation on a river section (Doulatyari et al., 2014)
- 2015 Link of the ability of the model to capture the statistical features of high flows to the degree of non-linearity of the catchment hydrologic response (Basso et al., 2015b)
- 2015 Coupling to water balance models and a geomorphological recession flow model to apply the model to ungaged catchments (Doulatyari et al., 2015)
- 2015 Coupling with sediment rating curves (Basso et al., 2015a)
- 2015 Extension to develop an analytical model for the persistence time pdf (Dralle et al., 2016)
- 2017 Investigation of the spatial correlation of daily flows based on the model (Betterle et al., 2017)
- 2017 Proposition of a method to predict the variability of streamflows at seasonal and annual time scale (Dralle et al., 2017a)
- 2018 Extension to study long term fluvial erosion rates (Deal et al., 2018)
- 2018 Study of the extension of Mejía et al. (2014) under nonstationary conditions (Jovanovic et al., 2018)
- 2018 Use to assess fish habitat quality (Fabris et al., 2018)

Figure 2.2 – Timeline of key model developments

Table 2.1 – Model applications and main characteristics

| Reference | Region | # cases | Climate/Seasons | Type of recession | Particularities |
|---|---|---|---|---|---|
| Botter et al. (2007a) | USA | 7 | Varied, avoids snow | Linear | First observational validation |
| Botter et al. (2008) | USA | 1 | Humid subtropical, all seasons and year | Linear | |
| Botter et al. (2009) | USA | 1 | Summer | Nonlinear | Fist application of nonlinear model |
| Botter et al. (2010) | Italy | 18 | Alpine,summer | Linear | Evaluate alterations of intra-annual streamflow variability |
| Ceola et al. (2010) | Italy and USA | 14 | Various, mostly summer | Linear/nonlinear | Tested different parameter estimation methods |
| Botter (2010) | Italy | 1 | Alpine,summer | Linear (stochastic) | Stochastic recession rates |
| Pumo and Noto (2013) | Italy (Sicily) | 1 | Mediterranean, active period | Linear | Studies the elasticity of the model to different climatic scenarios |
| Schaefli et al. (2013) | Italy and Switzerland | 14 | Alpine, winter | Linear | Considers snow accumulation |
| Botter et al. (2013) | USA and Italy | 44 | Varied, avoids snow | Linear | Proposes a classification of river regimes into erratic or persistent |
| Mejía et al. (2014) | USA | 11 | Varied | Linear | Urbanized catchments |
| Ceola et al. (2014) | Austria | 1 | Prealpine, summer | Linear | Ecohydrological studies |
| Müller et al. (2014) | Australia, USA and Nepal | 38 | Dry | Linear | Development for dry climates |
| Botter (2014) | USA | 1 | Temperate, negligible snow | Linear | Study about the influence of climate and landscape change on river flow regimes |
| Doulatyari et al. (2014) | Italy and USA | 2 | Erratic and Persistent, summer | Linear | Comparison between regimes |
| Lazzaro and Botter (2015) | Italy | 2 | Alpine,spring to autumn | Linear | Model used to assess hydrologic alteration |
| Basso et al. (2015b) | Italy, USA and Switzerland | 16 | Varied, avoids snow | Linear/nonlinear | Investigates how the model framework capture the statistical features of high flows |
| Doulatyari et al. (2015) | USA | 11 | Varied, avoids snow | Nonlinear | Ungaged catchments |
| Müller and Thompson (2016) | Nepal | 25 | Various | Nonlinear | Comparison with statistical methods for ungaged catchments |
| Doulatyari et al. (2017) | Switzerland | 6 | Meteorological seasons, mostly rainfall driven | Nonlinear | Spatial variability of parameters and regimes over a catchments and its sub-catchments. |
| Dralle et al. (2017a) | USA and Puerto Rico | 7 | Variable | Linear | Study about the variability of streamflows |

It is interesting to notice that, despite the gain in performance obtained with the incorporation of nonlinear storage-discharge relationships, the linear model remains popular, particularly in works that extend the model to new conditions. This happens because the resulting probabilistic streamflow distribution for the linear model is a gamma distribution, which has well known properties and allows a better theoretical treatment of results.

Another particularity of the previous case studies is that most of them are applications to the meteorological seasons. This allows the assumption of steady state conditions within each season with good model performances, but meteorological seasons may not be suitable in cases with transference of water between seasons. The only study to adopt case specific seasons was the one that dealt with carry-over effect between a wet and a dry season (Müller et al., 2014). Also, most of the studies avoid seasons affected by glacier and/or snow processes deliberately because they have particular streamflow producing conditions that were not studied in the model framework context. The exception to this is the work of Schaefli et al. (2013) that extended the model to snow accumulation conditions and applied it to a meteorological winter.

One more key application in this thesis context is the one by Ceola et al. (2010), who tested different methods of estimation of the frequency of streamflow producing events and of the recession parameters. They recommended that the frequency of streamflow producing events is best estimated from a combination of streamflow and precipitation data and could not conclude about any particular recession analysis method. Finally, they propose to obtain recession methods using statistical inference methods, but they do not test this systematically.

### 2.4.2 Maximum Likelihood Estimation

The model results in a parametric probabilistic curve, because of that, when observed streamflow data are available, statistical inference methods can also be used to estimate the model parameters. In parameter estimation, those methods associate a probabilistic model for a random variable to a sample of observed data to infer information about the population (Naghettini, 2016).

Ceola et al. (2010) were the first to attempt to use this group of methods to estimate nonlinear recession parameters to be used with the analytical model. They tested two methods: least squares (LS) and maximum likelihood estimation (MLE) and this second yield the best results.

MLE is considered to be an efficient method for parameter estimation. It maximizes a function of the distribution parameters, known as the likelihood function. The formulation of the MLE for the estimation of nonlinear recession parameters based on the model is shown in Equation 2.7:

$$\mathscr{L}(a, k_n) = \prod_{i=1}^{N} p(\tilde{Q}; a, k_n), \tag{2.7}$$

where $\tilde{Q}$ is the observed streamflow, $N$ is the number of available observations and $p(\tilde{Q}; a, k_n)$ is the probability density. This likelihood function is obtained following the general definition of a likelihood function, i.e. the joint probability of all observed data points (Naghettini, 2016). For the model of Equation 2.6, this joint probability corresponds to the product of $p(\tilde{Q})$ for all sample points.

## 2.5 Hydrological regimes and mountain hydrology

Mountainous regions are the source of important rivers, such as the Rhine, the Ganges, and the Columbia. They produce more streamflow than lowlands and supply a great part of the world population with water, being called natural “water towers” (Viviroli and Weingartner, 2004).

In mountainous regions, where the weather is colder, precipitation can occur in the form of snow, which accumulates until the temperature rises enough to melt it. When the climate supports the prolonged presence of snow, the accumulation may happen trough period long enough to become a perennial glacier.

It is possible to distinguish between three main types of streamflow regimes according to its drivers (Musy and Higy, 2010; Hänggi and Weingartner, 2012):

- Pluvial or rainfall dominated: Streamflow production is driven mainly by rainfall and evapotranspiration and, frequently, streamflows and rainfall patterns are similar.
- Snow dominated: Precipitation can occur in the form of snow that accumulates and melts completely intra-annually, and the greater streamflows generally occur at the end of spring or beginning of summer, influenced by snow melt. Annual streamflows tend to correlate positively with the annual precipitation, but there is a delay between the moment when snow falls (i.e., winter) and the moment when it becomes streamflow (i.e., spring).
- Glacier: In addition to snow, glacier melt also influences streamflows. The increase of streamflows is not limited by the amount of snow available for melting, so streamflows peak when temperature (i.e., energy) peaks and peak streamflows tend to occur in the middle of summer. Additionally, flows are lower from the end of autumn to the beginning of spring. Snow accumulates interannually, and the total annual streamflows depend not only on precipitation but also on temperature.

Modelling processes of snow accumulation and melt is complex, it depends on the knowledge of the characteristics of the snow packs and of energy fluxes, which can be rather complex in turn, specially because the monitoring networks in high mountains can be sparse, so modelling those processes require simplifications. Some modelling difficulties are particular from mountainous catchments namely (Musy et al., 2014):

- High spatial variability of meteorological variables (Hingray et al., 2012);
- High variability in space and time of the form of precipitation (Froidurot et al., 2014);
- High spatial variability of hydrological processes that depends on the meteorology on the topography and land uses (Kirnbauer, 1992; Tobin et al., 2013);
- Dependence of initial conditions in terms of soil saturation and snow conditions (Schaefli et al., 2005);
- Sparse observations of hydro-climatic variables in high elevations (Magnusson et al., 2014).

### 2.5.1 Swiss hydrology

Switzerland has an area of 41 285 $km^2$ mostly situated in mountainous regions. Its elevations range from 372 m asl to 4634 m asl and it is crossed by the Alps in the east-west direction. This geography results in varied hydrological regimes.

The streamflow regimes in Switzerland are usually classified in sixteen types (Haller et al., 2004). First, the country is divided into three regions: Northern part of the Alps (and Jura), Inner zone of the Alps and Southern zone of the Alps (Botter et al., 2019) then, for each of those regions, some characteristic Pardé coefficients were calculated, and they define the regimes. Pardé coefficients are the ratios between monthly streamflows and the annual streamflow (Weingartner and Aschwanden, 1994; Spreafico and Weingartner, 2005). Figure 2.3 illustrates the streamflow regimes for Switzerland and Figure 2.4 shows their spatial occurrence.

Figure 2.3 confirms that the Alpine regimes, that are mostly dominated by snow and glaciers have their higher streamflows during the warmer seasons when snow-melt occurs. Accordingly, during the colder seasons, the streamflows are very low. For the glacier regimes, the peak occurs later, during summer, while for the purely snow dominated regimes it happens before, during spring. Nivo-pluvial regimes tend to have two peaks, one during spring, due to snow melt and a second one during the autumn, due to high precipitation. The streamflows in the pluvial regimes tend to follow the same trends of precipitation.

Such varied regimes must be studied in different catchments with different characteristics, so 25 catchments were selected to be used as case studies in this thesis. Chapter 3 presents all those cases. The criteria for the selection were:

- Catchment with non-regulated streamflow, keeping approximately natural regimes (catchment without dams and lakes or important withdraws);

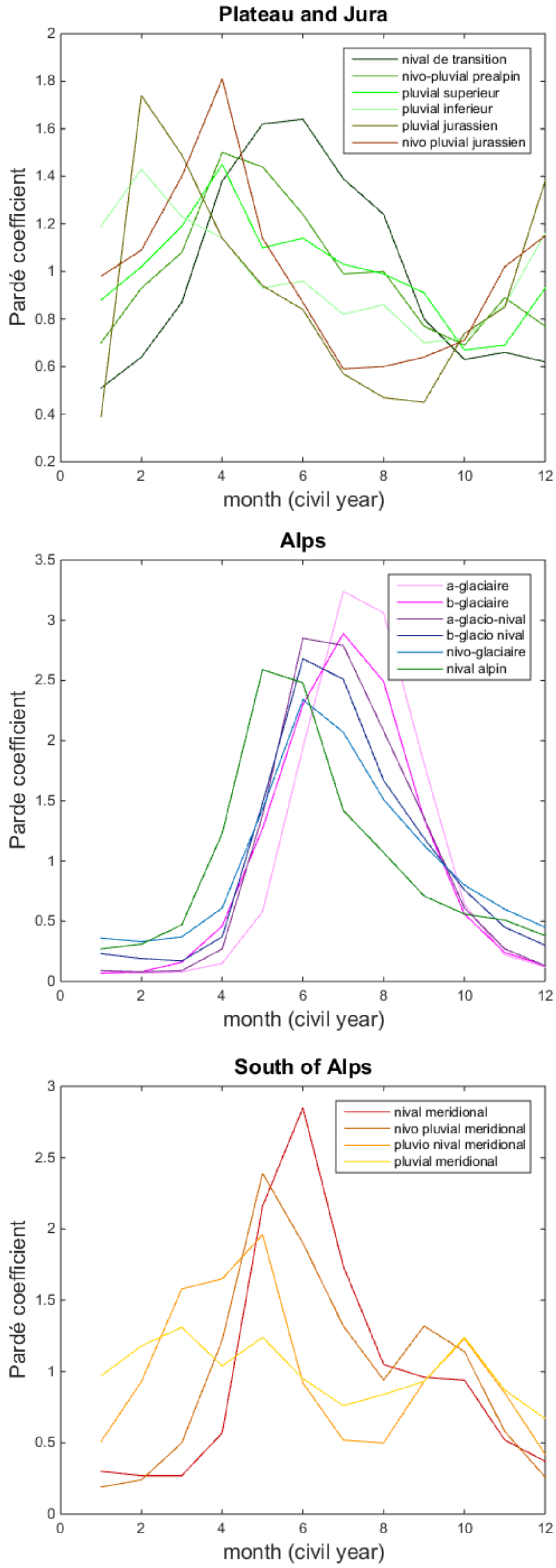


Figure 2.3 – Swiss streamflow regimes (Haller et al., 2004)

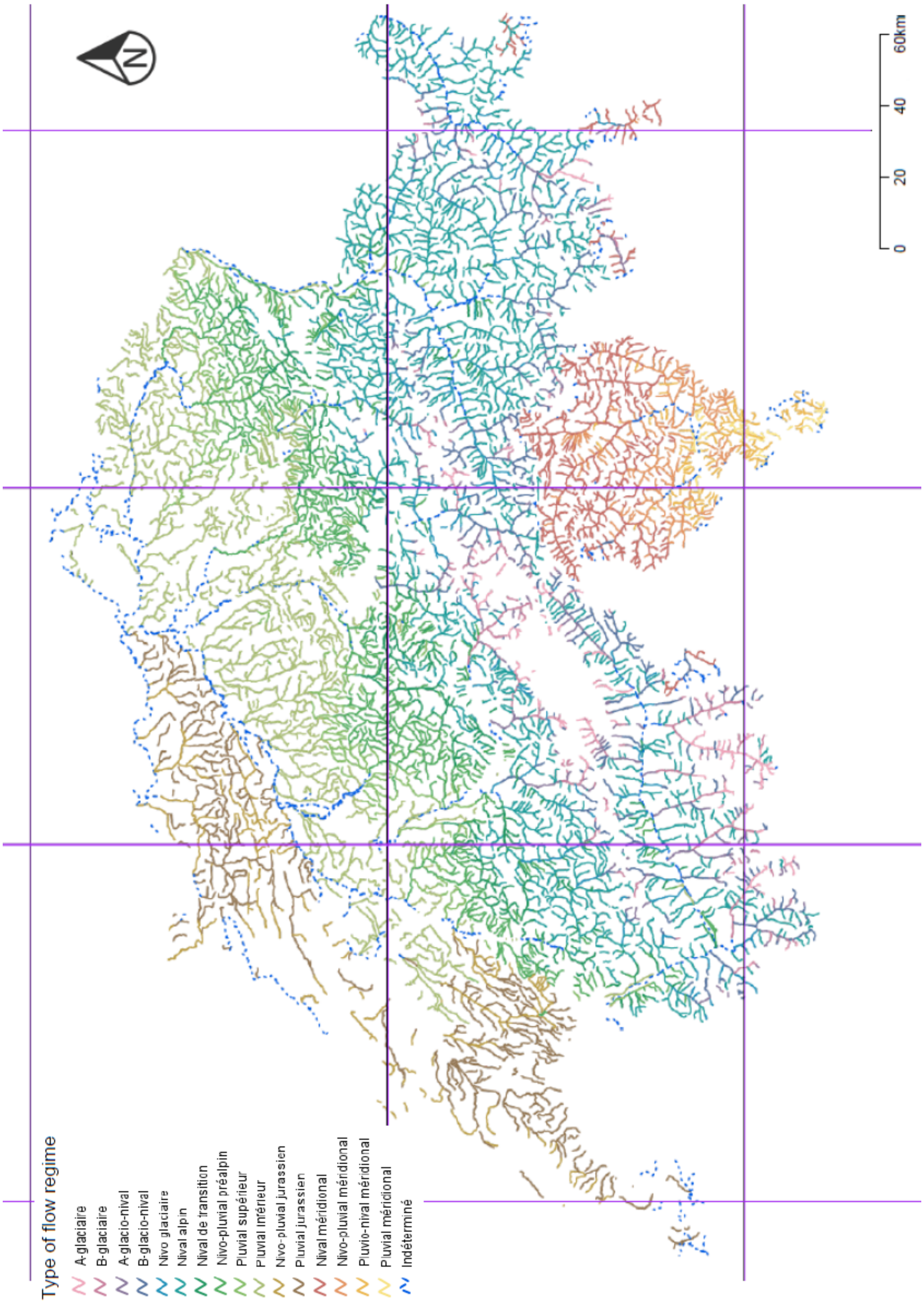


Figure 2.4 – Regions where for the streamflow regimes happen in Switzerland (Haller et al., 2004)

– Availability of long series of streamflow data;
– Representativeness of the different Swiss streamflow regimes.

The Swiss Federal Office for the Environment (FOEN) provided daily streamflow data for each catchment (FOEN, 2017). Meteoswiss provided gridded daily precipitation (MeteoSwiss, 2011) and gridded daily temperature data (MeteoSwiss, 2014). In 2018, Meteoswiss updated the gridded daily precipitation databases, but at the time all the calculations related to Chapters 3 to 4 were finished based on the old databases and they were not updated. The time series obtained with both databasis were compared and the differences do not affect the conclusions.

## 2.6 Research needs

The literature review revealed the following research gaps related to the application of the probabilistic daily streamflow model to Alpine streamflow regimes:

– The model framework has few parameters and because of that, each one of them can affect modelling results significantly. One can make different methodological choices to estimate those parameters, but there is no consensus about the best methods. The values of recession parameters are particularly susceptible to methodological choices that affect the model performance strongly. The calculation of recession parameters using statistical inference methods (MLE) has been proposed, but has not been tested systematically.
– Most of the previous applications of the model framework excluded case studies impacted by snow dynamics. In snow dominated regions, the model is adapted only for periods of snow accumulation. The model should be tested for snow melting conditions and adapted to those conditions.
– The model has not being tested for glacier regimes, this should be done to identify needs of developments and then to implement those developments.

The objectives presented in the Introduction of the thesis try to fill those gaps. Chapter 3 studies the model behaviour for cases with different hydrological regimes seeking to define the gaps better, then, Chapters 4 and 5 are focused on the definition of better recession analysis methods, and finally Chapter 6 applies the model to glacier and/or snow dominated catchments all over the year defining the conditions of application and the adaptations needed for both regimes.

# Scientific developments Part II

# 3 Analytical flow duration curves for summer streamflow in Switzerland

*This chapter proposes a systematic assessment of the performance of an analytical modelling framework for streamflow probability distributions for a set of 25 Swiss catchments. These catchments show a wide range of hydroclimatic regimes, including namely snow-influenced streamflows. The model parameters are calculated from a spatially averaged gridded daily precipitation data set and from observed daily streamflow time series, both in a forward estimation mode (direct parameter calculation from observed data) and in a inverse estimation mode (maximum likelihood estimation). The performance of the linear and the nonlinear model versions is assessed in terms of reproducing observed flow duration curves and their natural variability. Overall, the nonlinear model version outperforms the linear model for all regimes, but the linear model shows a notable performance increase with catchment elevation. More importantly, the obtained results demonstrate that the analytical model performs well for summer streamflow for all analyzed streamflow regimes, ranging from rainfall-driven regimes with summer low flow to snow and glacier regimes with summer high flow. These results suggest that the model's encoding of streamflow-generating events based on stochastic soil moisture dynamics is more flexible than previously thought. As shown in this chapter, the presence of snow- or icemelt is accommodated by a relative increase of the streamflow-generating frequency, a key parameter of the model. Explicit quantification of this frequency increase as a function of mean catchment meteorological conditions is left for future research.* [1]

[1] This chapter is an adapted version of Santos et al. (2018)

## 3.1 Introduction

Knowledge of the availability and variability of daily streamflows in a given stream section proves useful for many engineering applications (e.g. the design of hydro-power plants or water supply systems), as well as for studies about stream ecology alterations and sediment transport or about water quality and allocation (Basso et al., 2015b; Ceola et al., 2010; Searcy, 1959; Vogel and Fennessey, 1995). For many such applications, knowledge of the probability distribution of daily streamflows rather than of their exact temporal occurrence is sufficient.

In hydrology, the probability distribution of daily streamflows is traditionally not represented as a probability density function (pdf) but in terms of flow duration curves (FDCs) that associate an exceedance probability to each streamflow value (Vogel and Fennessey, 1994) and that correspond to the complement of the cumulative distribution function (cdf).

Different methods exist to estimate FDCs (ie. to estimate their shape), the most straightforward method being the assignment of empirical probabilities to observed ranked data (yielding empirical FDCs) (Vogel and Fennessey, 1994). FDCs can also be obtained from statistical methods that relate the FDC shape to catchment characteristics (Castellarin et al., 2013).

An important category of FDC models are process-based models that combine climate controls and catchment characteristics to estimate the shape of FDCs. Such models describe the shape of FDCs either based on long term simulations of the system behavior or based on a direct parameterization of the FDC shape as a function of key hydrological controls. One such model is the model developed by Botter et al. (2007c), who derived an analytical description of streamflow distributions as the result of subsurface flow pulses triggered by stochastic rainfall and censored by the soil moisture dynamics. The resulting streamflow distribution is characterized by only a few parameters: the mean rainfall depth and the frequency of rainfall events that produce streamflow, the area of the catchment and the mean residence time of the catchment.

In the previous applications of the model, the focus was generally on the study of signatures of streamflow regimes under different climates and landscape conditions (Botter et al., 2007a, 2013), where the shape of the pdf was more important than the accuracy of the predicted streamflow probabilities. Furthermore, all previous applications deliberately excluded all catchments or seasons that where snowmelt affected (Botter et al., 2007a, 2013; Ceola et al., 2010; Doulatyari et al., 2015).

The objective of this research is to assess and compare the performance of the model in its linear and nonlinear forms for summer streamflows for a range of Alpine streamflow regimes. The selected set of case studies covers all Swiss catchments that have a natural (unperturbed) streamflow regime and long term streamflow monitoring. Compared to existing studies (eg. Basso et al., 2015b; Ceola et al., 2010; Doulatyari et al., 2017), this chapter provides a systematic analysis of all model parameters and of their seasonality, and a comprehensive analysis of a wide range of streamflow regimes, including namely rainfall-driven and snowfall-influenced regimes. This allows a first detailed view on the suitability of the modelling framework for Alpine summer streamflows (influenced by rain and snow) and an assessment of the model performance as a function of the streamflow regime.

The chapter is organized as follows: Section 3.2 provides a description of the methods adopted in this chapter to estimate the model parameters and to assess the model performance, followed by a presentation of the Swiss case studies (Section 3.3). The obtained results for the linear and nonlinear model versions (Section 3.4) are discussed in Section 3.5 with a particular focus on the model performance under different hydrological regimes. The conclusions are summarized in Section 3.6.

## 3.2 Methods

Hereafter, we present the two different methods adopted for parameter estimation and for model performance assessment. All methods are applied only to the summer season (June $1^{st}$ to August $31^{st}$, see also Section 3.3). The model evaluation framework adopted here is synthesized in Figure 3.1, starting from the empirical cdfs as references for performance evaluation. Next, the precipitation frequency $\lambda_p$ is estimated from precipitation and the streamflow-producing frequency $\lambda$ from observed streamflow (Equation 3.1, Section 3.2.1). The recession parameters are obtained in forward mode (Section 3.2.1) or inverse mode (Section 3.2.2). Based on these parameters, the model cdf is calculated from the linear model (Equation 2.4) or from the nonlinear model (Equation 2.6). The model performance is evaluated based on two classical performance indicators and by comparison to the natural variability of the observed cdfs (Section 3.2.3).

### 3.2.1 Parameter estimation 1: forward estimation

We use the term "forward parameter estimation" to emphasize that the parameters are estimated directly from observed data, without calibration. This method is generally used in the context of this modelling framework for the estimation of the parameters related to the stochastic inputs ($\lambda_p$, $\alpha$, $\lambda$), and this method is always used for these parameters in the present paper. However, the recession parameters ($k$, $k_n$ and $a$) are either estimated in a forward mode (Botter et al., 2007c, 2009; Ceola et al., 2010; Schaefli et al., 2013) or in an inverse mode (Ceola et al., 2010) (see Section 3.2.2).

The computation of the precipitation parameters first involves the computation of a reference catchment-scale precipitation time series (here obtained from gridded data, see Section 3.3). Then interception losses ($I$) are subtracted from the observed daily precipitation depths. These losses are in fact evaporated (or sublimated in case of snow) before participating to soil moisture dynamics. Following Rodriguez-Iturbe et al. (1999), previous model applications generally assumed that these losses are accounted for

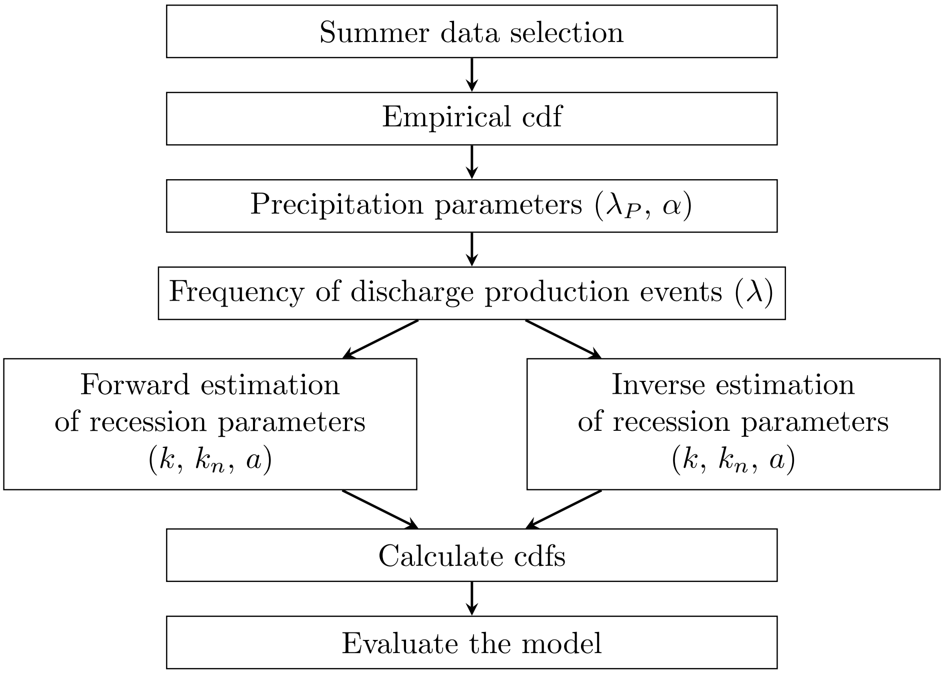


Figure 3.1 – Sketch of the adopted workflow for model parameter estimation and performance assessment.

when the frequency of precipitation events is corrected to the frequency of streamflow-producing events. In view of understanding how the model parameters vary in space, it was decided here to treat interception losses explicitly with minimal assumptions about this process: different maximum interception depths are attributed to four different land covers: 4 mm for forests, 2 mm, for low vegetation, 1 mm for impervious areas, 0 mm for water bodies (Gerrits, 2010). The catchment-scale maximum interception depth is obtained as the land use-weighted average of these values, but a minimum interception depth of 1 mm is imposed. This catchment-scale interception depth is subtracted from daily precipitation depths, assuming that at a daily time step, all intercepted water re-evaporates during the same time step.

Instead of correcting the frequency of precipitation events $\lambda_p$ according to Equation 2.3, the frequency of streamflow-producing events $\lambda$ is estimated directly from the theoretical relationship between the mean streamflow and the precipitation parameters, $\overline{Q} = \lambda\alpha$ (see Equation 2.4). Replacing the mean modelled streamflow $\overline{Q}$ with the mean observed streamflow $\overline{\tilde{Q}}$, it follows that

$$\lambda = \frac{\overline{\tilde{Q}}}{\alpha}. \tag{3.1}$$

Estimating $\lambda$ from the above equation rather than directly from the soil properties as in

Equation 2.3, has been shown by Ceola et al. (2010) to provide much better results, and this method was used by the majority of studies since then (e.g. Ceola et al., 2010; Botter et al., 2013; Basso et al., 2015b).

The recession parameter for the linear model is calculated directly from observed daily streamflow based on a classical Brutsaert-Nieber recession analysis (Brutsaert and Nieber, 1977; Biswal and Marani, 2010; Biswal and Nagesh, 2014; Mutzner et al., 2013), considering, however, only streamflows below a certain threshold, fixed to 95%. The nonlinear recession parameters, $k_n$ and $a$ are also obtained based from a recession analysis, using the same streamflow threshold via linear regression of the logarithm of $(-dQ/dt)$ versus the logarithm of $Q$, where $a$ is the slope and $k_n$ the intercept.

### 3.2.2 Parameter estimation 2: inverse estimation

To objectively compare the potential of the linear and the nonlinear model formulations to capture observed flow-duration curves, the recession parameters for the linear model ($k$) and for the nonlinear model ($k_n, a$) are also estimated in a classical inverse estimation mode where the model parameters are obtained by maximizing the likelihood function formulated for the model (Equation 2.7).

### 3.2.3 Model evaluation criteria

To objectively compare different models, we propose to use the Kolmogorov-Smirnov distance between the cdfs corresponding to different models (Ceola et al., 2010; Schaefli et al., 2013), i.e. the maximum difference between the values of the empirical and the modelled cumulative distributions:

$$c^{\mathrm{KS}} = \sup_x |F(\tilde{Q}) - F(Q)|, \tag{3.2}$$

where $F(\tilde{Q})$ corresponds to the empirical cumulative distribution of the streamflows and $F(Q)$ to the modelled cumulative distribution of the streamflows. A good model should have a low $c^{\mathrm{KS}}$ value.

Since the nonlinear model formulation has an additional parameter, the linear and the nonlinear models are also compared based on the Akaike information criterion (Burnham and Anderson, 2004; Laio et al., 2009; Ceola et al., 2010):

$$c^{\mathrm{AIC}} = 2n_m - \ln(\hat{\mathscr{L}}), \tag{3.3}$$

where $n_m$ is the number of parameters of the model and $\ln(\hat{\mathscr{L}})$ is the logarithm of the maximum likelihood function obtained by maximizing Equation 2.7. As for $c^{\mathrm{KS}}$, a good model should have a low $c^{\mathrm{AIC}}$ value.

Based on the above criterion, we measure the relative performance increase from the linear to the nonlinear model as follows:

$$r^{\mathrm{AIC}} = -\left(\frac{c_n^{\mathrm{AIC}} - c_l^{\mathrm{AIC}}}{c_l^{\mathrm{AIC}}}\right), \tag{3.4}$$

where ${c_n}^{\mathrm{AIC}}$ is the Akaike criterion for the nonlinear model and $c_l^{\mathrm{AIC}}$ for the linear model. Taking the opposite of the relative difference between the Akaike criteria ensures that a higher $r^{\mathrm{AIC}}$ value indicates a stronger performance increase (recall that the Akaike criterion is to be minimized).

In addition to assess the performance difference between different models, the obtained models are compared to the natural variability of the observed streamflow cdfs. Therefore, an empirical long term cdf is constructed, obtained by ranking the observed data in ascending order and dividing the rank numbers by the total sample size. Furthermore, to assess the natural yearly variability, individual cdfs are constructed for each summer season of each civil year (Vogel and Fennessey, 1994). From this collection of annual cdfs, envelopes are obtained based on the maximum and minimum values of streamflow for each probability class of the annual cdfs. A reliable model should yield a cdf contained between these curves and should be as close as possible to the long term cdf.

## 3.3 Case studies

In this paper, we analyze 25 Swiss catchments with areas ranging from 1.05 km$^2$ to 377 km$^2$ and with mean elevations ranging from 615 m asl. (meters above sea level) to 2945 m asl. (Table 3.1, Figure 3.2). These catchments correspond to all streamflow gauging stations run by the Swiss Federal Office for the Environment (FOEN) (FOEN, 2017) that have unperturbed streamflows (i.e. minimal anthropogenic influence).

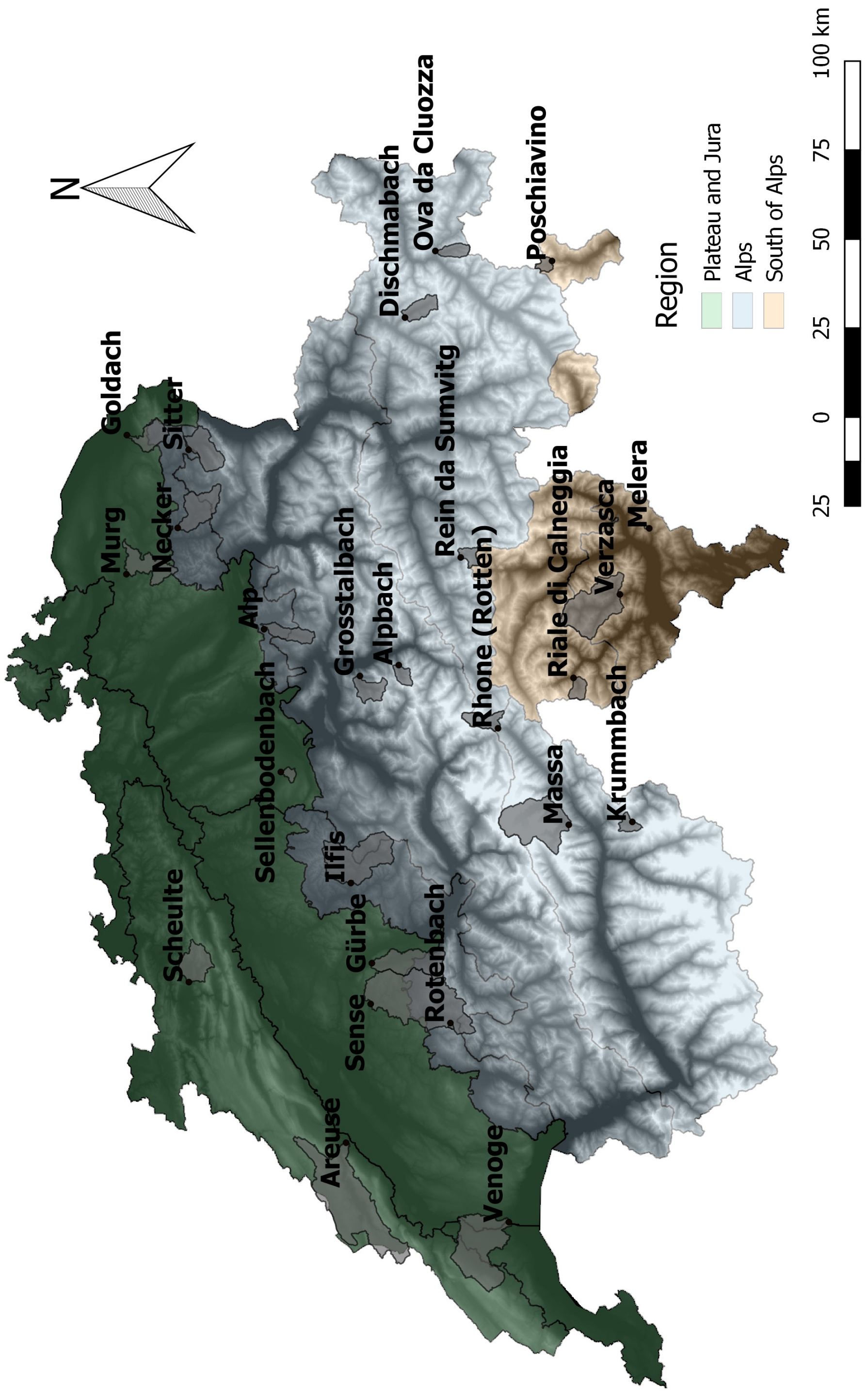


Figure 3.2 – Location of the case study catchments in Switzerland. The six biogeographical regions of Switzerland (FOEN, 2004) are summarized here into three main regions. Data source: Digital elevation model (SwissTopo, 2005a), catchments: (Helbling, 2016).

Table 3.1 – Characteristics of Swiss case study catchments as given in the FOEN database, including: the FOEN identification code (ID), the catchment name, the Swiss coordinates of the gauging station, the drainage area, the mean elevation of the catchment and the gauging station elevation, the percentage of glacier-cover of the catchment, the mean annual precipitation, the mean annual temperature, the period of data acquisition.

| | ID | Name | Coordinates (CH1903) | Area ($km^2$) | Mean elevation (m asl.) | Station elevation (m asl.) | Glaciation (%) | P (mm) | $\overline{T}$ ($^oC$) | Data period |
|---|---|---|---|---|---|---|---|---|---|---|
| 1 | 2430 | Rein da Sumvitg - Sumvitg, Encardens | 718810 / 167690 | 21.8 | 2450 | 1490 | 6.7 | 1707 | -1,19 | 15-09-1977 to 31-12-2014 |
| 2 | 2327 | Dischmabach - Davos, Kriegsmatte | 786220 / 183370 | 43.3 | 2372 | 1668 | 2.1 | 1021 | -0,62 | 24-07-1961 to 31-12-2014 |
| 3 | 2308 | Goldach - Goldach, Bleiche | 753190 / 261590 | 49.8 | 833 | 399 | 0 | 1446 | 7,39 | 01-01-1974 to 31-12-2014 |
| 4 | 2374 | Necker - Mogelsberg, Aachsäge | 727110 / 247290 | 88.2 | 959 | 606 | 0 | 1777 | 6,47 | 01-01-1972 to 31-12-2014 |
| 5 | 2112 | Sitter - Appenzell | 749040 / 244220 | 74.2 | 1252 | 769 | 0.08 | 1904 | 5,10 | 01-01-1961 to 31-12-2014 |
| 6 | 2126 | Murg - Wängi | 714105 / 261720 | 78.9 | 650 | 466 | 0 | 1357 | 7,90 | 01-01-1961 to 31-12-2014 |
| 7 | 2610 | Scheulte - Vicques | 599485 / 244150 | 72.8 | 785 | 463 | 0 | 1325 | 7,27 | 01-01-1992 to 31-12-2014 |
| 8 | 2159 | Gürbe - Belp, Mülimatt | 604810 / 192680 | 117 | 837 | 522 | 0 | 1295 | 7,21 | 01-01-1961 to 31-12-2014 |
| 9 | 2251 | Rotenbach - Plaffeien, Schwyberg | 587980 / 170590 | 1.65 | 1454 | 1275 | 0 | 1910 | 5,81 | 01-09-1961 to 31-12-2014 |
| 10 | 2179 | Sense - Thörishaus, Sensematt | 593350 / 193020 | 352 | 1068 | 553 | 0 | 1479 | 6,29 | 01-01-1961 to 31-12-2014 |
| 11 | 2480 | Areuse - Boudry | 554350 / 199940 | 377 | 1060 | 444 | 0 | 1531 | 5,41 | 01-01-1961 to 31-12-2014 |
| 12 | 2603 | Ilfis - Langnau | 627320 / 198600 | 188 | 1051 | 685 | 0 | 1719 | 6,22 | 01-04-1989 to 31-12-2014 |
| 13 | 2608 | Sellenbodenbach - Neuenkirch | 658530 / 218290 | 10.5 | 615 | 515 | 0 | 1230 | 8,72 | 12-09-1980 to 31-12-2014 |
| 14 | 2299 | Alpbach - Erstfeld, Bodenberg | 688560 / 185120 | 20.6 | 2200 | 1022 | 27.7 | 1645 | 0,68 | 01-01-1961 to 31-12-2014 |
| 15 | 2276 | Grosstalbach - Isenthal | 685500 / 196050 | 43.9 | 1820 | 767 | 9.3 | 1801 | 2,22 | 01-01-1961 to 31-12-2014 |
| 16 | 2609 | Alp - Einsiedeln | 698640 / 223020 | 46.4 | 1155 | 840 | 0 | 2005 | 5,43 | 27-02-1991 to 31-12-2014 |
| 17 | 2268 | Rhône - Gletsch | 670810 / 157200 | 38.9 | 2719 | 1761 | 52.2 | 2066 | -2,98 | 01-01-1961 to 31-12-2014 |
| 18 | 2161 | Massa - Blatten bei Naters | 643700 / 137290 | 195 | 2945 | 1446 | 65.9 | 2423 | -3,18 | 01-01-1961 to 31-12-2014 |
| 19 | 2432 | Venoge - Ecublens, Les Bois | 532040 / 154160 | 231 | 700 | 383 | 0 | 1181 | 9,29 | 01-01-1979 to 31-12-2014 |
| 20 | 2206 | Melera - Melera (Valle Morobbia) | 726988 / 114670 | 1.05 | 1419 | 944 | 0 | 1716 | 4,74 | 01-01-2005 to 31-12-2014 |
| 21 | 2605 | Verzasca - Lavertezzo, Campiòi | 708420 / 122920 | 186 | 1672 | 490 | 0 | 2051 | 4,37 | 01-09-1989 to 31-12-2014 |
| 22 | 2356 | Riale di Calneggia - Cavergno, Pontit | 684970 / 135960 | 24 | 1996 | 890 | 0 | 1918 | 2,54 | 01-01-1967 to 31-12-2014 |
| 23 | 2244 | Krummbach - Klusmatten | 644500 / 119420 | 19.8 | 2276 | 1795 | 3 | 1475 | 1,92 | 01-01-1995 to 31-12-2014 |
| 24 | 2366 | Poschiavino - La Rösa | 802120 / 142010 | 14.1 | 2283 | 1860 | 0.35 | 1512 | 0,02 | 01-01-1970 to 31-12-2014 |
| 25 | 2319 | Ova da Cluozza - Zernez | 804930 / 174830 | 26.9 | 2368 | 1509 | 2.2 | 963 | -1,36 | 24-07-1961 to 31-12-2014 |

The average precipitation at the country scale is around 1300 mm yr$^{-1}$ (Blanc and Schädler, 2013). The complex topography leads to a high diversity of hydrologic regimes (Weingartner and Aschwanden, 1992), which can be grouped into i) pluvial or rainfall-driven regimes, ii) snow-dominated regimes and iii) glacier regimes (Table 3.2). Pluvial regimes are rainfall-dominated with sporadic snowfall events during winter; these regimes occur on the Swiss Plateau and in the Jura region (Figure 3.2). Snow-dominated regimes result from a seasonal snow cover, roughly at elevations above 900 m asl. In these catchments, solid precipitation accumulates during several weeks up to several months during the cold season (winter) and is entirely released in the following spring and early summer. Glacier regimes result from perennial snow and ice accumulation at elevations roughly beyond 3000 m asl. Most snow-dominated and glacier regimes are located in the Alps region (Figure 3.2), few of them are located in the South of Alps region, which overall has a warmer climate and presents higher precipitation than the other two regions.

Table 3.2 – Regrouping of the 16 regime classes of Weingartner and Aschwanden (1992) into three classes (details are available in the Appendix A).

| | ID | Name | Regime 16 | Regime 3 |
|---|---|---|---|---|
| 1 | 2430 | Rein da Sumvitg - Sumvitg, Encardens | b-glacio nival | glacier |
| 2 | 2327 | Dischmabach - Davos, Kriegsmatte | b-glacio nival | glacier |
| 3 | 2308 | Goldach - Goldach, Bleiche | pluvial supérieur | pluvial |
| 4 | 2374 | Necker - Mogelsberg, Aachsäge | nivo-pluvial préalpin | snow-dominated |
| 5 | 2112 | Sitter - Appenzell | nival de transition | snow-dominated |
| 6 | 2126 | Murg - Wängi | pluvial inférieur | pluvial |
| 7 | 2610 | Scheulte - Vicques | nivo-pluvial jurassien | snow-dominated |
| 8 | 2159 | Gürbe - Belp, Mülimatt | pluvial supérieur | pluvial |
| 9 | 2251 | Rotenbach - Plaffeien, Schwyberg 4 | nivo-pluvial préalpin | snow-dominated |
| 10 | 2179 | Sense - Thörishaus, Sensematt | nivo-pluvial préalpin | snow-dominated |
| 11 | 2480 | Areuse - Boudry | pluvial jurassien | pluvial |
| 12 | 2603 | Ilfis - Langnau | nivo-pluvial préalpin | snow-dominated |
| 13 | 2608 | Sellenbodenbach - Neuenkirch | pluvial inférieur | pluvial |
| 14 | 2299 | Alpbach - Erstfeld, Bodenberg | b-glaciaire | glacier |
| 15 | 2276 | Grosstalbach - Isenthal | nival alpin | snow-dominated |
| 16 | 2609 | Alp - Einsiedeln | nivo-pluvial préalpin | snow-dominated |
| 17 | 2268 | Rhône - Gletsch | a-glaciaire | glacier |
| 18 | 2161 | Massa - Blatten bei Naters | a-glaciaire | glacier |
| 19 | 2432 | Venoge - Ecublens, Les Bois | pluvial jurassien | pluvial |
| 20 | 2206 | Melera - Melera (Valle Morobbia) | nivo-pluvial méridional | snow-dominated |
| 21 | 2605 | Verzasca - Lavertezzo, Campiòi | nivo-pluvial méridional | snow-dominated |
| 22 | 2356 | Riale di Calneggia - Cavergno, Pontit | nival méridional | snow-dominated |
| 23 | 2244 | Krummbach - Klusmatten | nival méridional | snow-dominated |
| 24 | 2366 | Poschiavino - La Rösa | nival méridional | snow-dominated |
| 25 | 2319 | Ova da Cluozza - Zernez | nivo glaciaire | snow-dominated |

Most Swiss streamflow regimes show a strong seasonality (Weingartner and Aschwanden, 1992), illustrated in Figure 3.3 for typical examples of the three regime main types; air temperature is shown here as a proxy for snow and evapotranspiration processes. The pluvial Goldach river (GOL) shows the typical summer low flow resulting from evapotranspiration; the Dischmabach shows a snow regime with high summer flows resulting from the release of snowmelt stored in the subsurface during the main snowmelt period (spring) and from residual snowmelt during summer. The Rhône river (RHG) with its

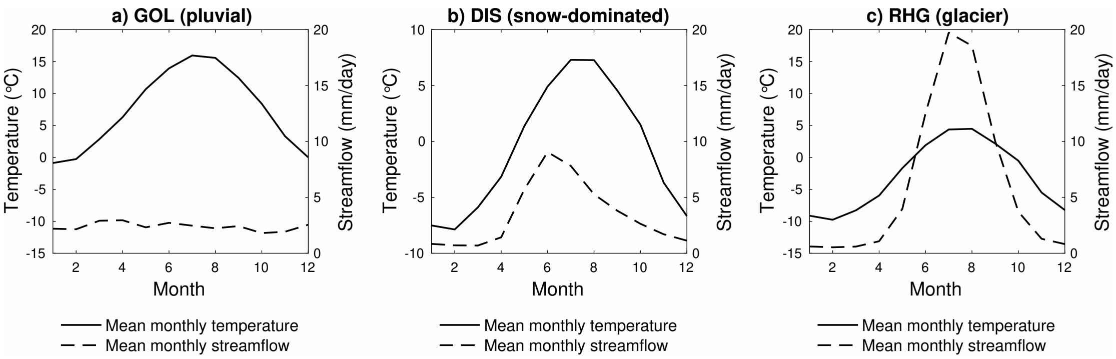


Figure 3.3 – Annual cycle of streamflow and air temperature for three selected catchments representing three different hydrologic regimes (pluvial, snow-dominated and glacier regime). Shown are the mean monthly values computed over the entire observation period for each catchment (see Table 3.1).

50% glacier cover shows a glacier regime, with significant ice melt during summer, and with monthly streamflow peaking for the same month as air temperature (July).

It is noteworthy that surface runoff processes can play a certain role for extreme events in all regions of Switzerland (Bernet et al., 2017), but all hydrologic regimes are dominated by subsurface runoff processes, a pre-condition for the application of the modelling framework developed by Botter et al. (2007c).

Besides observed daily streamflow, the model requires catchment-scale daily precipitation as input. Most of the previous applications of the models used precipitation from one or several meteorological stations as input (Botter et al., 2007c,a, 2013; Ceola et al., 2010; Basso et al., 2015b; Schaefli et al., 2013), which is potentially limiting for the model performance since good area-averaged input estimates are critical. Recent progress in spaceborne precipitation observation, and in particular the Global Precipitation Measurement (GPM) mission, potentially offers an interesting new data source for area-averaged precipitation estimates, even in such complex terrain as the Swiss Alps (Gabella et al., 2017), with the drawback of covering only short historical periods. Here, we use the relatively new spatial precipitation data set of MeteoSwiss with a nominal resolution of 2.2 km and an effective resolution between 15 km and 20 km and extending back to 1961 (MeteoSwiss, 2011). This data set can be assumed to give relatively good estimates of area-averaged precipitation (Paschalis et al., 2014; Addor and Fischer, 2015), even in mountainous areas where there are only few meteorological stations.

Corresponding catchment-scale average precipitation time series per case study catchment are obtained by averaging the daily precipitation time series of all pixels contained in the catchment (a list of pixels per catchment is included in the Appendix A ). In addition, we also used the corresponding gridded temperature data set (MeteoSwiss, 2014) to support the analysis of parameter seasonality. As for precipitation, the catchment-scale average temperature data set is obtained by averaging the daily time series of all pixels.

Before estimating rainfall frequency ($\lambda_p$) and average rainfall depth on raindays ($\alpha$), the catchment-scale precipitation time series are pre-processed to remove losses from interception. This step requires information about land use. Of the retained 25 case study catchments, 22 are part of what is called "hydrological study areas" and have an associated extended data set, including land use (Aschwanden, 1996). For the other catchments (i.e. the Areuse, Rhône-Gletsch and Venoge), land use is obtained from the Swiss land use database (FOS, 2015). Details about the land use estimation are available in the Appendix A).

## 3.4 Results

### 3.4.1 Discharge regimes and parameter seasonality

To gain further insights into the hydrological processes underlying the different regimes, Figure 3.4 shows the within-year variability of the model parameters obtained by estimating the parameters in forward mode for moving and overlapping 90-day windows. The precipitation parameters $\alpha$ and $\lambda_p$ do not show strong seasonal patterns, except for a few catchments such as the Goldach river (Figure 3.4a). For snow and glacier regimes, the frequency of streamflow-producing events, $\lambda$, increases strongly at the beginning of spring (Figure 3.4b and c), which indicates the release of water from snow- or icemelt.

The inverse of the linear recession coefficient $\tau = k^{-1}$ shows a coherent annual cycle for all catchments, independent of the underlying streamflow regime (Figure 3.5). This seasonal pattern with consistently low $\tau$ values during summer for all catchments clearly justifies the choice of a common summer season (June, July, August) for all regimes. The amplitude of the annual cycle (the difference between high and low $\tau$ values) is stronger for snow or glacier regimes, which reflects the fact that in these regimes, parts of the catchment are effectively dormant during the winter (Schaefli et al., 2013).

### 3.4.2 Linear model

All estimated parameters for both forward and inverse estimations are summarized in Tables 3.3 and 3.4, together with the values of the performance indicator $c^{\text{KS}}$. It can be noted that for 11 catchments (i.e. Rein da Sumvitg, Dischmabach, Alpbach, Grosstalbach, Rhône à Gletsch, Massa, Verzasca, Riale di Calneggia, Krumbach, Poschiavino and Ova da Cluozza), $\lambda$ exceeds $\lambda_p$, contradicting the original description of the model (Botter et al., 2007b), which states that the streamflow-producing frequency $\lambda$ is smaller than the precipitation frequency $\lambda_p$. Such an exceedance of $\lambda$ over $\lambda_p$ should only happen in catchments or seasons with an additional source of water (in addition to rainfall), which in the present case is snow- or icemelt.

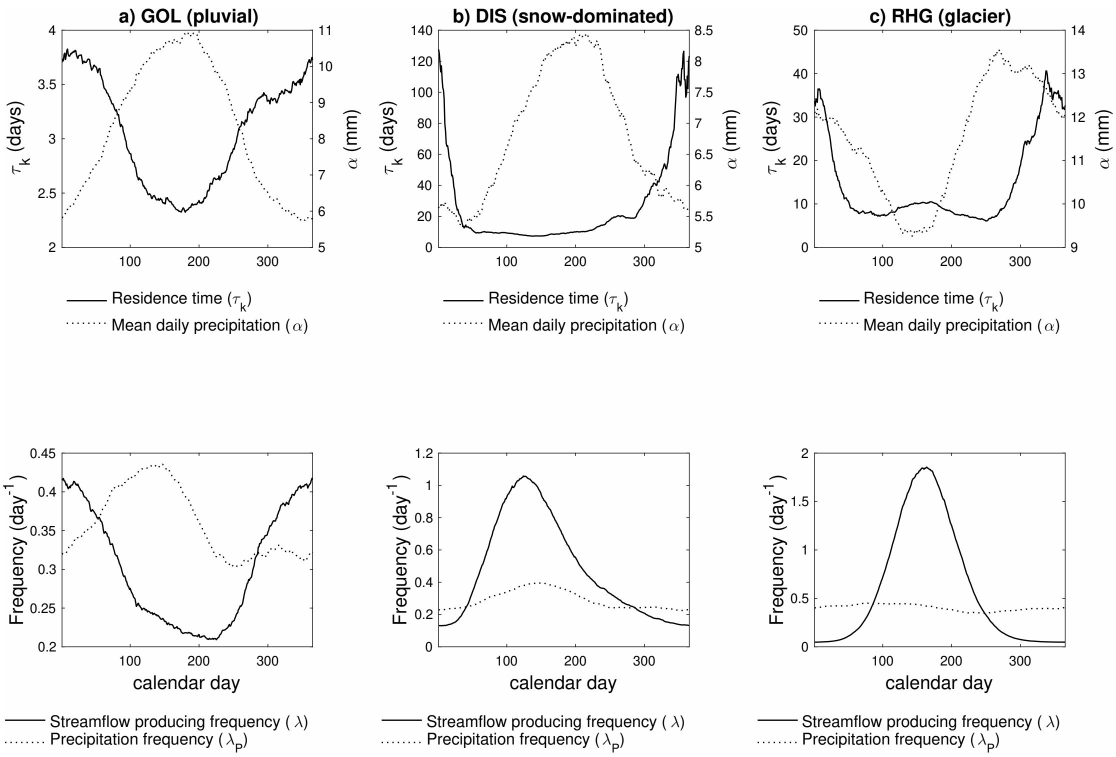


Figure 3.4 – Examples of the temporal variation of the model parameters over the course of a year. The parameters are calculated for 90 days intervals beginning at the calendar day for which the value is plotted; for a given time window, the data points corresponding to this window in all available civil years are pooled together. Top row: residence time $\tau_k$ and mean daily precipitation depth $\alpha$; bottom row: precipitation frequency $\lambda_p$ and streamflow-producing frequency $\lambda$.

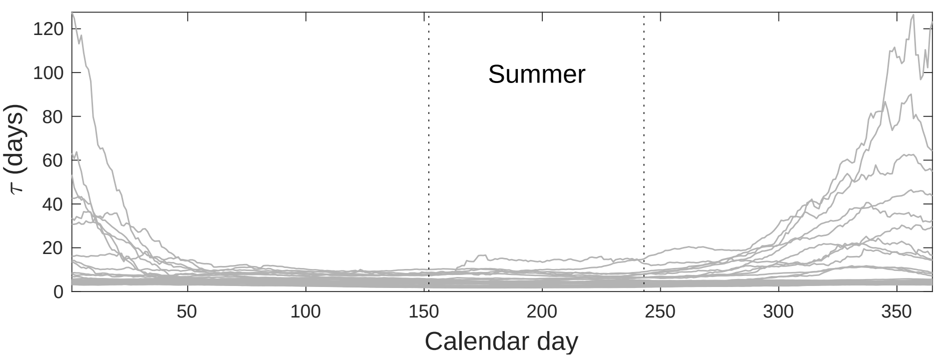


Figure 3.5 – Temporal variation of the residence time ($\tau_k = k^{-1}$) for the 25 catchments. The temporal variation is obtained as in Figure 3.4.

Table 3.3 – Parameter values for all the catchments for summer common to the linear and nonlinear models. $\overline{Q}$ stands for the mean observed streamflow, $P_s$ the mean total precipitation during summer, $\overline{T_s}$ the mean temperature during summer, $I$ for interception depth.

| Name | $\overline{Q}$ (mm/d) | $P_s$ (mm) | $\overline{T_s}$ ($^oC$) | $\alpha$ (mm/d) | $\lambda_p$ (1/d) | $I$ (mm/d) | $\lambda$ (1/d) |
|---|---|---|---|---|---|---|---|
| Rein da Sumvitg - Sumvitg, Encardens | 13,8 | 532 | 5,62 | 12,4 | 0,410 | 1,83 | 1,115 |
| Dischmabach - Davos, Kriegsmatte | 7,4 | 378 | 6,49 | 8,2 | 0,377 | 2,29 | 0,906 |
| Goldach - Goldach, Bleiche | 2,5 | 513 | 15,15 | 11,0 | 0,376 | 3,13 | 0,224 |
| Necker - Mogelsberg, Aachsäge | 3,3 | 600 | 14,22 | 12,2 | 0,393 | 3,30 | 0,273 |
| Sitter - Appenzell | 5,4 | 648 | 12,30 | 12,5 | 0,433 | 3,06 | 0,427 |
| Murg - Wängi | 1,7 | 432 | 16,07 | 9,6 | 0,348 | 3,13 | 0,174 |
| Scheulte - Vicques | 1,5 | 388 | 15,10 | 9,1 | 0,312 | 3,46 | 0,162 |
| Gürbe - Belp, Mülimatt | 2,1 | 450 | 15,15 | 9,9 | 0,355 | 3,06 | 0,210 |
| Rotenbach - Plaffeien, Schwyberg | 4,3 | 616 | 13,29 | 14,0 | 0,378 | 3,16 | 0,309 |
| Sense - Thörishaus, Sensematt | 2,2 | 483 | 13,98 | 10,7 | 0,356 | 3,22 | 0,208 |
| Areuse - Boudry | 1,7 | 383 | 13,10 | 8,8 | 0,316 | 3,37 | 0,191 |
| Ilfis - Langnau | 2,7 | 567 | 13,79 | 12,4 | 0,373 | 3,40 | 0,220 |
| Sellenbodenbach - Neuenkirch | 2,0 | 431 | 16,86 | 9,7 | 0,357 | 2,99 | 0,207 |
| Alpbach - Erstfeld, Bodenberg | 16,5 | 457 | 7,29 | 8,9 | 0,477 | 1,28 | 1,858 |
| Grosstalbach - Isenthal | 6,0 | 598 | 8,97 | 11,8 | 0,444 | 2,35 | 0,504 |
| Alp - Einsiedeln | 4,7 | 687 | 13,03 | 14,1 | 0,415 | 3,40 | 0,335 |
| Rhône - Gletsch | 17,1 | 473 | 3,58 | 9,0 | 0,505 | 1,00 | 1,905 |
| Massa - Blatten bei Naters | 17,1 | 739 | 3,48 | 13,9 | 0,533 | 1,00 | 1,228 |
| Venoge - Ecublens, Les Bois | 0,7 | 298 | 17,39 | 7,9 | 0,268 | 3,14 | 0,090 |
| Melera - Melera (Valle Morobbia) | 3,1 | 562 | 12,64 | 18,1 | 0,273 | 3,87 | 0,174 |
| Verzasca - Lavertezzo, Campiòi | 6,0 | 581 | 12,03 | 17,9 | 0,313 | 3,00 | 0,333 |
| Riale di Calneggia - Cavergno, Pontit | 8,9 | 482 | 9,96 | 13,5 | 0,332 | 2,04 | 0,655 |
| Krummbach - Klusmatten | 6,0 | 317 | 9,30 | 9,2 | 0,294 | 2,35 | 0,656 |
| Poschiavino - La Rösa | 5,4 | 424 | 7,83 | 11,1 | 0,323 | 2,49 | 0,490 |
| Ova da Cluozza - Zernez | 5,2 | 329 | 6,58 | 8,4 | 0,342 | 1,77 | 0,619 |

Table 3.4 – Parameter values and performance indicators for all the catchments for summer with linear model and forward estimation, summer linear model and inverse estimation, summer nonlinear model and forward estimation, winter nonlinear model and inverse estimation, winter linear model and forward estimation. $c^{KS}$ stands for the Kolmogorov-Smirnov distance. The indices stand for: $f$ forward estimation, $i$ inverse estimation, $l$ linear model, $n$ nonlinear model.

| Name (1/d) | $k_f$ | $c_{lf}^{KS}$ (1/d) | $k_i$ | $c_{li}^{KS}$ | $c_{li}^{AIC}$ | $k_{nf}$ | $a_f$ | $c_{nf}^{KS}$ | $k_{ni}$ | $a_i$ | $c_{ni}^{KS}$ | $c_{ni}^{AIC}$ |
|---|---|---|---|---|---|---|---|---|---|---|---|---|
| Rein da Sumvitg - Sumvitg, Encardens | 0,201 | 0,179 | 0,383 | 0,075 | 21550 | 0,029 | 1,46 | 0,296 | 0,110 | 1,52 | 0,057 | 21387 |
| Dischmabach - Davos, Kriegsmatte | 0,136 | 0,065 | 0,163 | 0,048 | 22300 | 0,013 | 1,73 | 0,201 | 0,031 | 1,86 | 0,022 | 21972 |
| Goldach - Goldach, Bleiche | 0,370 | 0,187 | 0,236 | 0,130 | 13494 | 0,145 | 1,50 | 0,126 | 0,174 | 1,81 | 0,023 | 11990 |
| Necker - Mogelsberg, Aachsäge | 0,435 | 0,183 | 0,275 | 0,125 | 16467 | 0,125 | 1,63 | 0,107 | 0,156 | 1,81 | 0,023 | 15015 |
| Sitter - Appenzell | 0,393 | 0,109 | 0,308 | 0,108 | 25067 | 0,066 | 1,69 | 0,179 | 0,115 | 1,76 | 0,029 | 23888 |
| Murg - Wängi | 0,282 | 0,293 | 0,105 | 0,120 | 13636 | 0,099 | 1,70 | 0,062 | 0,081 | 1,98 | 0,019 | 11978 |
| Scheulte - Vicques | 0,264 | 0,274 | 0,133 | 0,158 | 5262 | 0,099 | 1,72 | 0,106 | 0,117 | 2,20 | 0,027 | 3978 |
| Gürbe - Belp, Mülimatt | 0,271 | 0,266 | 0,096 | 0,095 | 15070 | 0,068 | 1,76 | 0,036 | 0,063 | 1,76 | 0,023 | 14108 |
| Rotenbach - Plaffeien, Schwyberg | 0,550 | 0,202 | 0,339 | 0,161 | 22856 | 0,080 | 1,81 | 0,218 | 0,154 | 1,87 | 0,043 | 20753 |
| Sense - Thörishaus, Sensematt | 0,344 | 0,275 | 0,127 | 0,105 | 16401 | 0,084 | 1,85 | 0,010 | 0,082 | 1,86 | 0,009 | 15069 |
| Areuse - Boudry | 0,261 | 0,214 | 0,132 | 0,120 | 14013 | 0,078 | 1,85 | 0,106 | 0,116 | 1,77 | 0,032 | 12785 |
| Ilfis - Langnau | 0,362 | 0,287 | 0,149 | 0,123 | 8210 | 0,068 | 1,96 | 0,042 | 0,069 | 2,04 | 0,025 | 7303 |
| Sellenbodenbach - Neuenkirch | 0,381 | 0,165 | 0,285 | 0,161 | 6617 | 0,184 | 1,38 | 0,181 | 0,271 | 1,49 | 0,077 | 5776 |
| Alpbach - Erstfeld, Bodenberg | 0,171 | 0,081 | 0,276 | 0,014 | 30444 | 0,057 | 1,17 | 0,168 | 0,156 | 1,21 | 0,020 | 30420 |
| Grosstalbach - Isenthal | 0,195 | 0,128 | 0,106 | 0,053 | 22256 | 0,017 | 1,88 | 0,070 | 0,025 | 1,86 | 0,016 | 21768 |
| Alp - Einsiedeln | 0,521 | 0,204 | 0,318 | 0,144 | 9763 | 0,089 | 1,76 | 0,160 | 0,110 | 1,97 | 0,036 | 8870 |
| Rhône - Gletsch | 0,092 | 0,197 | 0,419 | 0,064 | 32412 | 0,107 | 0,87 | 0,216 | 0,897 | 0,70 | 0,043 | 32234 |
| Massa - Blatten bei Naters | 0,130 | 0,112 | 0,272 | 0,049 | 32418 | 0,052 | 1,13 | 0,181 | 0,585 | 0,70 | 0,034 | 32274 |
| Venoge - Ecublens, Les Bois | 0,194 | 0,355 | 0,056 | 0,124 | 3737 | 0,119 | 1,65 | 0,103 | 0,104 | 2,00 | 0,030 | 2706 |
| Melera - Melera (Valle Morobbia) | 0,142 | 0,176 | 0,079 | 0,096 | 2918 | 0,054 | 0,92 | 0,161 | 0,031 | 1,94 | 0,057 | 2702 |
| Verzasca - Lavertezzo, Campiòi | 0,287 | 0,127 | 0,294 | 0,125 | 11649 | 0,041 | 1,70 | 0,261 | 0,081 | 1,94 | 0,030 | 10738 |
| Riale di Calneggia - Cavergno, Pontit | 0,173 | 0,192 | 0,352 | 0,071 | 25838 | 0,014 | 1,79 | 0,336 | 0,077 | 1,79 | 0,039 | 24958 |
| Krummbach - Klusmatten | 0,117 | 0,253 | 0,297 | 0,102 | 8673 | 0,032 | 1,37 | 0,354 | 0,064 | 1,99 | 0,060 | 8345 |
| Poschiavino - La Rösa | 0,125 | 0,162 | 0,199 | 0,087 | 19679 | 0,014 | 1,75 | 0,318 | 0,042 | 2,05 | 0,035 | 18837 |
| Ova da Cluozza - Zernez | 0,215 | 0,047 | 0,192 | 0,058 | 21954 | 0,030 | 1,70 | 0,180 | 0,083 | 1,58 | 0,034 | 21673 |

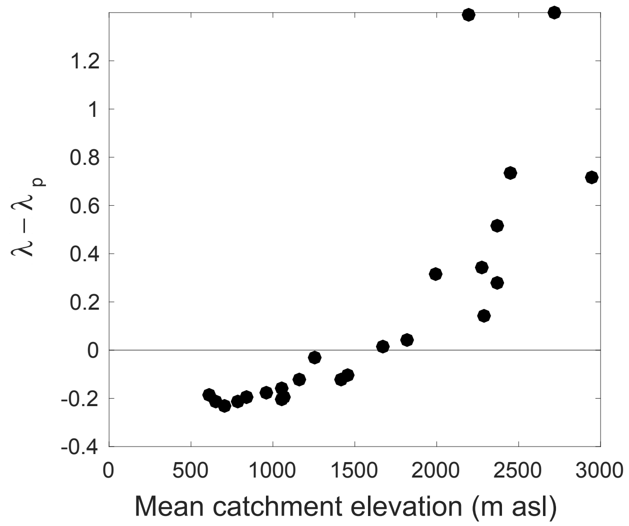


Figure 3.6 – Difference between $\lambda$ and $\lambda_p$ as a function of mean catchment elevation.

The exceedance of $\lambda$ over $\lambda_p$ increases with mean catchment elevation (Figure 3.6), the limit of $\lambda = \lambda_p$ being at around 1500 m asl. This important result is further discussed in Section 3.5.

The cdfs obtained from all estimated parameters are presented in Figure 3.7 for the three example case studies. For the catchment with rainfall-driven streamflows (GOL), it can be seen that the probabilities of occurrence of low flows are largely overestimated with forward estimation (Figure 3.7a). This is a typical indication that the recession time scale is underestimated. The model values even exceed the envelopes that represent the natural variability of the streamflows. In the presence of snow, the linear model in forward estimation mode tends to underestimate low flows, with satisfactory results for some cases, such as the Dischmabach (Figure 3.7b).

Overall, there is a strong increasing trend of the linear model performance with mean catchment elevation (Figure 3.9a). Despite of this, the results of the linear model are not satisfactory for the forward estimation method for any of the regimes.

The inverse estimation of the model parameters improves the results significantly, but the $c^{\mathrm{KS}}$ performance indicator shows relatively high values and the curves are visually not accurate, especially for pluvial regimes. This suggests that the model with a linear streamflow decay is overall not suitable for the studied catchments.

### 3.4.3 Nonlinear models

The results obtained from inverse parameter estimation for the nonlinear model are very good (Figure 3.8, Tables 3.3 and 3.4), and the nonlinear model outperforms the linear model for all catchments, both in terms of the KS performance and in terms of the Akaike criterion (Table 3.4). The relative model performance increase (as measured

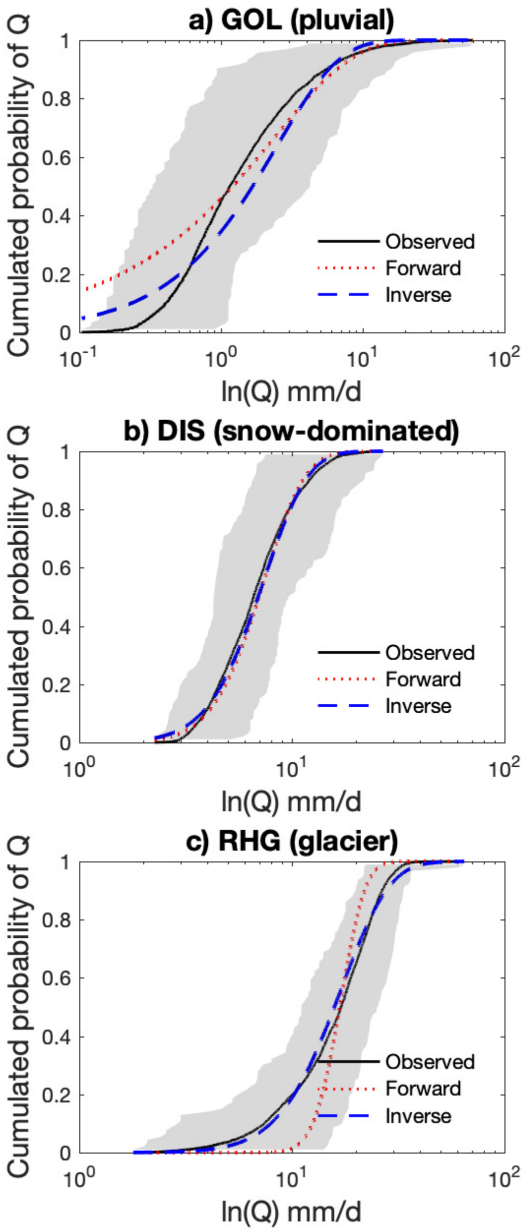


Figure 3.7 – Modelled linear cdfs with forward and inverse parameter estimation for the three selected catchments. The shaded area is located between the cdf envelopes and represents the natural variability of the daily streamflows.

by $r^{AIC}$) shows furthermore a strong inverse trend with mean catchment elevation (Figure 3.10), which results from the increasing performance of the linear model with increasing elevation (Figure 3.9b).

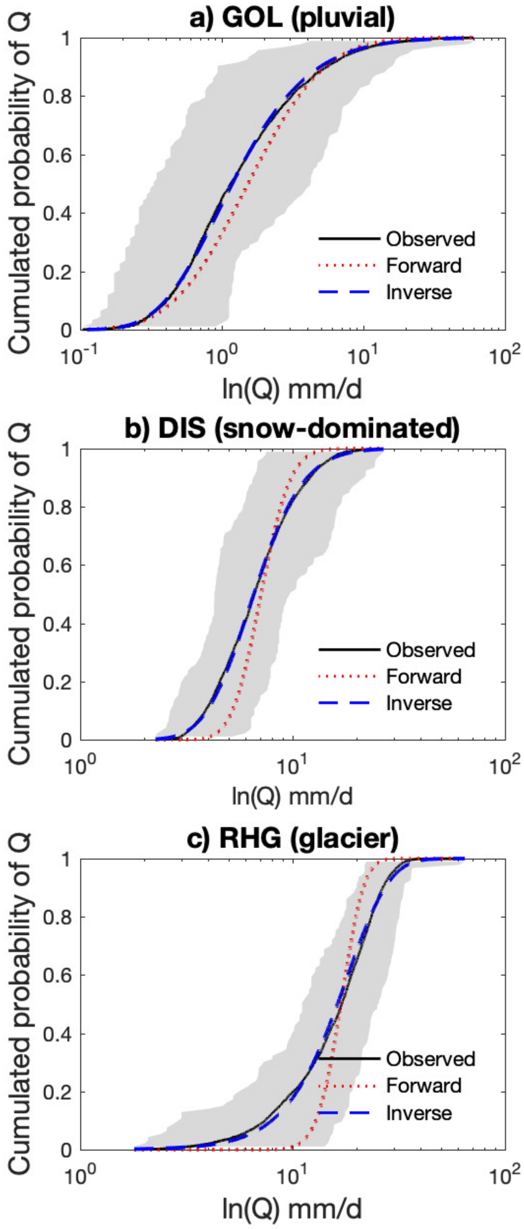


Figure 3.8 – As Figure 3.7 but for the nonlinear model.

It is noteworthy that the two catchments for which the performance increase of the nonlinear model over the linear models exceeds 20% are the two catchments that have a strongly karst-influenced regime (Scheulte at Vicques and Venoge at Ecublens).

As for the linear model, the forward estimation mode gives less good results than the inverse estimation mode. For some catchments (i.e. Murg-Wängi, Gürbe, Sense, Ilfis, and Grosstalbach), the forward estimation mode gives nevertheless very good results with $c^{\mathrm{KS}}$ below 0.1. In general, for the catchments where the discrepancies between modelled and observed cdfs are due to an underestimation of $\tau$, the nonlinear model yields a significant improvement. For catchments where the recession time scale is overestimated with the linear model, the nonlinear model in forward model leads to a performance decrease.

## 3.5 Discussion

Our results show that analytical modelling framework for streamflow distributions proposed by Botter et al. (2007c) performs well for the 25 Swiss catchments across all studied streamflow regimes. A detailed comparison between the performance of the linear and the nonlinear models considering the optimized parameters obtained from the inverse approach shows that the results for the nonlinear model are always better than for the linear model. This underlines that the nonlinear recession suits better the hydrological conditions of all studied catchments, which is inline with previous results (Ceola et al., 2010; Basso et al., 2015b).

In forward estimation mode, the linear model outperforms the nonlinear model for catchments with summer high flows; the nonlinear model outperforms the linear model for catchments with rainfall-driven regimes (i.e. summer low flows). This results from the fact that for regimes with summer high flow, the linear model overestimates the recession time scale (resulting in a underestimation of the streamflow variance). For regimes with summer low flow, the linear model in exchange underestimates the recession time scale. Given that the nonlinear model yields longer recessions, the nonlinear model shows accordingly a better performance for regimes with summer low flow.

The comparison between the forward and inverse estimation methods shows a clear underestimation of $k_n$ for most of the catchments, which was already discussed by Dralle et al. (2015) and which is inline with previous work that tried to improve the results of the model in forward estimation mode, for the linear and the nonlinear formulation (Ceola et al., 2010; Basso et al., 2015b). There is clearly a need to further improve the methods to estimate the recession parameters. Our results pinpoint that a key hereby might be the detailed investigation of recession analysis methods along elevational gradients and related hydrologic regimes.

Overall, the good model performance in many different catchments with different regimes indicates that the modelling framework is suitable for the prediction of FDCs in Switzerland. A more detailed model temporal model validation (e.g. with a split sample test, Klemeš, 1986) is not possible for this framework since the model parameters are obtained directly from observed data for each time period (i.e. they vary from period to period). The obtained model performances are comparable to the results obtained in previous studies, e.g. in the work of Ceola et al. (2010). They obtained for different case studies in Italy and the US $c^{KS}$ values varying between 0.030 and 0.409 for the nonlinear model using different methods of forward estimation, and $c^{KS}$ values between 0.021 to 0.051 for inverse estimation. For the linear model, Ceola et al. (2010) obtained $c^{KS}$ values between 0.054 and 0.567. Basso et al. (2015b) and Doulatyari et al. (2017) studied some case studies that are included in the present paper (Sitter at Appenzell and Murg at Wängi).

Recomputing their results with their model parameters yields slightly different $c^{KS}$ values for the nonlinear model for the Sitter (0.12 compared to our 0.19) and for the Murg (0.05 to 0.06 compared to our 0.06). These differences are small and can be explained by different data periods and by the methodological choices in the calculation of parameters.

The most remarkable result of the presented analysis is the fact that the modelling framework is applicable in its original formulation to catchments where summer flow is influenced by snow processes. The additional source of water from snow or icemelt is accommodated by increasing the frequency $\lambda$ of streamflow-producing events. This is inline with a common assumption in catchment-scale precipitation-runoff modelling (e.g. Schaefli et al., 2005), which is that runoff from snowmelt can be modelled with exactly the same functional relationships as for rainfall, by simply feeding so-called equivalent precipitation (sum of rainfall and simulated snowmelt) into the runoff generation module.

The increase of the streamflow-producing frequency to account for snow or icemelt is furthermore also coherent with the original description of the analytic modelling framework, which incorporates losses as a decrease of the streamflow-producing frequency. This type of behavior can be identified in previous studies. Basso et al. (2015b) obtained for the Sitter at Appenzell $\lambda$ values that are close to the precipitation frequency $\lambda_p$ during spring; for the Thur at Jonschwil they obtain $\lambda = \lambda_p$ for spring. Both catchments have a mean elevation above 1000 m asl., which suggests the presence of snow processes. Later on, Doulatyari et al. (2017) discussed that snow accumulation and melt could be affecting the streamflow pdf estimation for the Sitter at Appenzell, without, however, exploring the issue further.

As can be seen in Figure 3.6, the switch from $\lambda < \lambda_p$ to $\lambda_p$ to $\lambda > \lambda_p$ is located at around 1500 m asl. This corresponds to a relatively low mean catchment elevation; for this mean elevation, it can a priori not be assumed that significant snowmelt continues throughout the summer. In fact, for most snow-influenced catchments, the majority of snowmelt happens during spring. Summer flows are nevertheless directly influenced by spring snowmelt since the summer streamflow results from a continuous release of melt water stored in the catchment during the preceding snowmelt period. For high elevation catchments, the exceedance of $\lambda$ over $\lambda_p$ is directly related to significant snow- and icemelt inputs throughout the summer.

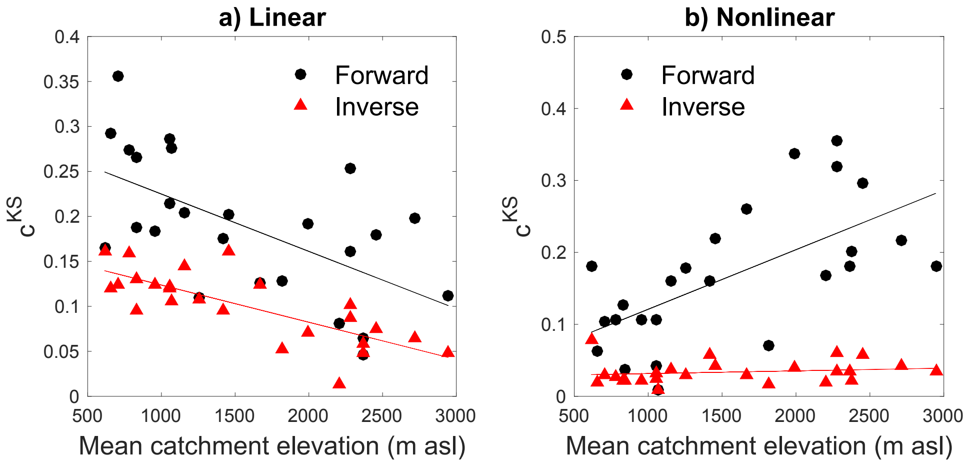


Figure 3.9 – Performance of the linear model and nonlinear model as a function of mean catchment elevation. The shown performance measure, $c^{\mathrm{KS}}$ is zero for a perfect model.

It should be kept in mind here, that for the present study, $\lambda$ is estimated directly from the relation between streamflow and precipitation (see section 3.2.1 and Equation 3.1). The question of how to estimate this parameter directly from catchment characteristics based on long term snow cover statistics and data on glacier cover remains to be answered in future work.

Besides the important result that the model is applicable to snow-influenced catchments, additional insights can be obtained from the highlighted model performance trends with mean catchment elevation (Figure 3.9 and 3.10). These performance trends are explained by the evolution of the regimes with mean catchment elevation, from rainfall-dominated (pluvial) regimes with summer low flow to snowfall-influenced (nival and glacier) regimes with summer high flow. This result suggests that mean catchment elevation is a good proxy for regime shifts, despite the fact that many other catchment characteristics vary strongly across the set of studied catchments (area, hypsometric curve, land use etc.). Given the strong link between mean catchment elevation, mean catchment air temperature and snow accumulation, this opens interesting perspectives for parameter regionalization.

## 3.6 Conclusions

This application of the analytic framework of Botter et al. (2007c) to estimate summer streamflow probability distributions for 25 Swiss catchments shows that this framework performs well without any further methodological adjustments across a wide range of streamflow regimes, including rainfall-driven regimes with summer low flows, but also regimes with snow- and glacier melt influenced summer high flows. Given that the original framework was developed for purely rainfall-driven regimes, this result is unexpected. For snow-influenced catchments, the model has been shown here to

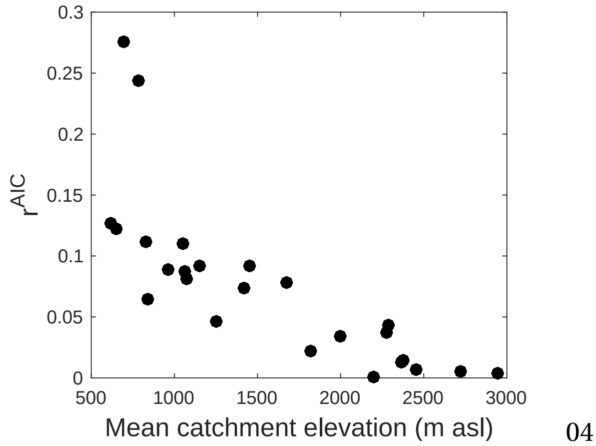


Figure 3.10 – Relative increase of the performance of the nonlinear model with respect to the linear model (as measured by $r^{\text{AIC}}$) as a function of mean catchment elevation. All model parameters are estimated in inverse mode.

accommodate the additional source of water from snowmelt by a relative increase of the streamflow-producing frequency, which is coherent with the underlying analytic framework.

The detailed comparison between the performance of the linear and the nonlinear model formulation shows that the description of Swiss summer flows strongly benefits from using a nonlinear storage-streamflow relationship, in particular for catchments with summer low flow and for the karst catchments. In general, the linear model performance increases for increasing total summer flows or, equivalently, for catchments with higher mean elevation. Future work will focus on improving the model parameter estimation directly from observed data (without parameter optimization), which is a pre-condition for parameter regionalization. Better insights into the physical grounds of the different parameters will also open new perspectives for the extension of the model framework to all four seasons for all Swiss streamflow regimes.

# 4 Estimation of streamflow recession parameters: new insights from an analytic streamflow distribution model

*Streamflow recession analysis characterizes the storage-outflow relationship in catchments. This relationship, which typically follows a power law, summarizes all catchment-scale subsurface hydrological processes and has long been known to be a key descriptor of the hydrologic response. In this chapter, we tested a range of common recession analysis methods (RAMs) and propose the use of an analytic streamflow distribution model as an alternative method for recession parameter estimation and to objectively compare different RAMs. The used analytical model assumes power law recessions, in combination with a stochastic process for streamflow triggering rainfall events. This streamflow distribution model is used in the present framework to establish reference values for the recession parameters via maximum likelihood estimation (MLE). The model-based method has two main advantages: i) joint estimation of both power law recession parameters (coefficient and exponent), which are known to be strongly correlated; ii) parameter estimation based on all available streamflow data (no recession selection). The approach is applied to five rainfall-dominated catchments in Switzerland with 40 years of continuous streamflow observations. The results show that the estimated recession parameters are highly dependent on methodological choices and that some RAMs lead to biased estimates. The recession selection method is shown to be of prime importance for a reliable description of catchment-scale recession behavior, in particular in presence of short streamflow records. The newly proposed model-based RAM yields robust results, which supports the further development of this method for comparative hydrology and opens new perspectives for understanding the recession behavior of catchments.* [1]

[1] This chapter is an adapted version of Santos et al. (2019)

## 4.1 Introduction

Recession analysis is a classical tool in hydrology to understand subsurface storage - outflow relationships in absence of water input at the catchment scale (Brutsaert and Nieber, 1977). Many analytical expressions can be used to model a streamflow recession. The one that is adopted in the present work as well as in most studies available in the literature, is presented in Equation 4.1. This expression was derived by Brutsaert and Nieber (1977) from the Boussinesq equation. Boussinesq (1904) proposed an exact solution for this equation which was later refined by Polubarinova-Koch (2015), who solved it for the beginning of the recession. According to this expression, recessions can be described by two parameters that relate streamflow ($Q$) to its variation in time ($dQ/dt$): $k_n$, or the recession coefficient and $a$, or the recession exponent.

$$\frac{dQ}{dt} = -k_n Q^a. \tag{4.1}$$

It is noteworthy that each recession event in a catchment might have a unique pair of parameters. It has, in fact, long been known that the hydrologic recession behavior is dynamic; each recession event reflects the antecedent moisture and recharge conditions for that particular event (Biswal and Nagesh, 2014). Nevertheless, we need effective constant parameters to describe the overall behavior of different catchments, to compare those catchments across hydroclimatic gradients, to understand hydrologic similarity among them or to build models. This necessarily raises the need for methods to define a pair of constant recession parameters from streamflow records, which are known as Recession Analysis Methods (RAMs) (Stoelzle et al., 2013). The many methods proposed in the literature have usually specific purposes (Tallaksen, 1995), such as low flow studies (Aksoy and Wittenberg, 2011; Bako and Hunt, 1988; Gottschalk et al., 1997; Sugiyama, 1996), rainfall-runoff modelling (Kirchner, 2009; Müller et al., 2014; Rupp and Woods, 2008), the estimation of groundwater storage variations at catchment scale (Kirchner, 2009; Vogel and Kroll, 1992), or studies on the geomorphologic origin of streamflow (Biswal and Marani, 2010; Biswal and Nagesh, 2014; Mutzner et al., 2013). Recession analysis has also been used to study catchment similarity (Sawicz et al., 2011), hydrological regimes (Botter et al., 2013) or to study how land use can affect the recession behavior (Bogaart et al., 2016; Sawaske and Freyberg, 2014). In hydrologic modelling, recession analysis has become widely used to derive hydrologic signatures to be used in model calibration (e.g. McMillan et al., 2017). An early example is the work of Harlin (1991). Recent work in this field focuses on the question of how to account for different sources of uncertainties in hydrological signatures (Westerberg, 2015).

The application of a selected RAM implies a number of methodological choices. Any RAM can be divided into two main steps: i) Recession extraction and ii) parameter estimation. Recession extraction is the process of selecting a streamflow data portion where recession is the only streamflow generation process. It can be based only on streamflow data or include other types of data, such as precipitation. Parameter estimation, in turn, consists of fitting parametric curves to the selected data portions to estimate the recession parameters. There exists a wide variety of methods to perform both steps, leading to a large choice of possible combinations and accordingly, to a considerable spread of corresponding results (Arciniega-Esparza et al., 2017; Chen and Krajewski, 2016; Dralle et al., 2017b; Stoelzle et al., 2013). Some authors even propose supplementary steps, such as filtering the noise of observed streamflow as suggested by Roques et al. (2017).

One classical way to extract recessions is the graphical method consisting of inspecting the hydrograph represented on a semi-logarithmic scale and searching for the long-enough segments where the hydrograph fits a straight line (Horton, 1941; Rorabaugh, 1964). Given that this is not practical to automatize, different methods have been proposed to mimic this process. Brutsaert and Nieber (1977) consider only series of streamflows starting at least 5 days after a rainfall event, requiring not only streamflow data, but also precipitation data. Vogel and Kroll (1992) proposed an algorithm based on 3-day moving averages of daily streamflows and a minimum length of 10 days of recession that also excludes the beginning of the recession (to exclude surface runoff). Later, Brutsaert (2008) described new criteria to extract recessions based only on streamflow data: decreasing streamflow portions are selected and the start and end points of an event are eliminated. Dralle et al. (2017b) summarized all decisions involved in recession extraction in terms of: i) the minimum allowable length of events, ii) the definition of the beginning and of the end of an event and iii) concavity. They furthermore showed that results are significantly improved when concavity is considered in the recession selection.

The range of parameter estimation methods proposed in the literature can be classified into two types: i) based on a collection of individual events or ii) assuming that all events come from a single master recession. Master recession curve methods fit the ensemble of data at once in log-log scale but different fitting methods exist: the original method of Brutsaert and Nieber (1977) suggested to estimate the recession parameters from lower envelopes of all data points. Some authors apply a regression to all data points (e.g Ceola et al., 2010). Kirchner (2009) proposed to bin the data.

Another approach is fitting parametric curves to individual recession events, called "per event" approach hereafter. The methods based on individual events estimate the parameters for each selected event and then take either the average (Ye et al., 2014) or the median (Basso et al., 2015b; Biswal and Marani, 2010; Mutzner et al., 2013) of the resulting parameter sets. Given that the parameters $k_n$ and $a$ are always correlated to some degree (Dralle et al., 2015), such an approach might induce biases. Dralle et al. (2015) thus proposed a method to overcome this limitation.

Some authors, such as Chen and Krajewski (2016); Dralle et al. (2017b); Stoelzle et al. (2013) studied the inherent uncertainties in the choice of a RAM and how methodological choices can affect the values of parameters, with only partly conclusive results. The recent paper by Dralle et al. (2017b) studies exclusively the per event recession methods and provides a clear recommendation about the best method to use in this case: non-linear fitting in combination with a concavity criterion for recession selection. Stoelzle et al. (2013) on the other hand, studied exclusively methods based on the regression of master recession curves, concluding that each application of recession models (e.g. the use of a particular model or for a particular climate) may require a different RAM and must be studied individually.

A critical point for comparing different RAMs is the fact that all methods are approximations. An exception is the work of Roques et al. (2017) who used synthetic recessions as a reference. In the present chapter, we build on this existing work and extend it to understand how well classical RAMs can capture the actual storage-discharge behavior of catchments. To overcome the aforementioned limitation, we use a simple hydrologic model to objectively compare the model parameters obtained with different RAMs. The retained model is the analytic streamflow duration curve model developed by Botter et al. (2007c, 2009), which derives an analytic expression for the probabilistic distribution of daily streamflows as a function of stochastic rainfall properties and the recession parameters $k_n$ and $a$.

In this model context, the recession parameters have generally been estimated with the master recession approach, with binning (Ceola et al., 2010) or, mostly without binning (Ceola et al., 2010; Santos et al., 2018; Schaefli et al., 2013) or with an event-scale recession analysis with a linear regression of data (Basso et al., 2015b; Botter et al., 2007a, 2009, 2013, 2008; Müller et al., 2014).

A major advantage of using this analytic model for a systematic comparison of different RAMs is the fact that we can obtain a reference recession parameter set via maximum likelihood estimation (MLE). This was first attempted by Ceola et al. (2010) who assessed the model performance for different recession parameter estimation methods, including traditional RAMs and statistical curve-fitting methods. Since in their analysis, MLE provided the best results, it was later used by Santos et al. (2018) to obtain linear and nonlinear recession parameters and will build the basis for parameter comparison in this chapter.

Recession parameters correspond to effective parameters that are used to describe the storage-discharge relationship of a catchment. Even if they are estimated based on physical considerations, e.g. from groundwater flow analysis, they can usually not be related directly to actual catchment properties. Some authors, such as Biswal and Marani (2010); Biswal and Nagesh (2014); Mutzner et al. (2013), tried to relate the recession parameters to geomorphological features, in a first step to tie them firmly to the physiographic characteristics of a catchment. However, the recession behavior at the scale of an entire catchment results from the interplay of saturated and unsaturated flow, which makes its description rather complex (Tallaksen, 1995).

In this context, the model-based approach proposed in the present chapter offers two important advantages over traditional RAMs: i) It extracts information about the recession behavior from all observed streamflow records collectively without prior recession selection. ii) The proposed framework estimates the two recession parameters ($a$ and $k_n$) jointly, which is crucially lacking in most existing methods. The method has thus the potential to provide a more holistic view of the recession characteristics at the catchment scale.

The overall objective of the chapter is twofold: i) assess the value of the model-based approach for recession parameter comparison; and ii) understand the advantage of using MLE in combination with the model of Botter et al. (2007c, 2009) over established RAMs. An essential part of this analysis is a detailed assessment of the different parameter estimation methods in the presence of short streamflow records. All methods are tested for five Swiss case studies.

The chapter is organized as follows: Section 4.2 presents RAMs that are tested in this work, Section 4.3 provides a description of the case studies, followed by the results (Section 4.4) and discussion of results (Section 4.5). Our main conclusions are summarized in Section 4.6.

## 4.2 Methods

### 4.2.1 Recession Analysis Methods

The different Recession Analysis Methods (RAMs) analyzed in this chapter are presented in detail hereafter. The range of analyzed methods results from all possible combinations of three recession extraction methods and three parameter estimation methods.

#### Recession extraction

Recessions are periods with decreasing streamflows, in absence of rainfall input (or snow-melt input in snow-influenced areas), but many features of the measured streamflow series can be used to make a more refined selection of recession events. Therefore, in general, additional criteria are adopted to guarantee the choice of representative stretches of the streamflow series. As discussed above, the following additional criteria are typically used: the definition of minimum length of recession periods, the number of days before or after a positive jump in streamflows (Chen and Krajewski, 2016), the concavity of the series of streamflow data, peak characteristics and differences between successive values (Dralle et al., 2017b).

In this study we select three commonly used methods, ranging from a very permissive method (E1), to an intermediate method, based on simple criteria (E2) to a more strict method recommended recently in the literature (Dralle et al., 2017b) for recession extraction (E3):

1. E1: Comprises all segments of streamflow series that decay for at least two consecutive days (Kirchner, 2009; Schaefli et al., 2013).

2. E2: This method excludes 3 daily data points after a positive jump and 4 data points before the next positive jump (Brutsaert, 2008).
3. E3: This method is based on the work of Dralle et al. (2017b), who proposed to select only concave recessions with a minimum length of four days. Based on their results, we also retain only recessions that begin with a streamflow higher than the mean streamflow in the period of analysis. This type of criteria for peak selectivity has been adopted previously by Biswal and Marani (2010); Mutzner et al. (2013).

**Parameter estimation**

The three analyzed parameter estimation methods are: the classical master recession curve method of Brutsaert and Nieber (1977), called here method P1, an event-based method (P2) and the method proposed by Dralle et al. (2015) that overcomes parameter biases (P3):

1. P1: It consists of a linear regression of all values of $\log(Q)$ against $\log(-dQ/dt)$ with the values of $Q$ being the means of the values of two successive days, and $dQ/dt$ the decrease of $Q$ between these days (Brutsaert and Nieber, 1977). We do not calculate the parameters from the lower envelope, as suggested in the original paper since it is known to bias $k_n$ to lower values (Dralle et al., 2015).
2. P2: This linear least-squares method is analogous to method P1 but it fits a recession parameter set ($k_{nj}$ and $a_j$) to each selected recession event. The exponent $a$ is then taken as the median value of the fitted $a_j$ values, where $j$ is an index for individual recessions. Once $a$ is fixed, the curves are fitted again to estimate $k_n$ as the median of the recalculated $k_{nj}$ (Basso et al., 2015b; Mutzner et al., 2013).
3. P3: This is also an estimation per event, but with nonlinear curves fitted directly to individual recessions according to Equation 4.1, without linearization in a $\log-\log$ space. Following Dralle et al. (2015), we use a decorrelation method to avoid biases arising from the mathematical correlation between $k_n$ and $a$. The first step is to fit curves for each of the selected recessions, obtaining a set of parameters $k^d_{nj}$ and $a^d_j$, where $d$ distinguishes the parameters from those obtained by other methods and $j$ identifies parameters for an individual recession. Then the streamflow values are rescaled, by a constant $q_0$ (Eq. 4.2) so that $a$ and $k_n$ become independent. Finally, curves are fitted again and the parameters are obtained as the median values of the new fitted parameters.

$$q_0 = \exp\left[\frac{\sum_{j=1}^{n}(a^d_j - \overline{a^d})(\log k^d_{nj} - \overline{\log k^d_n})}{\sum_{j=1}^{n}(a^d_j - \overline{a^d})^2}\right] \tag{4.2}$$

where $\overline{\log k^d_n}$ is the mean of the logarithm of the set $k^d_{nj}$ and $\overline{a^d}$ is the mean of the set $a^d_j$.

The RAMs obtained from combining all parameter estimation methods with all recession extraction methods are summarized in Table 4.1.

Table 4.1 – Synthesis of the adopted RAMs

| Symbol | Description | References |
|---|---|---|
| E1 | Permissive recession extraction | Kirchner (2009); Schaefli et al. (2013) |
| E2 | Intermediate recession extraction | Brutsaert (2008) |
| E3 | Recession extraction with concavity criteria | Dralle et al. (2017b) |
| P1 | Parameter estimation based on master recession curve | Brutsaert and Nieber (1977) |
| P2 | Parameter estimation with linear least square method per event | Basso et al. (2015b); Mutzner et al. (2013) |
| P3 | Decorrelation parameter estimation per event | Dralle et al. (2015) |

#### Maximum likelihood estimation of parameters

The values of $k_n$ and $a$ can be obtained by statistical inference as being the parameters that provide the best fit of the probabilistic model (Eq. 2.6) to the observed data, i.e. the parameters obtained via maximum likelihood estimation (MLE). The parameter values obtained by MLE for the observed long term data sets are called reference values hereafter.

The MLE is obtained by maximizing (numerically) the likelihood function (Equation 2.7) that can be formulated for observed streamflow values.

A Matlab implementation of MLE for the model of Equation 2.6 is given in the Appendix B.

### 4.2.2 Comparison criteria

The recession parameter values obtained with different RAMs are analyzed in terms of their joint effect on the analytic model (Eq. 2.6). In fact, since the parameters $k_n$ and $a$ are always correlated (Dralle et al., 2015), a direct comparison between their values is not completely meaningful. Assessing their effect on the analytic model of Equation 2.6 considers the joint effect of the pair of parameters. The performances of the recession parameter sets obtained for the different RAMs is assessed adopting the Kolmogorov-Smirnov distance ($c^{KS}$). This indicator corresponds to the maximum distance between the analytical cumulative distribution function (cdf) and the empirical long term cdf, previously adopted as a measure of performance for this type of model framework (Ceola et al., 2010; Santos et al., 2018; Schaefli et al., 2013).

We also assess the RAMs and MLE as a function of data availability, estimating the values of $k_n$ and $a$ for different scenarios of short streamflow record lengths (i.e. time-overlapping periods of 1 year, 2 years or 5 years). Such a short sample analysis shows how the variability of the estimated parameters decreases with the record length for the different methods. In addition, it gives a more complete picture of the parameter range

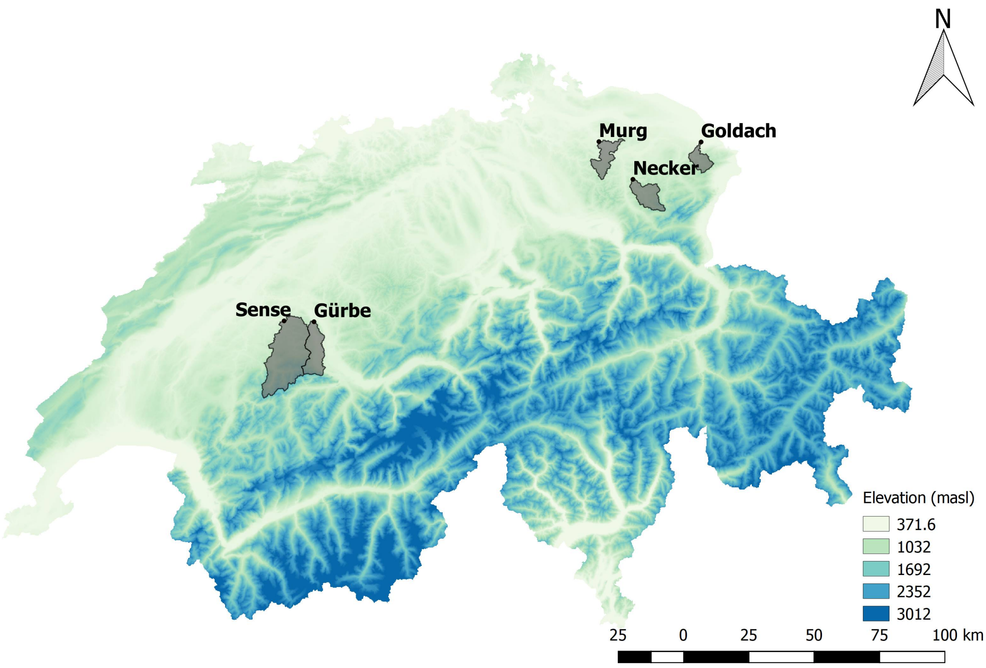


Figure 4.1 – Localization of the 5 case studies in Switzerland over a topographic map

obtained for each method.

## 4.3 Case studies

The proposed framework for RAM inter-comparison is applied to five case studies in Switzerland (Figure 5.1). The requirements for their selection were: gauged catchments with unperturbed streamflows (i.e. minimal anthropogenic influence, including changes in land-use and engineering works), with a rainfall-dominated regime, not strongly karst-influenced and with a continuous series of measured daily streamflows from 1975 to 2014. These case studies do not show considerable snow influences and a visual inspection of the precipitation and streamflow time series does not show strong seasonalities (see Appendix B). Accordingly, the RAMs are applied without consideration of seasons.

Daily streamflow data for each catchment have been provided by the Swiss Federal Office for the Environment (FOEN, 2017). Daily precipitation data have been extracted from the gridded database RhiresD (MeteoSwiss, 2011). The catchment scale average precipitation time series are obtained by averaging the data from all grid cells contained in a catchment (based on shape files available from MeteoSwiss (2011). The suitability of the analytical model hypotheses for this data set was carefully checked (see Santos

Table 4.2 – Characteristics of case studies in Switzerland as given in the FOEN database; $P$ stands for the mean annual precipitation, $\overline{T}$ is the mean annual temperature, $\lambda$ is the annual frequency of streamflow producing events and $\alpha$ is the annual mean precipitation depth.

| ID | Code | Name | Coordinates (CH1903) | Area ($km^2$) | Mean elevation (m asl) | Station elevation (m asl) | $P$ (mm) | $\overline{T}$ ($^oC$) | $\lambda$ day$^{-1}$ | $\alpha$ mm |
|---|---|---|---|---|---|---|---|---|---|---|
| 2308 | GOL | Goldach - Goldach, Bleiche | 753190 / 261590 | 49.8 | 833 | 399 | 1446 | 7.39 | 0.27 | 8.63 |
| 2374 | NEC | Necker - Mogelsberg, Aachsäge | 727110 / 247290 | 88.2 | 959 | 606 | 1777 | 6.47 | 0.32 | 10.04 |
| 2126 | MUW | Murg - Wängi | 714105 / 261720 | 78.9 | 650 | 466 | 1357 | 7.90 | 0.24 | 8.22 |
| 2159 | GUR | Gürbe - Belp, Mülimatt | 604810 / 192680 | 117 | 837 | 522 | 1295 | 7.21 | 0.31 | 8.85 |
| 2179 | SEN | Sense - Thörishaus, Sensematt | 593350 / 193020 | 352 | 1068 | 553 | 1479 | 6.29 | 0.22 | 8.97 |

Table 4.3 – Reference values of the recession coefficient $k_n$ , the mean values obtained for the three scenarios of short record length ($\overline{k^{(1)}}_n$, $\overline{k^{(2)}}_n$, $\overline{k^{(5)}}_n$). The coefficient of variation, $CV$ (mean divided by standard deviation) of the three scenarios is also indicated.

| | Ref. $k_n$ | $\overline{k^{(1)}}n$ | $CV_{k_n^{(1)}}$ | $\overline{k^{(2)}}n$ | $CV_{k_n^{(2)}}$ | $\overline{k^{(5)}}n$ | $CV_{k_n^{(5)}}$ |
|---|---|---|---|---|---|---|---|
| GOL | 0,161 | 0,148 | 0,239 | 0,156 | 0,205 | 0,161 | 0,147 |
| NEC | 0,170 | 0,159 | 0,243 | 0,165 | 0,156 | 0,171 | 0,107 |
| MUW | 0,094 | 0,084 | 0,289 | 0,088 | 0,207 | 0,095 | 0,171 |
| GUR | 0,070 | 0,056 | 0,452 | 0,063 | 0,321 | 0,065 | 0,204 |
| SEN | 0,087 | 0,079 | 0,320 | 0,084 | 0,223 | 0,087 | 0,134 |

et al., 2018, and Appendix B) .

Table 4.2 shows some key characteristics of the selected catchments, including the codes that are used to refer to the catchments in the following tables and figures. Additional data about the catchments including their land-use and karstic influence can be found in the work of Aschwanden (1996).

## 4.4 Results

### 4.4.1 MLE parameter values

The reference parameter values obtained via MLE estimation (Eq. 2.7) for the full streamflow record length (40 years) are presented in Tables 4.3 and 4.4. We consider these values as a reference because they give the best results for the model used in this study. The corresponding parameter ranges obtained for short streamflow records are shown in Figure 4.2.

As expected, the shorter record lengths result in a higher variability of the estimated parameter values (Figure 4.2 and Tables 4.3 and 4.4). Especially for the exponent of the recession, $a$, the variability decreases strongly with the length of the observed streamflow series. The reference values are all contained in the estimated interquartile range for the different record lengths scenarios, but using very short data portions (1 or 2 years) clearly leads to a bias of the estimated median value compared to the reference

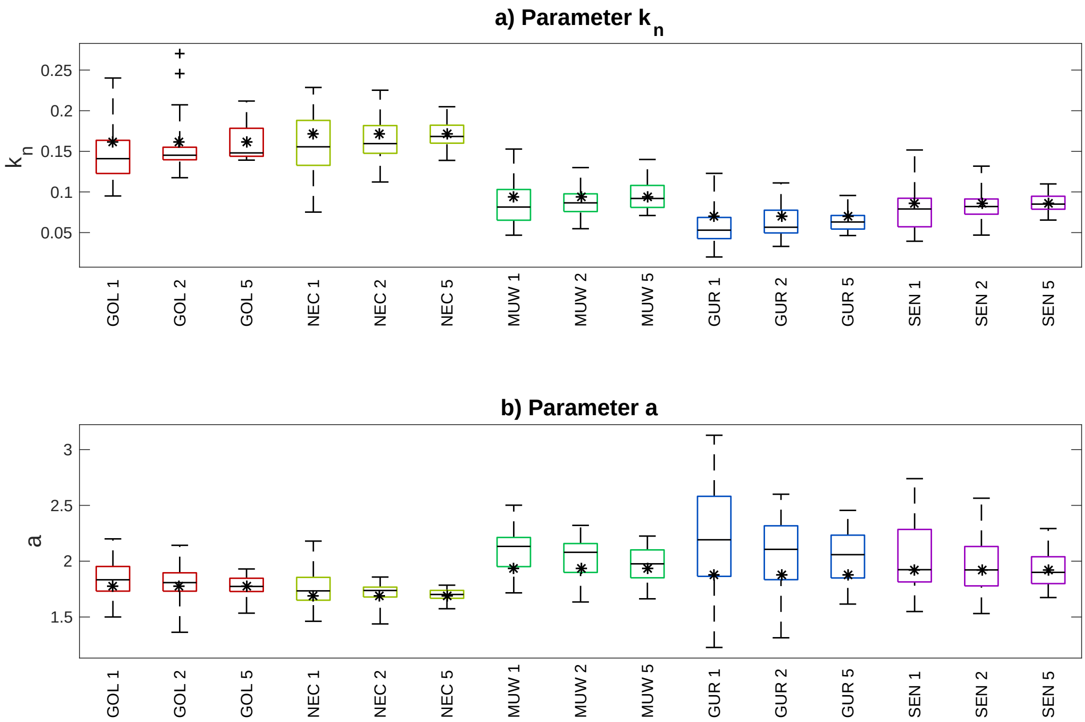


Figure 4.2 – Box-plots of the MLE recession parameters $k_n$ and $a$ for the three different scenarios of short record lengths. The box-plots represent the interquartile range (box), outliers are marked as crosses. The stars represent the reference MLE values (obtained for full record length).

Table 4.4 – Values of the recession exponent $a$ and the mean values obtained for the three scenarios of short record length ($\overline{a^{(1)}}_i$, $\overline{a^{(2)}}_i$, $\overline{a^{(5)}}_i$). The coefficient of variation of the three scenarios is also indicated.

| | Reference $a$ | $\overline{a_i^{(1)}}$ | $CV_{a^{(1)}}$ | $\overline{a_i^{(2)}}$ | $CV_{a^{(2)}}$ | $\overline{a_i^{(5)}}$ | $CV_{a^{(5)}}$ |
|---|---|---|---|---|---|---|---|
| GOL | 1,77 | 1,86 | 0,098 | 1,81 | 0,086 | 1,77 | 0,055 |
| NEC | 1,69 | 1,76 | 0,081 | 1,72 | 0,049 | 1,70 | 0,033 |
| MUW | 1,94 | 2,09 | 0,091 | 2,04 | 0,087 | 1,98 | 0,079 |
| GUR | 1,88 | 2,21 | 0,193 | 2,07 | 0,160 | 2,03 | 0,110 |
| SEN | 1,92 | 2,04 | 0,160 | 1,98 | 0,128 | 1,93 | 0,089 |

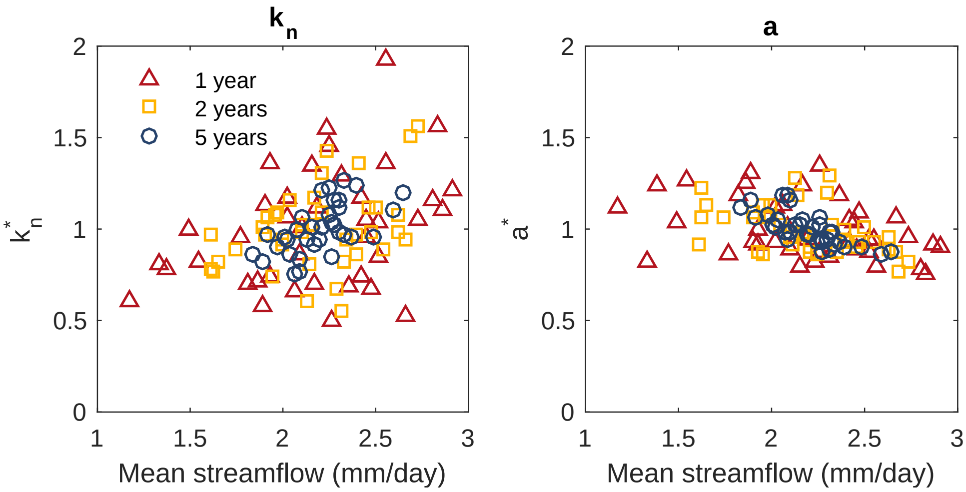


Figure 4.3 – Scatter plot of the normalized MLE recession parameters $k_n^*$ (left) and $a^*$ (right) against observed mean daily streamflow for the three different scenarios of short record lengths for the Sense catchment. The parameters are normalized by the mean value of each scenario.

values (Figure 4.2). For records of 5 years, the median values are, in exchange, close to the reference values (i.e. there is a low bias), except for the value of $a$ for the Gürbe catchment.

The variability of the values of $a$ is smaller than the variability of $k_n$ (see the coefficients of variation in Tables 4.3 and 4.4), which might be expected. Some authors argue, in fact, that $k_n$ depends on soil moisture conditions and that $a$ is more related to the (more static) geomorphological characteristics of the catchment (Biswal and Marani, 2010; Biswal and Nagesh, 2014; Brutsaert and Nieber, 1977; Dralle et al., 2017b); others, such as Harman et al. (2009), argue that $a$ differs from 1 as a consequence of catchment heterogeneity and that it could also be sensitive to antecedent soil moisture conditions in sufficiently heterogeneous catchments. This dependence on the soil moisture conditions can also be seen when plotting the normalized parameter values against mean daily streamflow (see Figure 4.3 for an example).

It is interesting to notice that there is a correlation between the model parameters that seems to be approximately the same for all the catchments even if they are located in

Table 4.5 – Value of $k_n$ from the nine tested RAMs. The reference value obtained via MLE from the full record length and the 95% range ($R^{(1)}$) obtained from MLE with a single year are also indicated.The lowest and highest value for each catchment are highlighted in bold

| | Ref. $k_n$ | $R^{(1)}$ | E1P1 | E1P2 | E1P3 | E2P1 | E2P2 | E2P3 | E3P1 | E3P2 | E3P3 |
|---|---|---|---|---|---|---|---|---|---|---|---|
| GOL | 0,161 | 0,099-0,240 | 0,114 | 0,107 | 0,148 | **0,075** | 0,095 | 0,101 | 0,141 | 0,151 | **0,152** |
| NEC | 0,170 | 0,087-0,227 | 0,098 | 0,077 | 0,118 | **0,076** | 0,099 | 0,104 | 0,128 | 0,139 | **0,142** |
| MUW | 0,094 | 0,047-0,137 | 0,064 | 0,054 | 0,068 | 0,045 | **0,039** | 0,049 | **0,088** | 0,063 | 0,067 |
| GUR | 0,070 | 0,020-0,123 | 0,049 | **0,030** | 0,050 | 0,036 | 0,036 | 0,034 | **0,070** | 0,053 | 0,055 |
| SEN | 0,087 | 0,041-0,137 | 0,063 | 0,050 | 0,090 | **0,045** | 0,054 | 0,079 | 0,089 | 0,099 | **0,104** |

different parts of the parameter space (Figure 4.4). This correlation between recession parameters has been described before for individual recession events (Dralle et al., 2015).

To gain further insights into the variability of the estimated parameter values for short records, Figure 4.5 shows their temporal evolution for the Murg-Wängi catchment and for the Goldach catchment. For the Murg-Wängi catchment, we see a strong pattern for the short series values of $k_n$; this might be related to interannual fluctuations of average soil moisture, which is known to influence the value of $k_n$ (Biswal and Marani, 2010; Biswal and Nagesh, 2014; Brutsaert and Nieber, 1977; Dralle et al., 2017b). The corresponding values of $a$ follow an anti cyclic pattern, which is to be expected given the known correlation between the two parameters (e.g Dralle et al., 2017b). A special case is the Goldach catchment, which shows a clear change in the pattern of $k_n$ around the year 2000. According to the data provider (FOEN, 2017), there was a modification of a weir to increase the minimum flow in 1999. The mean results concerning this catchment for the full record length are, however, not strongly affected by this change.

As expected, the above results suggest that overall a considerable reduction of the variability in the parameter values occurs for longer time periods. The effect is even more apparent if considering the model performance corresponding to these parameter values, i.e. the Kolmogorov-Smirnov distance $c^{KS}$ (Section 4.2.2, Figure 4.6), which shows a much lower variability for two years of data than for one year.

### 4.4.2 Parameter values obtained from nine different RAMs

To compare the different RAMs, the recession parameters are calculated by adopting the nine possible combinations of the three recession extraction methods (E1 to E3) with the three parameter estimation methods (P1 to P3, Section 4.2.1). The results are presented in Tables 4.5 and 4.6 together with the reference values obtained by MLE for the full record (40 years) and the interquartile ranges obtained via MLE with a single year of streamflow data. Figure 4.7 shows the variation observed in the recession parameters for individual recession events for each catchment and each recession extraction method.

The direct comparison of the parameter values obtained with the different RAMs is not meaningful since this cannot capture the joint effect of both parameters on a recession model. We can nevertheless observe that the methods per event (P2 and P3) tend to

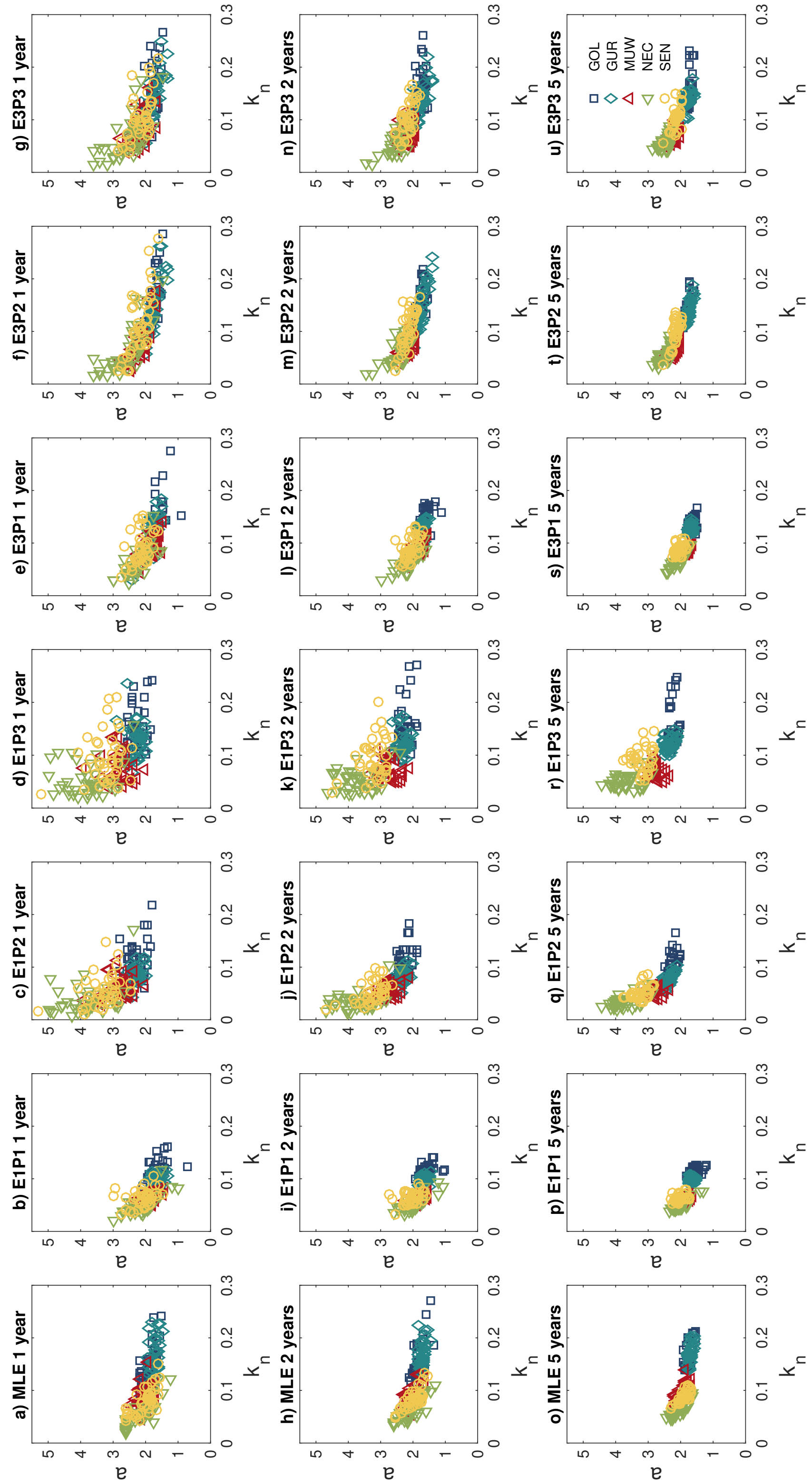


Figure 4.4 – Scatter plots of the recession parameters ($a$ and $k_n$) obtained for the three scenarios of short record lengths and for all estimation methods (rows correspond to different record lengths, columns to different estimation methods; methods based on P1 are excluded, see text). One data point ($a = 1.87$ $k_n = 0.37$) for GOL is out of the domain in d.

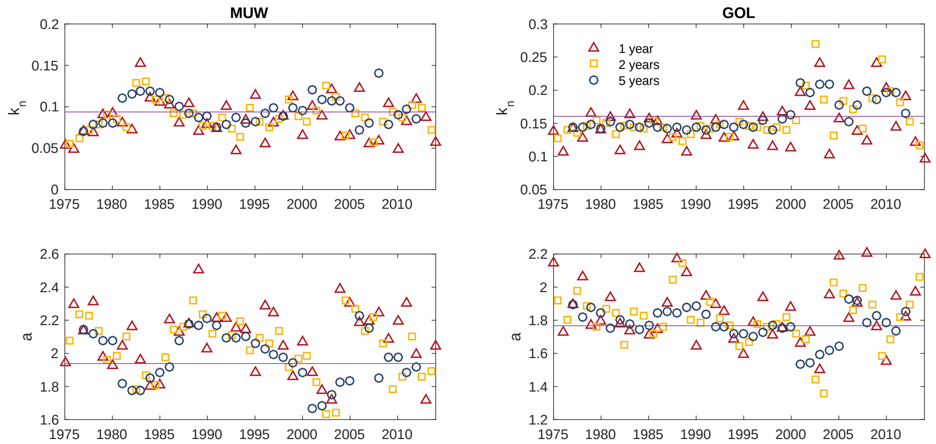


Figure 4.5 – Temporal evolution of the MLE parameters obtained by MLE for the three scenarios of short record lengths for two case studies: Murg-Wängi (MUR) (left) and Goldach (GOL) (right).

Table 4.6 – Value of $a$ from the nine tested RAMs. The reference value obtained via MLE from the full record length and the 95% range ($R^{(1)}$) obtained from MLE with a single year are also indicated. The lowest and highest value for each catchment are highlighted in bold

| | Ref. $a$ | $R^{(1)}$ | E1P1 | E1P2 | E1P3 | E2P1 | E2P2 | E2P3 | E3P1 | E3P2 | E3P3 |
|---|---|---|---|---|---|---|---|---|---|---|---|
| GOL | 1,77 | 1,53-2,20 | **1,57** | **2,29** | 2,28 | 1,66 | 1,91 | 1,91 | 1,64 | 1,74 | 1,74 |
| NEC | 1,69 | 1,50-2,08 | 1,65 | **2,33** | 2,31 | **1,57** | 1,96 | 1,96 | 1,68 | 1,76 | 1,76 |
| MUW | 1,94 | 1,73-2,45 | 1,80 | **2,85** | 2,78 | **1,74** | 2,60 | 2,60 | 1,79 | 2,22 | 2,22 |
| GUR | 1,88 | 1,34-2,99 | **1,91** | **3,68** | 3,63 | 1,96 | 2,82 | 2,82 | 2,01 | 2,49 | 2,49 |
| SEN | 1,92 | 1,37-2,71 | **1,99** | **3,24** | 3,19 | 2,24 | 3,14 | 3,13 | 2,01 | 2,13 | 2,13 |

give larger values for $a$ than the master recession method P1. Additionally, for the less selective extraction methods (E1 and E2), the values of $k_n$ are smaller than for method E3 considering also the concavity of events as a selection criterion.

The corresponding model performances are mostly poor compared to the ones obtained with MLE parameters. The mean of all $c^{KS}$ values from all RAMs for all catchments is around 0.12, compared to 0.02 for the MLE reference values. The extraction method E3, recommended by Dralle et al. (2017b) has a distinguished better performance, with mean $c^{KS}$ around 0.08 over all catchments. Considering the different parameter estimation methods, none of them yields noticeably better results.

To give a better view on how well the parameter sets obtained with the different RAMs are able to describe the observed streamflow probability distributions, Figure 4.8 presents the cdfs resulting from the worst and the best performing RAM along with the curve resulting from observed data for all five catchments. While the best model fits the observed curve closely, the model with the lowest performance yields a cdf that lies outside the natural variability of annual cdfs.

We also assessed the variability of the RAM parameter values for different scenarios of

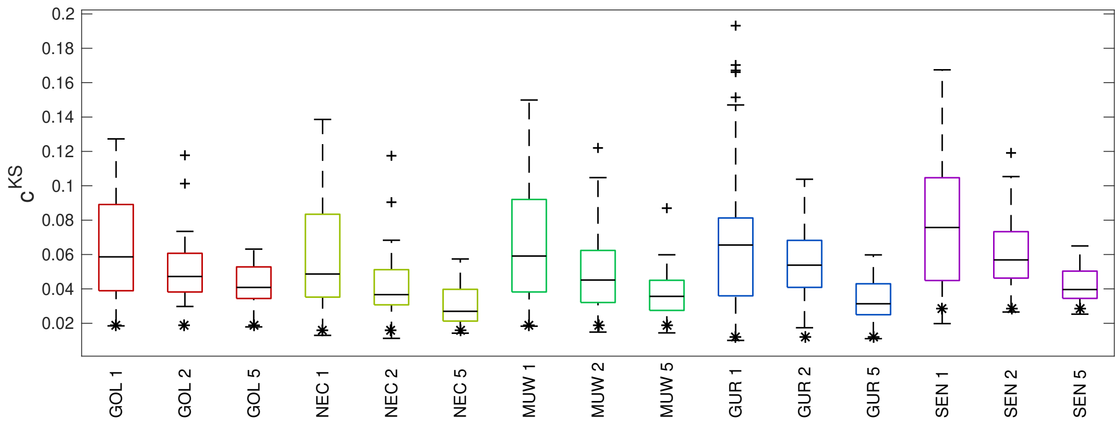


Figure 4.6 – Box-plots representing the model performances $c^K S$ of the MLE parameters for the three scenarios of short record lengths. The star represents the reference MLE values (full record length).

short streamflow record lengths (1 year, 2 years or 5 years). The extraction method E2 is very strict and samples too few recessions for short series estimation. Therefore, we tested only the short series scenarios for the RAMs based on the recession extraction methods E1 and E3. Figure 4.4 shows the results for the three record length scenarios for the six resulting combinations of methods.

Again, the parameters based on shorter record lengths vary more than the ones for longer series; the variability of the recession exponent $a$ decreases more than the one of $k_n$, with a particularly high variability for single year records for the flexible recession extraction E1 and the parameter estimation methods 'per event' (P2 and P3).

Comparing these last to parameter estimation methods shows that Dralle's (P3) estimation method leads to a lower correlation between the parameters than the simpler 'per event' estimation method P2). This confirms that Dralle's method reduces the mathematical correlation between parameters and suggests that the remaining correlation has a hydrological origin. Another remarkable aspect is that the parameter estimation method that considers the master curve (P1) gives precise results even for the shortest series.

## 4.5 Discussion

We discuss hereafter the key question underlying the presented analyses, namely if model-based recession parameter estimation presents an alternative to established RAMs but also in as far this new method allows new insights into recession behavior at catchment scale.

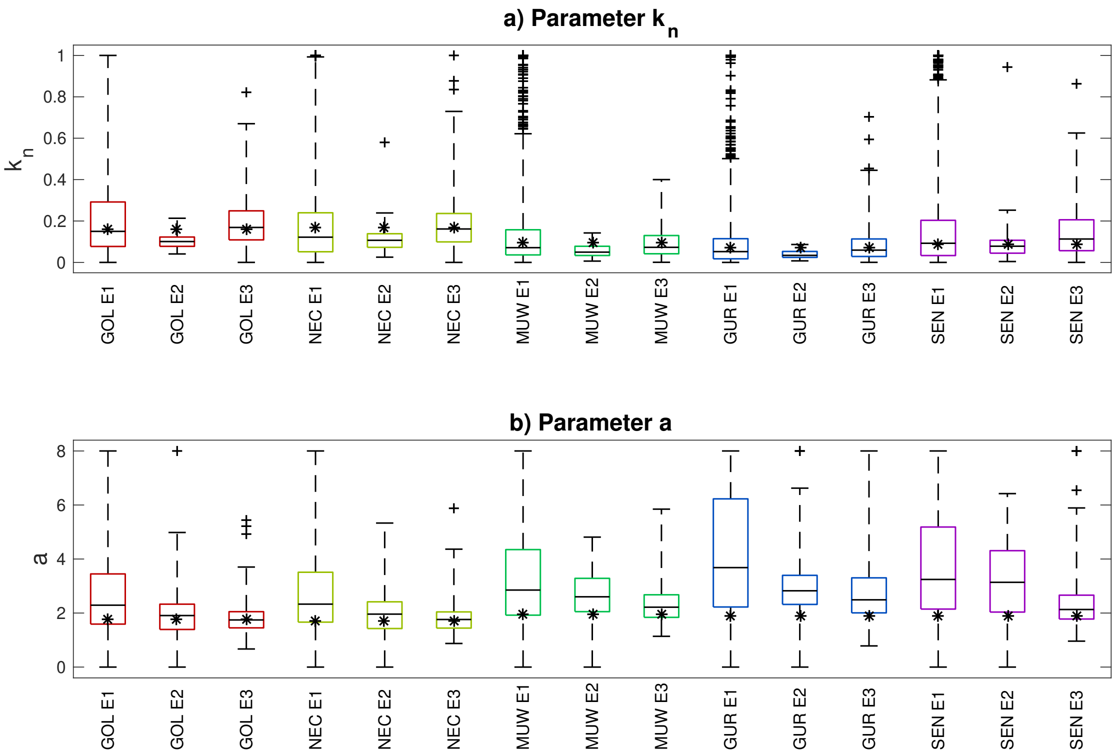


Figure 4.7 – Box-plots representing the recession parameters $k_n$ and $a$ for the individual recessions selected by the three different recession extraction methods. The star represents the MLE reference values (full record length).

### 4.5.1 Comparison of parameter ranges

The full record parameter values obtained for the 9 RAMs lie mostly within the 95% parameter intervals obtained with MLE for single year estimation (Tables 4.5 and 4.6), with the exception of methods E1P2 and E1P3. In other words, most of the methods provide parameter values that are similar to the MLE range; in particular RAMs selecting more representative recessions, which exclude most fast flow events (E2P* and E3P*), yield similar results as MLE. This important result is confirmed by the parameter domains spanned by all single year parameter sets (Figure 4.4, top row), which underlines that methods E1P2 and E1P3 are not compatible with the other methods.

Based on these results, it becomes clear that 'per event' parameter estimation (P2 and P3) should not be applied in combination with a permissive recession extraction method (E1). The parameter range comparison also shows that all methods based on the extraction method E3 proposed by Dralle et al. (2017b) show very similar ranges to the MLE estimates. More importantly, the original recession parameter analysis method proposed by Brutsaert and Nieber (1977) (E1P1) yields very robust and precise results for short samples, and $a$ values are in agreement with the parameter ranges obtained with MLE. This finding agrees with Brutsaert and Nieber (1977) who stated that this method reduces the uncertainties in recession parameters estimation; as our results

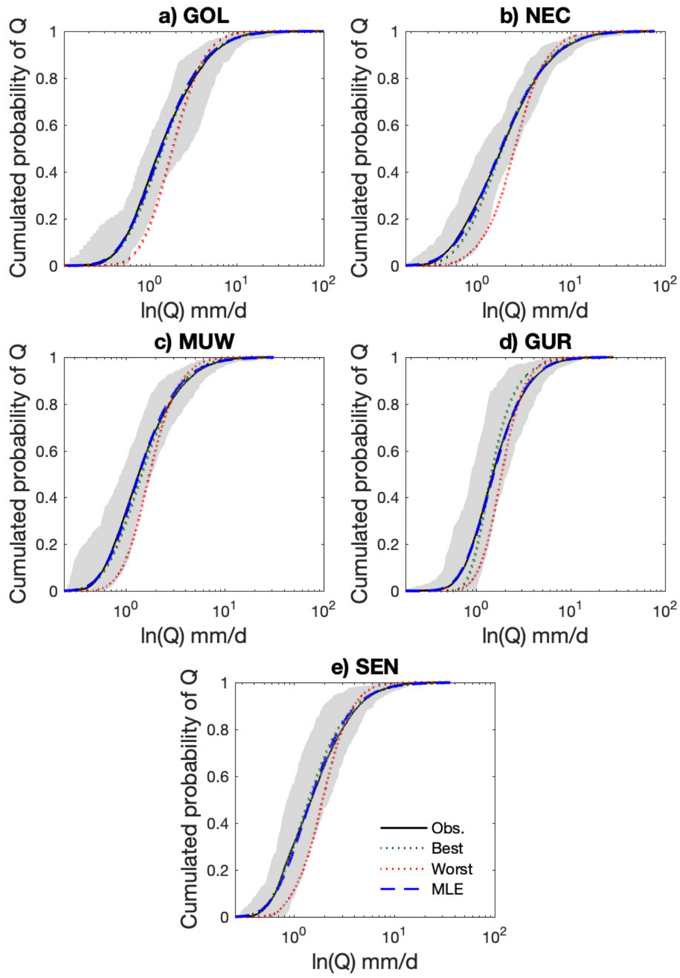


Figure 4.8 – Comparison of observed and modelled cdfs: shown are the curves corresponding to MLE parameters and to the best and the worst performing RAM parameters. The gray shaded area represents the envelop of the annual cdfs. All parameters and the cdfs are estimated over the full record lengths.

show, the method tends however to give relatively low $k_n$ values.

### 4.5.2 Insights of the model-based approach for RAM assessment

As discussed above, most of the RAMs yield parameter ranges that are similar to the ranges obtained by MLE estimation. This suggests that the model-based approach is well suited to further assess the behavior of the different RAMs.

From the model performance perspective, the methodological choice that has the highest positive impact is the recession extraction method. The method proposed by Dralle et al. (2017b), E3, gives the most reliable results. This underlines that choosing representative streamflow portions that correspond to actual recession events is the key for robust recession parameter estimation. This result is remarkable, in particular also in the context of previous studies using the same analytical streamflow distribution model, which focused on parameter estimation methods instead of on recession extraction methods (Ceola et al., 2010; Basso et al., 2015b; Müller et al., 2014).

Compared to the choice of the extraction method, selecting the parameter estimation method only marginally impacts the results (Table 4.7). And for a given extraction method, there is no parameter estimation method that systematically outperforms the others across all case studies. This result is coherent with the conclusions of Stoelzle et al. (2013) that recession characteristics correlate strongly for methods that use the same recession extraction method. From a hydrological process view point this can be interpreted as being related to the hydrological processes that are activated during the selected recessions.

Table 4.7 – Model performance in terms of $c^{KS}$ for the nine tested RAMs; the lowest $c^{KS}$ values (best model performance) are highlighted in bold. For the model performance evaluation, the full record length is used.

| | Reference $c^{KS}$ | E1P1 | E1P2 | E1P3 | E2P1 | E2P2 | E2P3 | E3P1 | E3P2 | E3P3 |
|---|---|---|---|---|---|---|---|---|---|---|
| GOL | 0,019 | 0,121 | 0,078 | 0,118 | 0,201 | 0,117 | 0,105 | 0,061 | 0,027 | **0,024** |
| NEC | 0,016 | 0,166 | 0,137 | 0,131 | 0,227 | 0,121 | 0,110 | 0,100 | 0,071 | **0,065** |
| MUW | 0,019 | 0,130 | 0,107 | 0,115 | 0,208 | 0,172 | 0,131 | **0,057** | 0,096 | 0,084 |
| GUR | 0,012 | 0,140 | 0,250 | 0,369 | 0,187 | 0,097 | **0,078** | 0,125 | 0,131 | 0,141 |
| SEN | 0,029 | 0,111 | 0,181 | 0,254 | 0,163 | 0,176 | 0,226 | **0,042** | 0,080 | 0,087 |

### 4.5.3 Robustness of MLE estimation

Given that maximum likelihood estimation (MLE) is a parameter optimization method, it necessarily outperforms all RAMs for the full streamflow record (Table 4.7). MLE performance for short record remains in general higher than the performance of most RAMs estimated over the full record length (compare the 95% quantile of the MLE model performances for different record lengths of Table 4.8 to the performances of the nine RAMs in Table 4.7). Even the MLE estimated parameters based on a single year of data have comparable performances to the ones obtained with most of the RAMs (except those based on extraction method E3) over the entire record. The exception is the Goldach catchment, for which the RAMs present remarkably good performances.

Table 4.8 – Values of the upper 95% quantile of the model performances ($c^{KS}$) adopting MLE parameters

| | $Q_{95}^{(1)}$ | $Q_{95}^{(2)}$ | $Q_{95}^{(5)}$ |
|---|---|---|---|
| GOL | 0,113 | 0,089 | 0,063 |
| NEC | 0,117 | 0,081 | 0,051 |
| MUW | 0,140 | 0,095 | 0,058 |
| GUR | 0,169 | 0,091 | 0,054 |
| SEN | 0,137 | 0,099 | 0,061 |

This analysis underlines that MLE estimation gives in general robust results in presence of short data records.

### 4.5.4 MLE as an alternative to RAMs?

The MLE parameters obtained from the full records are close to the values obtained from the best performing extraction method E3 (Dralle et al., 2017b) (compare Tables 4.3 and 4.4 and Tables 4.5 and 4.6) and the MLE estimates obtained from much shorter records are close to these long term estimates. These results indeed suggest that the MLE in combination with the model of Botter et al. (2007c, 2009) could become an interesting alternative RAM for catchments that meet the underlying assumptions about streamflow triggering mechanisms (exponentially distributed streamflow-triggering pulses resulting from Poisson rainfall, combined to nonlinear recession behavior).

A more detailed inspection of the performance of the RAM parameters reveals that the worst performances are obtained for RAMs that lead to high values of $a$. As Brutsaert and Nieber (1977) already discussed, values of $a > 3$ are related to fast flows. And they correspond to the exact solution of the Boussinesq equation for the beginning of the recessions, when the aquifer is close to be fully saturated.

Given that the streamflow distribution model is based on slow flow generation mechanisms, we repeated the 'per event' parameter estimations excluding recessions that show values of $a > 3$ (see Table 4.9 and Figure 4.9). The new parameter sets are significantly closer to the MLE parameters, both in terms of parameter values and in terms of model performance. This reinforces that model-based parameter estimation is an interesting alternative to existing RAMs.

Compared to existing RAMs, the model-based approach is computationally more demanding (maximization of a likelihood function) and it requires rainfall time series to estimate the parameter $\alpha$, the mean depth of rainfall events. The method does, in exchange, involve limited arbitrary choices for parameter estimation (or for recession extraction methods) because it uses all available streamflow records. In particular, this also implies that the model-based parameter estimation approach includes all possible

Table 4.9 – Recession parameters obtained from the six RAM per event (parameter estimation methods P2 and P3 combined with all the recession extraction methods), excluding recession events that characterize fast flows ($a > 3$)

| | E1P2 | | | E1P3 | | | E2P2 | | | E2P3 | | | E3P2 | | | E3P3 | | |
|---|---|---|---|---|---|---|---|---|---|---|---|---|---|---|---|---|---|---|
| | $k_n$ | $a$ | $c^{KS}$ | $k_n$ | $a$ | $c^{KS}$ | $k_n$ | $a$ | $c^{KS}$ | $k_n$ | $a$ | $c^{KS}$ | $k_n$ | $a$ | $c^{KS}$ | $k_n$ | $a$ | $c^{KS}$ |
| GOL | 0,130 | 1,88 | 0,043 | 0,140 | 1,84 | 0,031 | 0,096 | 1,85 | 0,121 | 0,101 | 1,85 | 0,109 | 0,154 | 1,73 | 0,024 | 0,148 | 1,73 | 0,033 |
| NEC | 0,108 | 1,99 | 0,101 | 0,118 | 1,94 | 0,086 | 0,100 | 1,87 | 0,127 | 0,104 | 1,87 | 0,120 | 0,142 | 1,74 | 0,067 | 0,136 | 1,74 | 0,078 |
| MUW | 0,074 | 2,12 | 0,068 | 0,068 | 2,01 | 0,096 | 0,049 | 2,28 | 0,146 | 0,047 | 2,28 | 0,153 | 0,071 | 2,13 | 0,076 | 0,076 | 2,13 | 0,063 |
| GUR | 0,067 | 2,05 | 0,121 | 0,067 | 1,76 | 0,122 | 0,041 | 2,43 | 0,063 | 0,034 | 2,42 | 0,092 | 0,079 | 2,16 | 0,169 | 0,077 | 2,16 | 0,163 |
| SEN | 0,091 | 2,11 | 0,064 | 0,104 | 2,02 | 0,067 | 0,065 | 2,01 | 0,102 | 0,071 | 1,94 | 0,086 | 0,118 | 2,02 | 0,090 | 0,106 | 2,02 | 0,068 |

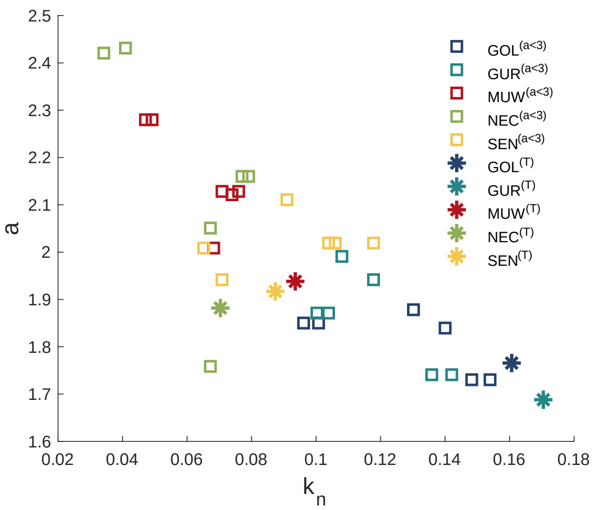


Figure 4.9 – Scatterplot of the recession parameters $a$ against $k_n$ obtained for MLE estimation (stars) and for all RAMs using 'per event' estimation (six methods per catchment, squares). All values are obtained over full record lengths. Recession events with $a > 3$ are excluded.

hydrological processes that have been activated during the observation period. This is argued to render our method robust for short-sample estimations.

Finally, it is noteworthy that this type of recession analysis framework could also be extended to other hydrological models as long as they are simple enough to guarantee unbiased parameter optimization.

### 4.5.5 Potential for new insights into recession behavior

The RAMs discussed in this chapter have been developed in the past to obtain insights in the water storage-release behavior of catchments and remain a key tool to understand low flows and water storage at catchment scale (e.g. Floriancic et al., 2018; Staudinger et al., 2017). Recent studies try to understand how the storage-release relationship is related to geomorphological and other physiographic catchment features (Biswal and Marani, 2010; Mutzner et al., 2013; Patnaik et al., 2018), with the ultimate goal to predict catchment-scale recession behavior from observable catchment characteristics. But the use of traditional RAMs for hydrological process analysis and comparative hydrology is inherently limited by the non-trivial interactions between methodological choices and resulting recession descriptors (estimated parameter values).

As shown in this chapter, the dominant source of parameter variability in traditional RAMs is the selection of recession events from observed streamflow. In rainfall dominated catchments, any decreasing event in observed streamflow either results from an actual catchment-scale recession, i.e. release of water stored in the subsurface in absence of rainfall input, or from the spatio-temporal evolution of non catchment-wide rainfall, which activates only parts of the catchment and thus leads to a decrease in streamflow. Accordingly, selecting actual representative recessions for entire catchments will remain challenging in the future. The model-based RAM proposed in this chapter overcomes this limitation by making assumptions about the stochastic nature of incoming rainfall and how it is partioned into streamflow (censoring small rainfall events). These assumptions have been shown to hold widely across the globe (Botter et al., 2013; Ceola et al., 2010; Müller et al., 2014; Santos et al., 2018). Accordingly, the model-based RAM opens new perspectives for comparative hydrology and to understand how recession behavior is linked to catchment characteristics under different climates.

## 4.6 Conclusions

Streamflow recession parameters are highly dependent on the used estimation method. Methodological choices involve two steps: the selection of recession events from observed streamflow records and the parameter estimation procedure. In this chapter, we compare the results of nine combinations of recession analysis methods (RAMs) resulting from three methods for each step. We also introduced an alternative, model-based estimation method involving maximum likelihood estimation (MLE) applied to the analytic streamflow distribution model proposed by Botter et al. (2007c, 2009). This model represents the probability distribution of daily streamflows assuming that it results from a stochastic succession of runoff-triggering rainfall events and ensuing linear or nonlinear recessions. Compared to traditional RAMs, this model-based method does not require extracting recession events from the streamflow series. Rather, it uses all available streamflow data to jointly estimate both recession parameters describing the power-law water storage-release behavior.

Comparing the full range of methods (RAMs and model-based) for different scenarios of streamflow record lengths for the selected five Swiss catchments reveals the following conclusions:

1. 'Per event' parameter estimation should not be applied in combination with a permissive recession extraction method. This, in fact, results in too variable parameter ranges, i.e. unreliable recession description.
2. The original method proposed by Brutsaert and Nieber (1977), estimating the

recession properties from all events jointly, yields too narrow parameter ranges, especially for the recession coefficient, $k_n$. This suggests that the corresponding parameter values are not representative of the actual recession behavior of a catchment, a conclusion that is supported by the low model performances obtained for this method.

3. The recession selection method is fundamental for reliable recession parameter estimation; some combinations of RAMs bias the parameter values, with ensuing low model performances for the model used in this chapter.

The restrictive extraction method, E3, provides parameters that are very similar to the model-based MLE estimates. This underlines that for classical RAMs, the selection of events and the hydrological processes activated during these events is crucial for recession analysis. It also supports the potential of the new, model-based parameter estimation approach as an interesting alternative to currently used RAMs; it represents an effective way of including all available observed data in terms of streamflow and rainfall, with potentially reduced sensitivity to observational errors typical occurring during very low flows.

Extending the recession analysis approach into a fully Bayesian framework to estimate posterior parameter distributions rather than single estimates would shed more light on the role of observational errors for recession parameter variability. This would in particular also bring new insights into which part of parameter variability stems from actual parameter errors, i.e. from the fact that actual parameters are not constant as assumed by the model.

Future work will also show if the recession parameters obtained from the model-based approach can be directly transferred to more complex hydrological models that use similar assumptions about streamflow recession and the potential of the approach for other hydro-climatological regimes, such as snow dominated or to semi-arid regimes. Finally, we would like to emphasize that the proposed method opens new perspectives for catchment classification and similarity assessment, capitalizing on an explicit separation between similarities in the rainfall forcing and similarities in recession behavior and underlying dominant hydrological processes.

# 5 Seasonal recession parameters in Switzerland

*In this chapter we expand the analyses presented in the previous chapters to answer the following questions: For pluvial regimes, how do the different recession analysis methods (RAMs) perform with respect to the analytical streamflow distribution model used in this thesis considering seasonal estimates? How variable are seasonal estimates of linear and nonlinear recession parameter estimates as compared to estimates based on annual data? And how do different recession estimation methods perform not only for nonlinear recession, as in Chapter 4, but also for linear recessions? The analyses are based on six Swiss case studies (including those from Chapter 4 and the Areuse catchment), three recession extraction methods and five parameter estimation methods: two for linear recessions and three for nonlinear recessions. The overall findings of these analyses are that the seasonal parameters are as good as annual parameters, especially for the nonlinear recessions, and they do not vary significantly along the year. For linear recessions, in general the methods per event result in high parameter values while methods based on a master recession curve result in low parameter values, but there is no methodological choice that results systematically in better results. This establishes a better basis for the estimation of recession parameters to be used with the model in broader contexts.*

## 5.1 Introduction

A hydrological recession is the gradual depletion of the streamflow in periods with scarce or no precipitation (Tallaksen, 1995). The literature proposes a wide range of recession analysis methods (RAM) to obtain recession parameters. Santos et al. (2019) explored the subject from view point of a streamflow distribution model framework and proposed a new approach to obtain recession parameters. The present chapter expands the analyses and presents some important complementary results.

As in the previous chapters, we refer to the method developed by Botter et al. (2007c), who described a simple physically-based model framework to estimate the probabilistic distribution of daily streamflows in rainfall-dominated regimes considering a stochastic rainfall forcing and a linear decay of streamflow due to the release of water from the subsoil. Within the framework allowed by those assumptions, daily streamflows follow a gamma distribution characterized by the mean depth of rainfall, the frequency of the rainfall events that produce streamflow, the area of the catchment and the mean residence time of the catchment (i.e. the inverse of the linear recession parameter). Later, Botter et al. (2009) extended the same streamflow distribution model framework to nonlinear recessions. This framework assumes steady state conditions, which generally implies its application on a seasonal basis.

Chapter 4 applied the model framework by assuming nonlinear recessions to five pluvial Swiss catchments with approximately analogous conditions around the entire year and studied different combinations of recession extraction and parameter estimation methods. It also investigated how the use of maximum likelihood estimates together with the model framework compares with usual RAMs and how both methods behave for short streamflow records. Two main gaps exist related to the original model assumptions: i) a comparison of linear recessions obtained from different RAMs, and ii) an analysis of seasonal recessions obtained from different RAMs The present chapter expand the work from Chapter 4 to fill those gaps.

RAMs can be divided into two steps: i) recession extraction, and ii) parameter estimation. We have chosen to test the combination of three recession extraction methods and five parameter estimation methods: two for linear recessions and three for nonlinear recessions, for seasonal and annual daily streamflow distribution curves. We tested them for six pluvial Swiss case studies with long term streamflow records.

The chapter is organized in six sections. Section 5.2 shortly describes the new RAMs and methods to assess the model performance. Section 5.3 presents the case studies. The obtained results for the linear and nonlinear model versions are presented in Section 5.4 and are discussed in Section 5.5 and the conclusions are summarized in Section 5.6.

## 5.2 Methods

### 5.2.1 Application time intervals

The model framework is suitable for steady-state conditions, at an annual or a seasonal scale, depending on the temporal variability of the model parameters (Botter et al., 2007a). Because of that, it is mostly applied separately to meteorological seasons (Basso et al., 2015b; Botter et al., 2013; Ceola et al., 2010; Müller et al., 2014): winter (01-December to 28-February), spring (01-March to 31-May), summer (01-June to 31-August) and autumn (01-September to 30-November).

However, annual daily streamflow distributions are of practical value. If the variation of model parameters (i.e. the recession parameters and the stochastic parameters) along the year is negligible, we can assume that the conditions are steady state and annual curves can also be obtained by the direct estimation of annual parameters, as done by Santos et al. (2019). Another possible approach to calculate annual streamflow distribution curves was proposed by Botter et al. (2008), who state that, for the linear model, the annual curve should be obtained by weighting the parameters of the underlying seasonal distributions. These authors used numerical investigations to show that for catchments where the model parameters do not vary significantly along the year, the temporal averaging of the seasonal model parameters leads to satisfactory estimates of the annual curves. We tested both approaches to obtain annual curves for the linear and nonlinear models. First, we tested the direct calculation of curves for the complete year (called hereafter Year C), then the calculation based on the temporal averaging of the seasonal model parameters (called hereafter Year S).

### 5.2.2 Stochastic inputs parameters

The model parameters related to the stochastic inputs are common to the linear and the nonlinear model. They are: the mean precipitation depth, $\alpha$, and the streamflow producing frequency, $\lambda$. Their estimation methods are the same as in Chapter 4.

Because here we adopt a seasonal basis, the values for maximum daily interception to be discounted from precipitation before the calculation of parameters are different. For summer it is obtained from land use and the maximum interception is set to 4 mm for forests, 2 mm, for low vegetation, 1 mm for impervious areas and 0 mm for water bodies (Gerrits, 2010; Santos et al., 2018). For winter, it is considered to be 1 mm. For spring and autumn, we considered a mean between the values for summer and winter. The maximum interception for any season is considered to be at least 1 mm.

### 5.2.3 Deterministic recession parameters

The recession parameters are obtained from streamflow observations adopting maximum likelihood estimation (MLE), that serves as a reference and by the aforementioned different RAMs. The combinations of methods result in six RAMs for linear recessions and nine RAMs for nonlinear recessions.

#### Recession extraction

There is a variety of methods that can be used to identify recession periods and literature reports that the choice of the method can influence the parameter values (Dralle et al., 2017b; Santos et al., 2019). Recessions comprise periods without precipitation or overland flow and with decreasing streamflows, but many features can be used to make a more refined selection of periods and to obtain representative recessions. We have chosen three methods for recession extraction to be tested for both, linear and nonlinear models. Two of those methods, E1 and E3, are the same as for Chapter 4, they are the simplest permissive method and the one with the best results. Since the method E2 was neither remarkably simple nor good, we have chosen to change it for another method.

1. E1: Includes all segments of observed streamflows that decay for at least two consecutive days (Santos et al., 2019).
2. E2: Includes the segments of observed streamflows for which the 3-days moving averages decrease for at least 10 consecutive days (Vogel and Kroll, 1992).
3. E3: Suggested by Dralle et al. (2017b), includes the segments of observed streamflows with a minimum length of four days, an upward concavity requirement and a peak selectivity criterion, which is selecting only recessions that begin with a streamflow observation higher than the mean streamflow in the period of analysis (Biswal and Marani, 2010; Mutzner et al., 2013; Santos et al., 2019).

#### Parameter estimation methods

We tested methods based on the master curve and the per event approaches for linear and nonlinear recessions. Two methods were tested for the linear model and three for the nonlinear model. For the linear model, the methods were:

1. PL1: Linear regression of $Q$ versus $-dQ/dt$ of the master recession curve (Brutsaert and Nieber, 1977). The values of $Q$ are the means of the same values of daily streamflows for two successive days used to calculate $-dQ/dt$.
2. PL2: Estimates the recession parameter as the median of recession coefficients from a linear regression of individual recessions.

For the nonlinear model, the methods were the same as the ones adopted by Chapter 4, namely:

1. PN1: Linear regression of the master recession curve $\log(Q)$ against $\log(-dQ/dt)$ (Brutsaert and Nieber, 1977).

2. PN2: Each recession event is linearized by adopting a log-log scale and fitted by linear least squares. The exponent of the recession ($a$) is the median value of the fitted $a$ values, then, $a$ is fixed and curves are fitted again to estimate $k_n$ as the median of all recalculated $k_n$ values (Mutzner et al., 2013; Basso et al., 2015b).
3. PN3: Is the per event "decorrelation method" (Dralle et al., 2015). The first step is to fit curves to each of the $j$ selected recessions, obtaining a set of parameters $k_{nj}$ and $a_j$. Then the streamflow values are rescaled by a constant $q_0$ and the rescaled recessions are fitted according to a coefficient (Equation 4.2), curves are fitted again and the parameters are the medians of the new fitted parameters.

### 5.2.4 Evaluation criteria

We evaluated the results in two different ways: i) qualitatively by a comparison with the reference MLE results and ii) quantitatively by their effect on model performances. The evaluation based on the model performance has the advantage of considering the joint effect of the pair of parameters. The performances of the model adopting the different recession parameters were assessed in relation to the empirical long-term cumulative distribution function (cdf) of daily streamflow adopting the Kolmogorov-Smirnov distance ($c^{KS}$). This indicator corresponds to the maximum distance between the analytical cdf and the empirical cdf, (Ceola et al., 2010; Santos et al., 2018, 2019; Schaefli et al., 2013).

## 5.3 Case studies

The methods for recession analysis and the probabilistic daily streamflow distribution model were applied to six case studies in Switzerland, selected based on three main criteria: i) gauged catchments with unperturbed streamflows (i.e. minimal anthropogenic influence), ii) with a predominantly rainfall-dominated regime, and iii) with at least 40 years of streamflow and precipitation observations (from 1975 to 2014). We did not apply a criteria of non-karsticity, so we added one more case to the cases in Chapter 4, the Areuse. Figure 5.1 shows the location of all the case studies and Table 5.1 shows their key characteristics.

Daily streamflow data for each catchment were provided by the Swiss Federal Office for the Environment (FOEN) (FOEN, 2017) and daily precipitation data were extracted from a gridded database (MeteoSwiss, 2011). Further description about the data can be found in Santos et al. (2018, 2019).

## 5.4 Results

Each RAM is identified by the combination of the codes for the recession extraction method and the parameter estimation method presented in Subsection 5.2.3. We present

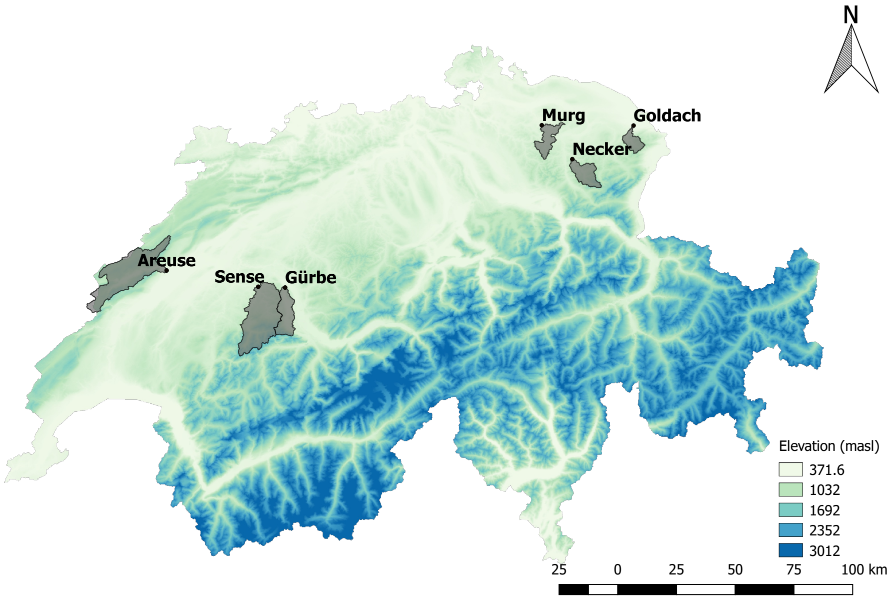


Figure 5.1 – Localization of the six Swiss case studies over a topographic map

Table 5.1 – Characteristics of case studies as given in the FOEN database, including the period for which streamflow and gridded precipitation are available; $P$ stands for the weighted mean annual precipitation, and $\overline{T}$ for the weighted mean annual temperature

| ID | Code | Name | Coordinates (CH1903) | Area ($km^2$) | Mean elevation (m) | Station elevation (m) | P (mm/year) | $\overline{T}$ ($^oC$) |
|---|---|---|---|---|---|---|---|---|
| 2308 | GOL | Goldach - Goldach, Bleiche | 753190 / 261590 | 49.8 | 833 | 399 | 1446 | 7,39 |
| 2374 | NEC | Necker - Mogelsberg, Aachsäge | 727110 / 247290 | 88.2 | 959 | 606 | 1777 | 6,47 |
| 2126 | MUW | Murg - Wängi | 714105 / 261720 | 78.9 | 650 | 466 | 1357 | 7,90 |
| 2159 | GUR | Gürbe - Belp, Mülimatt | 604810 / 192680 | 117.0 | 837 | 522 | 1295 | 7,21 |
| 2179 | SEN | Sense - Thörishaus, Sensematt | 593350 / 193020 | 352.0 | 1068 | 553 | 1479 | 6,29 |
| 2480 | ARE | Areuse - Boudry | 554350 / 199940 | 377.0 | 1060 | 444 | 1531 | 5,41 |

here only selected results; complete tables with all the calculated parameters and related model performances can be found in Appendix C.

### 5.4.1 Variability of recession parameters over the year

The climate in the selected Swiss case studies is humid, with precipitation well distributed all over the year, as shown by the seasonal stochastic input parameters in Figure 5.2 . Because of that, the recession parameters do also not vary strongly neither (Figure 5.3).As we will see later on, the variation among the parameters for one catchment adopting a specific RAM is smaller than the variation among the values obtained from different RAMs for a single season in a catchment.

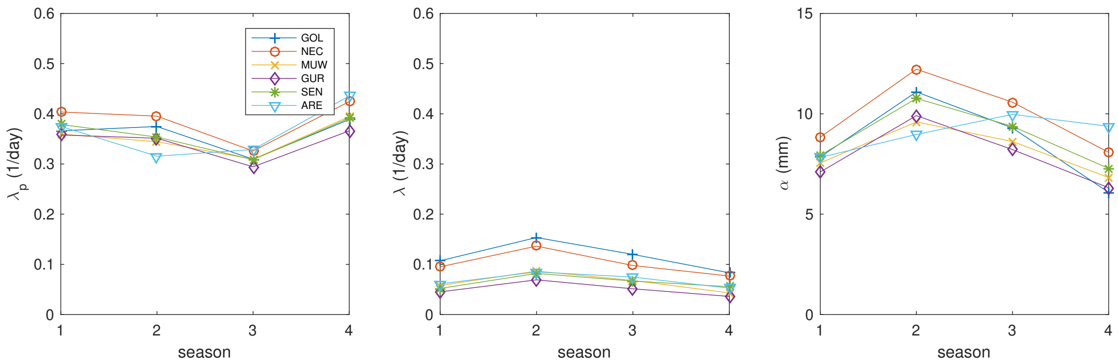


Figure 5.2 – Evolution of the stochastic parameters ($\lambda$, $\lambda_p$ and $\alpha$,) over the meteorological seasons in each catchment. On the abscissas: 1 stands for spring (01-Mar-31-May) , 2 for summer (01-Jun-31-Aug), 3 for autumn (01-Sep-30-Nov)), and 4 for winter (01-Dec-28-Feb)

### 5.4.2 Annual parameter values

This subsection presents only results for the annual time scale with parameters estimated once for the complete year (Year C) as a consequence of the small variation between the seasonal parameters shown in the previous subsection. Complete tables with parameters values can be found in Appendix C.

Figure 5.4 shows a comparison between the annual parameters obtained by the selected RAMs and MLE for the linear recession. The range of parameters for all the catchments vary between the RAMs, but is narrow for each RAM, except for E3PL2. Comparing the parameter estimation methods (i.e. the columns in Figure 5.4), the per event method (PL2) tends to result in higher values, in terms of recession extraction. E3 also leads to higher values, but overall the results from E3PL2 are much higher than the other results and completely off the range of the other RAMs, but not of the MLE values. In general, the parameter values are low for PL1, so it works better for catchments with low recession parameters. They tend to become much higher for PL2, which consequently works better for catchments with high recession parameters. There is no trend of general improvement for any method.

The nonlinear recession parameters are presented in Figure 5.5. Both parameters for the master curve estimation method PN1 are always more precise (i.e. less variable) than those estimated using the methods per event, PN2 and PN3 (compare columns of Figure 5.5). The PN1 values are also closer to the MLE values in terms of the recession exponent ($a$) but are mostly underestimated in terms of recession coefficient. On the other hand, the decorrelation method for parameter estimation (PN3) results in higher recession coefficients (even if still underestimated), but the values of recession exponent obtained by this method are mostly overestimated. The simpler per event method, PN2, had the worst results, overestimating $a$ and underestimating $k_n$. The choice of an extraction method (i.e. the rows in Figure 5.5) has an important role in the results, especially for the methods per event. As already pointed out by Santos et al. (2019), results for the

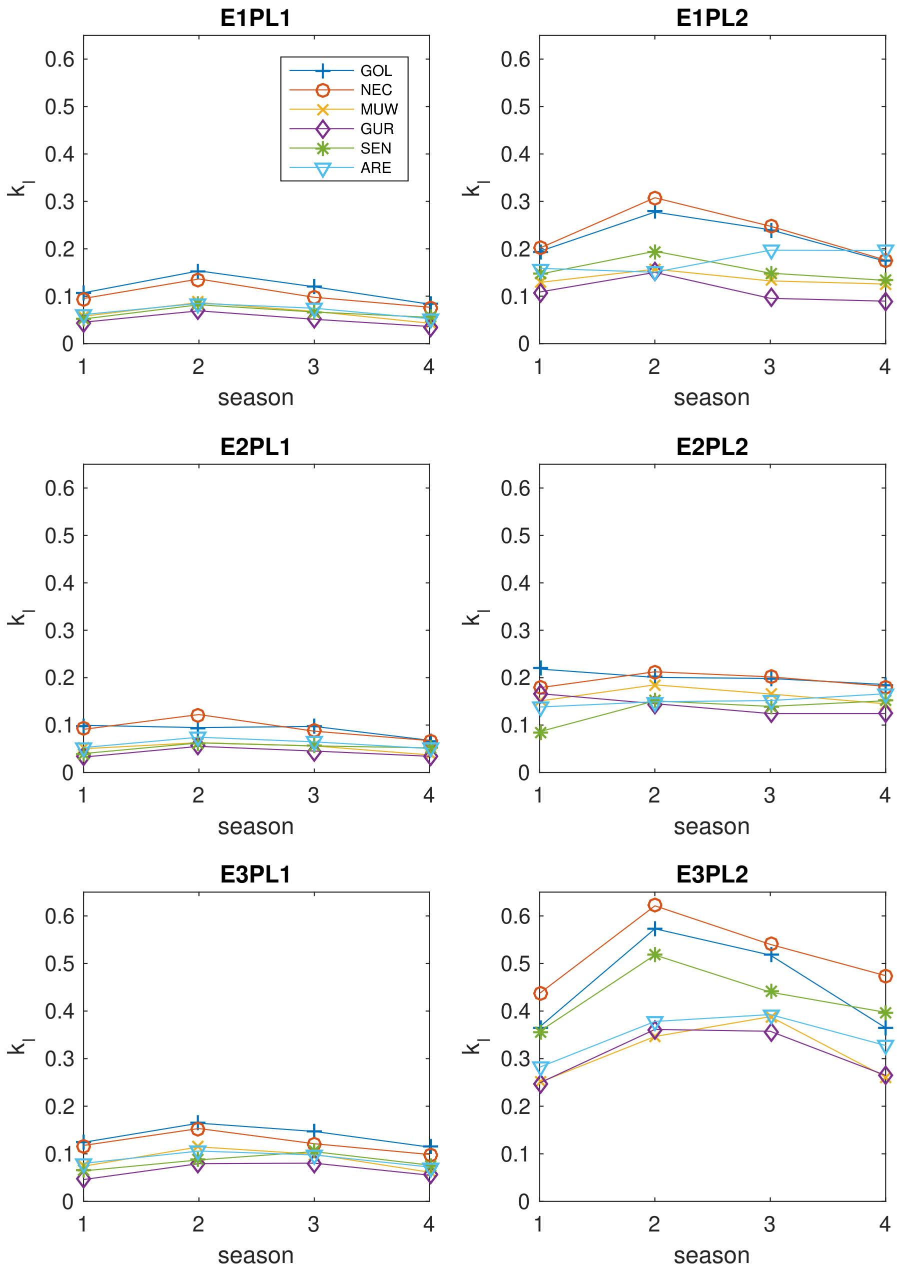


Figure 5.3 – Evolution of the linear recession parameters over the meteorological seasons in each catchment. On the abscissas: 1 stands for spring, 2 for summer, 3 for autumn, and 4 for winter

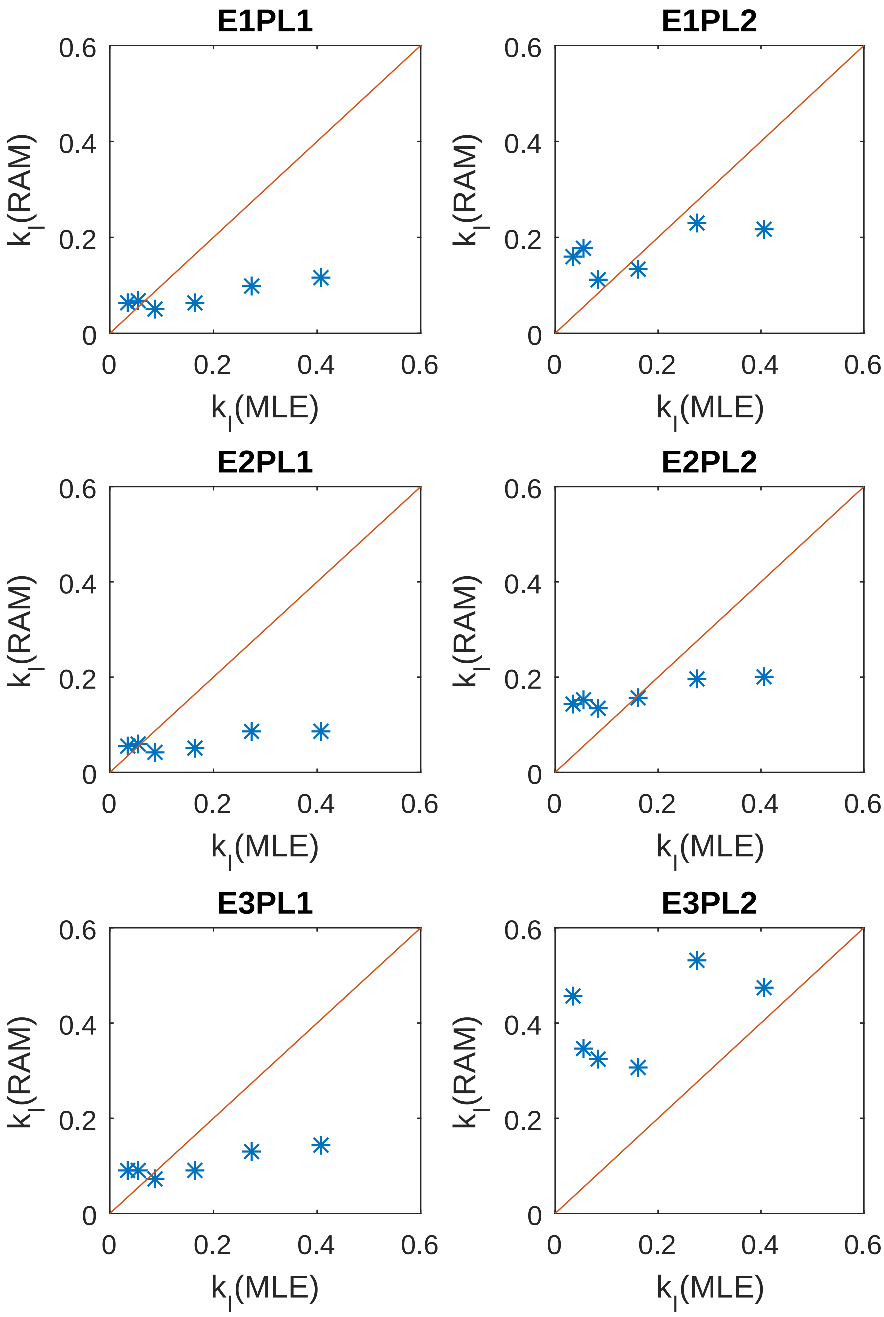


Figure 5.4 – Comparison between model parameters obtained by RAM and by MLE for each RAM combination for linear recession applied to all case studies

extraction method E3 are remarkably good; but the extraction method E2, that was not studied by Santos et al. (2019), also improves the quality (i.e. parameter values closer to MLE parameters) for the methods per event, albeit without yelding better results than E3.

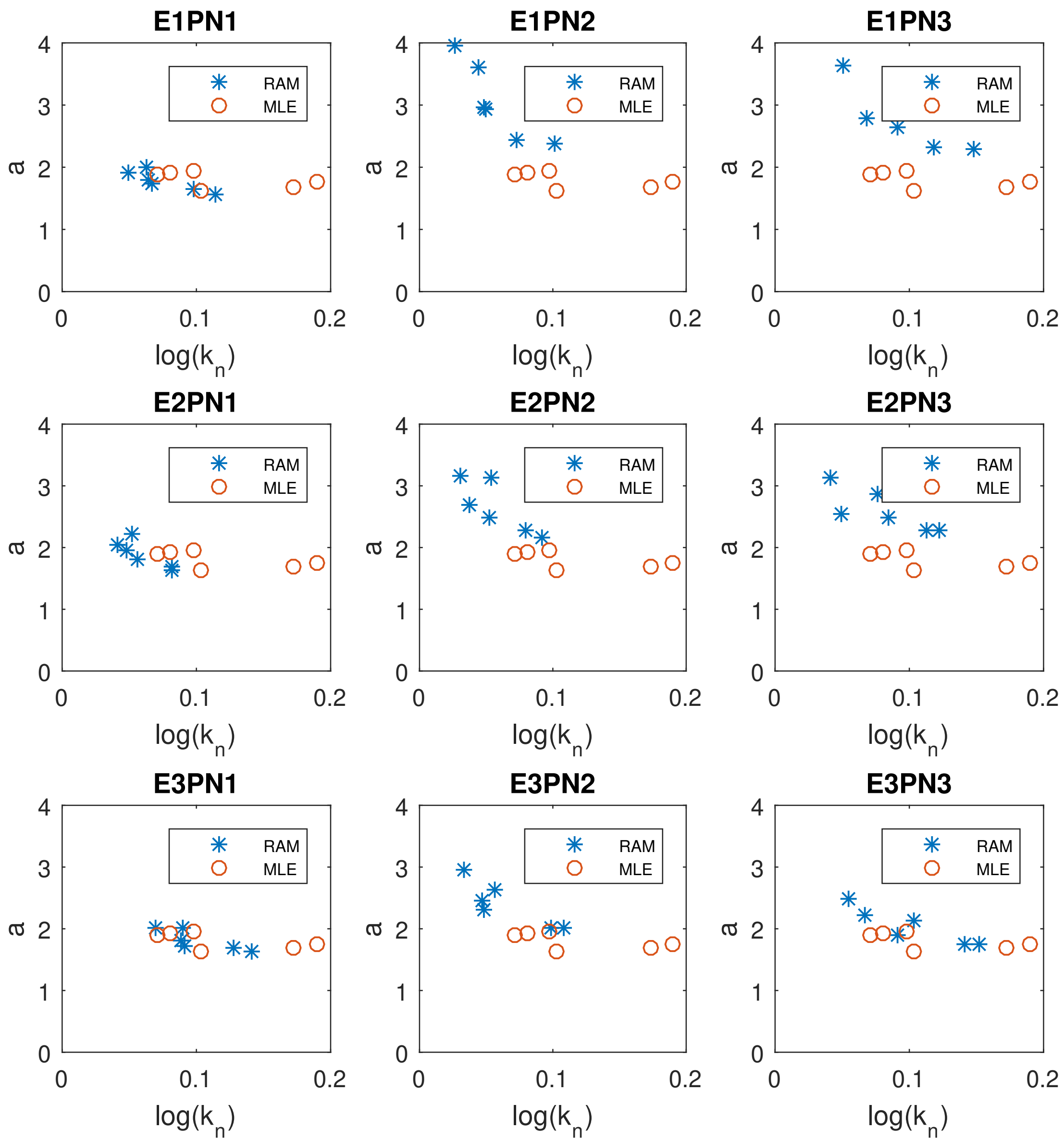


Figure 5.5 – Comparison between model parameters obtained by RAM and by MLE for each RAM combination for nonlinear recessions applied to all case studies.

### 5.4.3 Model performance

The model performance for all RAM parameters was measured by the Kolmogorov-Smirnov distance, $c^{KS}$, according to which the best values are the lowest ones. The

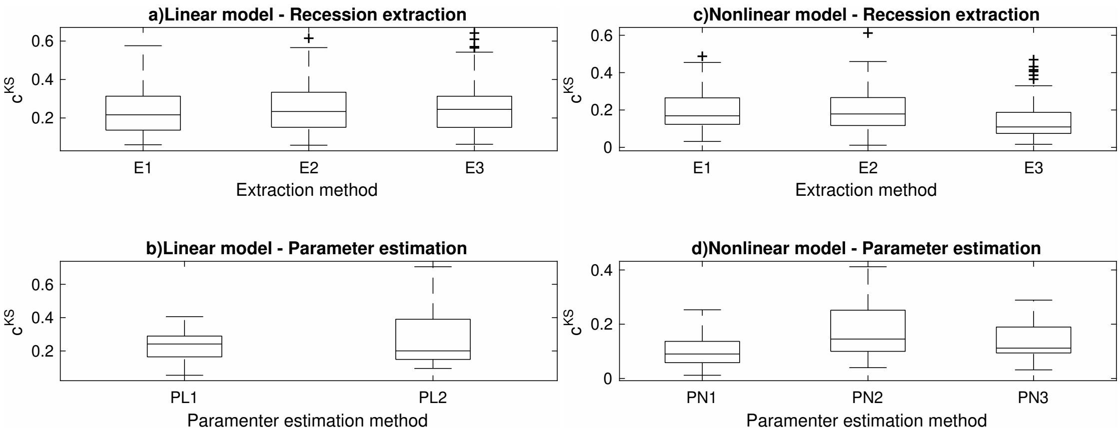


Figure 5.6 – Boxplots representing the comparison of the model performances for each RAM for the linear and nonlinear model with results aggregated per extraction method (a and c) and per parameter estimation method (b and d)

comparison between the extraction methods (Figure 5.6 a and c) shows that the linear recession parameters are not strongly affected by the extraction method, with similar median and variability. For the nonlinear recessions, the extraction method E3 gives better model performances, in terms of median and variability. The parameter estimation method (Figure 5.6 b and d) on the other hand, strongly affects the linear recessions and the parameter estimation method per event (PL2) is the one with better performances, but it is highly variable in comparison to PL1. For nonlinear recessions, the parameter estimation methods PN1 and PN3 show better performances.

We can also analyze the combinations of methods, which was first done by counting the number of times the performance for each RAM outperformed the performance for other RAMs, as shown in Table 5.2. This analysis takes into account the performance for each catchment for the four meteorological seasons and for Year C, resulting in 30 points of analysis for both, the linear and the nonlinear models. The annual results for the weighted parameters (i.e. Year S) were excluded of this analysis to avoid a bias. Table 5.2 shows that for the linear model, the best combination of methods was E3PL2, closely followed by E1PL2 and E2PL1, then by E3PL1. For the nonlinear model, the best combination was E3PN3, followed by E3PN1 and the results for every combination based on E2 and on PN2 are remarkably bad (i.e. 0 or 1 counts).

Table 5.2 – Number of times each combination of methods outperformed the others (lowest $c^{KS}$) for each catchment and each season and the complete year (Year C).

| | Linear | | Nonlinear | | |
|---|---|---|---|---|---|
| | PL1 | PL2 | PN1 | PN2 | PN3 |
| E1 | 2 | 6 | 5 | 1 | 2 |
| E2 | 6 | 4 | 0 | 1 | 0 |
| E3 | 5 | **7** | 9 | 0 | **12** |

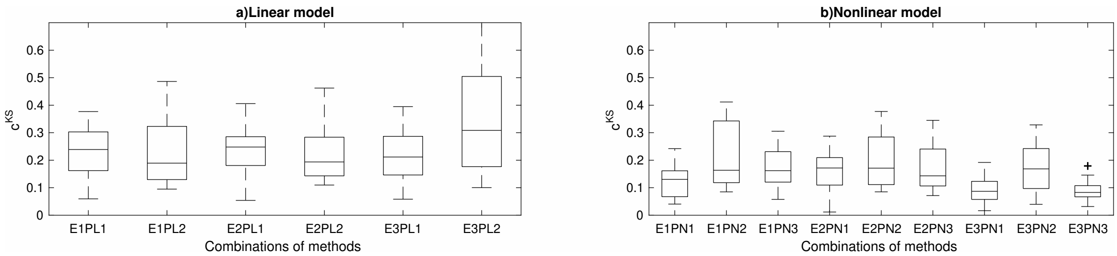


Figure 5.7 – Boxplots representing the variation of the model performances for each RAM for the linear (a) and nonlinear model (b)

Figure 5.7 brings more details about the model performances for each RAM and shows the variability of $c^{KS}$ for each combination of methods for each meteorological season and for Year C. For linear recessions, the combination E3PL2 has a very high variability despite the number of times it outperforms the others, implying that it has very good results for some cases and very bad results for others. E1PL2, E2PL1, and E3PL1, on the other hand, are slightly worse in terms of the number of times they outperform the other RAMs but they vary less and are better in general. The nonlinear results are coherent with Table 5.2, with the combination E3PN3 also being the best in terms of median and variability.

### 5.4.4 Seasonal model performance

The model performances can also be studied from a seasonal point of view. We present the results for one combination of methods for each type of recession to exemplify how the performances change from season to season. We have chosen the method combination according to the results shown in Table 5.2 and Figure 5.7. For the nonlinear model, the combination E3PL3 is remarkably good in both, Table 5.2 and Figure 5.7b. This method thus clearly outperforms the others. For the linear model, the choice of the best combination is not evident, but because E3PL1 shows good performances according to both criteria, we have chosen this RAM to exemplify the seasonal linear results. Figure 5.8 shows the seasonal model performances for all the catchments for these chosen RAMs. The nonlinear model clearly outperforms the linear one, when considering either best results for the Autumn or the worst ones for the Winter. On the other hand, it is difficult to identify the season with best and worse results for the linear model because model performances are highly variable for all the seasons.

### 5.4.5 Model framework on an annual basis

Comparing the results for annual estimations based on a single estimation of parameters for the complete year and those based on the weighted seasonal values (i.e respectively Year C and Year S), the calculation based on Year C yields better model performances than Year S. Figure 5.9 presents that comparison for the nonlinear recession parameters

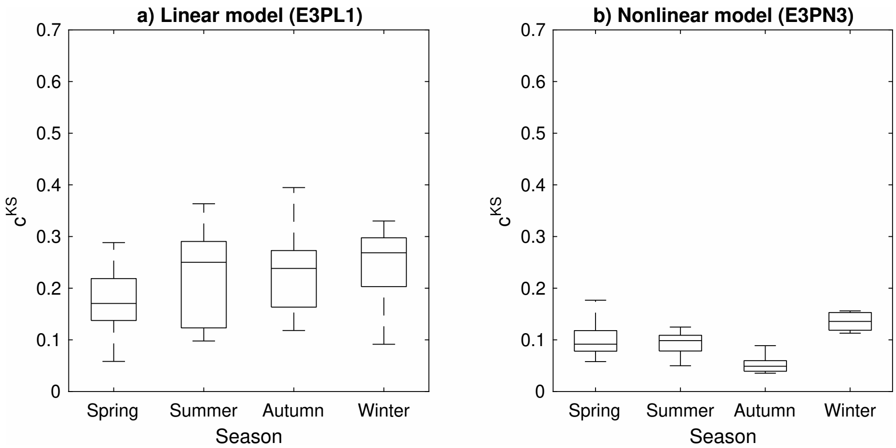


Figure 5.8 – Comparison between the model performance for each season for the combination E3PL1 for the linear model (a) and E3PN3 for the nonlinear model (b).

obtained with recession extraction E3 and all the parameter estimation methods. That confirms that the assumption of applying the model to the complete year made by Santos et al. (2019) can be hold for those cases.

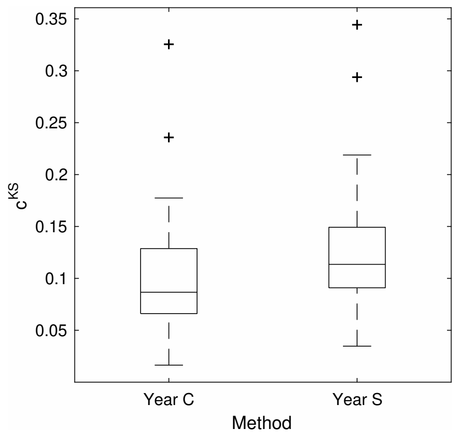


Figure 5.9 – Comparison between the results obtained for E3 for a single annual application and weighted seasonal parameters for all the catchments adopting the nonlinear model. The reported values correspond to the $c^{KS}$

## 5.5 Discussion

The recession parameters in the study catchments do not vary strongly along the year, allowing the study of the RAM on an annual basis with the assumption of single parameters calculated based on all the data or based on the ponderation of the seasonal parameters, as suggested by Botter et al. (2008). The calculation of single annual parameters, which was not tried before by other authors with the model framework, gives better results than the seasonal application. The calculation of recession parameters for the full year is novel just in the context of the model framework, Mutzner et al. (2013) calculated nonlinear annual parameters for the same cases and the results are close to ours in terms of ranges and also in terms of comparison between methods. Those authors also found that the Brutsaert and Nieber (1977) method gives lower values for the recession exponent ($a$) but did not study $k_n$, which hinds a comparison with our results.

For the linear recessions, the Brutsaert and Nieber (1977) method is good when the recession parameters are low, but tends to underestimate the parameters when they are higher. For those cases, the methods per event tend to work better because they tend to result in higher parameter values. Higher parameters values obtained from methods per events were also observed before for nonlinear recessions by Stoelzle et al. (2013).

Regarding the nonlinear recession parameters, one of the most used RAMs is the Brutsaert and Nieber (1977) method for nonlinear recessions and its results are remarkably good for $a$. This agrees with the argument of those authors that this method reduces the uncertainties in recession parameters estimation. Different studies also say that $k_n$ depends on soil moisture conditions and that $a$ is more related to the (more static) geomorphological characteristics of the catchment (Biswal and Marani, 2010; Biswal and Nagesh, 2014; Brutsaert and Nieber, 1977; Dralle et al., 2017b) however, our results varied more in relation to $a$ than in relation to $k_n$; seasonal results also confirm this statement.

Regarding nonlinear seasonal results, it is worth to mention that the worst results are the ones for winter (see Fig. 5.8). This season showed higher values of recession exponent in general, which implies that recessions are faster and may be more difficult to characterize.

## 5.6 Conclusions

Our results show that the model performances are strongly affected by the recession parameters, which are themselves highly affected by methodological choices made in their estimation. For the nonlinear model, between the two main methodological choices, namely recession extraction method and parameter estimation method, the one that affects overall results more strongly is the recession extraction method. Again, the recession extraction method that gave the best results was the one proposed by Dralle et al. (2017b) (E3), confirming the results from Santos et al. (2018). In terms of parameter estimation, PN1 is remarkably good to estimate the recession exponent ($a$) but underestimates the recession coefficients $k_n$, which is unsuitable for the model. Accordingly, the decorrelation parameter estimation method (PN3) works better, but must be applied to recessions selected with a strict method.

Linear recession parameters vary even more according to the RAM. In this case our results do not allow us to recommend a single combination of methods and it is better to use MLE if possible. We can only observe that the method based on the master curve, PL1, results in lower values of recession parameters than those for the per event methods, PL2, and consequently PL1 performs better for catchments with lower recession parameters and PL2 works better with catchments with higher parameters.

In terms of the estimation of annual flow duration curves, the quality of the annual results does not differ significantly from the seasonal results. In general, the results considering a full year are better than the ones obtained weighting seasonal parameters.

A study like this establishes a better basis for the estimation of recession parameters to be used with the model in different contexts that include not only annual nonlinear recession parameters, but also seasonal parameters and linear recession parameters, which can be useful in model applications.

# 6 Analytical annual streamflow distribution model for mountain catchments

*This chapter proposes an extension to the analytical streamflow distribution model studies in the previous Chapters to high flows in Alpine catchments in particular, in catchments where snow and glacier hydrology plays a major role. This extension adds to previous descriptions of daily streamflows for rainfall-driven regimes and of winter low flows and allows a description of the streamflow distributions all over the year in snow-dominated and glacier catchments, that have major relevance in water supply in many regions. We build on the model proposed by Botter et al. (2007c) by redefining the seasons of model application into an accumulation season and a melting season. Then we generalized a previous approach to winter flows (Schaefli et al., 2013) to estimate the amount of water accumulated as snow that is transferred to the melting season and incorporated to the model as equivalent precipitation. We tested this approach for ten Swiss catchments endowed with snow-dominated and glacier regimes. The novel framework yields good model performances even for the glacier catchments, for which some assumptions seem less viable. The proposed methodology may provide yet another perspective for the management of water resources in Alpine regimes.*

## 6.1 Introduction

Streamflow generating processes vary temporally and spatially according to the underlying climate conditions. In pluvial regimes, streamflow is generated in response to rainfall. In snow dominated regimes, typical for Alpine catchments with mean elevation higher than 1500 m asl. (Milano et al., 2015), streamflow is not only generated in response to rainfall but also by the melt of snow accumulated during the cold season. In glacier regimes, which are found in Switzerland in catchments with a significant part of the contributiong area above above 3500 m asl. (FOEN, 2013; Weingartner and Aschwanden, 1992), there is also an inter-annual storage of water in form of ice, which results in relatively constant streamflow production during the summer, when the melting conditions are playing a significant hydrologic role.

In snow-influenced catchments, the triggers of streamflow production vary throughout the year. In Alpine catchments, with often relatively low precipitation seasonality, the main driver of streamflow variations is air temperature. When air temperature is below some threshold, typically close to zero degree (Harpold et al., 2017), precipitation can be assumed to occur in the form of snow that accumulates on the ground; streamflows during this accumulation season are low (Schaefli et al., 2013). As air temperature in the catchment raises above zero degree, snow melt starts occurring. Streamflow resulting from snow melt and rainfall increases gradually throughout the melt period before decreasing again when either all the snow accumulated during the accumulation period is melted or, in catchments with permanent snow and ice, when air temperatures start falling again. During this period of decrease of streamflow, streamflow generation switches gradually from melt- and rainfall-driven to exclusively rainfall-driven, with the highest catchment parts potentially experiencing already the first snowfall events of the next accumulation season.

A typical way to represent the variability of streamflow in a river section is by flow duration curves, which represent the probability of exceedance of streamflow as a function of time. Botter et al. (2007c) developed an analytical description of such streamflow probability distributions as the result of subsurface flow pulses triggered by stochastic rainfall inputs that are censored by the soil moisture dynamics. The resulting streamflow distribution is characterized by only a few parameters: the mean rainfall depth on rain days, the frequency of rainfall events that produce streamflow and the mean recession coefficient of the catchment.

In the past, this streamflow distribution model was applied to rainfall-driven regimes across the globe (Botter et al., 2007c, 2009, 2013; Ceola et al., 2010; Santos et al., 2018), generally excluding explicitly seasons potentially affected by snow accumulation or melt processes (Botter et al., 2007a, 2013; Ceola et al., 2010; Doulatyari et al., 2015).

In this chapter, we propose an extension of the modelling framework of Botter et al. (2007c) to describe high flows during warm seasons in snow-influenced catchments. This adds to the extension proposed by Schaefli et al. (2013) for streamflow distributions during winter and yields streamflow distributions of snow-influenced catchments for the entire year, i.e. including the cold seasons (i.e. winter) low flows and warm seasons (i.e. spring and summer) high flows and incorporating the contributions of snow and glacier melt. The work presented here builds upon the work of Santos et al. (2018) that tested the model framework for summer flows in catchments with snow processes and concluded that the melt-related increase in summer streamflow can be incorporated in the stochastic modelling framework as an increase in the frequency of streamflow producing events. Some of the developments in this chapter draw on the model framework extension and numerical tests of Müller et al. (2014), who successfully modelled streamflow distributions in seasonally dry climates.

The presented developments are based on case studies from Switzerland, an Alpine country with different climates and elevations ranging up to 4634 m asl., which covers a wide range of mountainous hydrological regimes. The described model framework was applied here successfully in the past (Basso et al., 2015b; Doulatyari et al., 2017; Santos et al., 2018; Schaefli et al., 2013).

The chapter is organized as follows: Section 6.2 presents the methods used in this chapter, Section 6.3 provides a description of the case studies. Results are presented in Section 6.4, followed by their discussion (Section 6.5). The conclusions are summarized in Section 6.6.

## 6.2 Methods

We hereafter present the extension proposed to periods when streamflow is affected by glacier and/or snow melt and the criteria to identify the seasons of application of the model (i.e. accumulation and melting season). Then, we present the methods used for parameter estimation and the model performance assessment.

### 6.2.1 Model extension to snow-dominated catchments

#### Accumulation season

Schaefli et al. (2013) extended the analytical model in its linear version (Eq. 2.4) to account for snow accumulation occurring during winter in Alpine catchments. The extension is based on considering that low winter streamflows can be assimilated to a slowing down of the hydrologic response, and therefore to a reduction of the effectively contributing area. This which can be accounted for by an increase of the time scale associated with the hydrologic response (the inverse of the recession coefficient) and by a decrease of the responsive area of the catchment. The following relation has been derived for the streamflow pdf (Schaefli et al., 2013):

$$p(Q^{(w)}, t \to \infty) = \frac{1}{\Gamma\left(\frac{\lambda_p^{(w)}}{k^{(w)}}\right)} \frac{1}{Q} \left[\frac{Q}{\alpha^{(w)} k^{(w)} (1 - \frac{A^*}{A})}\right]^{\frac{\lambda_p^{(w)}}{k^{(w)}}} \exp\left[-\frac{Q}{\alpha^{(w)} k^{(w)} (1 - \frac{A^*}{A})}\right], \quad (6.1)$$

where $\lambda_p^{(w)}$ is the frequency of precipitation events during winter, $k^{(w)} = (\tau^{(w)})^{-1}$ is the winter recession coefficient, $\alpha^{(w)}$ is the mean depth of precipitation on days with precipitation, $A$ is the catchment area and $A^*$ is the non-responsive area of the catchment during the winter. $\tau^{(w)}$ is obtained as the sum of $\tau + \tau_D$, where $\tau$ is the residence time during periods without snow influence and $\tau_D$ is the delay caused by the presence of snow. In the original formulation of Schaefli et al. (2013), the winter was taken conventionally as the yearly period ranging from December to February. In the following, we adopt the more general term *accumulation period* and allow it to be of varying length (see Section 6.2.2).

The above extension for the accumulation period has to be completed with a proper model extension for the melting period. Based on the aforementioned assumptions, the precipitation that falls on the non-responsive area of the catchment does not generate streamflow; rather it is stored in the snowpack and produces streamflow later, in the melting season. The stored (accumulated) water can be quantified as:

$$S^{(a)} = \lambda_p^{(a)} \alpha^{(a)} l^{(a)} \frac{A^*}{A}, \quad (6.2)$$

where $\lambda_p^{(a)}$ is the precipitation frequency in the accumulation period, $\alpha^{(a)}$ is the mean depth of precipitation in the accumulation period, $l^{(a)}$ is the length of the accumulation period and $S^{(a)}$ is the specific accumulated water volume, ie. the volume of accumulated water divided by the catchment area.

#### Melting season

When air temperature raises above 0°C, the melting period starts, with a significant increase in the streamflows due to the contribution from snow melt and rainfall and an ensuing increase of streamflow production. As discussed by Santos et al. (2018), this increased input from melt can be accounted for by an increase of the streamflow generating frequency during the melting period, $\lambda^{(m)}$ beyond the actual rainfall frequency $\lambda_p^{(m)}$ during the same period, $\lambda^{(m)} > \lambda_p^{(m)}$ (where $m$ stands for the melting period).

The sum of melt and rainfall (what we call equivalent rainfall input) during the melt period cannot be unquestionably assumed to follow a marked Poisson. While the actual input amounts follow an exponential distributionas in the original model assumptions, a series of melt events typically comes clustered in time on days with melting conditions; accordingly equivalent precipitation shows lag-1 autocorrelations of up to 0.5. The numerical analysis of Müller et al. (2014) showed, however, that the model of Botter et al. (2007c, 2009) is robust with respect to this type of departure from the original assumptions about the Poissonian nature of the input process. We assume that the same conditions apply in this case.

Based on the above and assuming that the effect of snowmelt can be accounted for by $\lambda^{(m)} > \lambda_p^{(m)}$, we discuss here how to obtain two different estimates of $\lambda^{(m)}$, one directly from observed mean streamflow and one based on water balance considerations.

Under the presented modelling framework (linear or nonlinear formulation), the average amount of streamflow produced during the melting season can be written as:

$$\overline{Q^{(m)}} = \lambda^{(m)} \alpha^{(m)}, \tag{6.3}$$

where $\lambda^{(m)}$ is the streamflow generating frequency during the melting season and $\alpha^{(m)}$ the average amount of precipitation of the precipitation events during the melting season. This yields a first estimate of $\lambda^{(m)}$.

The average streamflow, $\overline{Q^{(m)}}$, can be split into a part, say $\overline{Q_a^{(m)}}$, originating from the water stored during the accumulation period in the non-responsive area (i.e. from $S^{(a)}$) and a part, say $\overline{Q_p^{(m)}}$, due to precipitation input during the melt season over the entire catchment area, i.e.

$$\overline{Q^{(m)}} = \overline{Q_a^{(m)}} + \overline{Q_p^{(m)}}, \tag{6.4}$$

where $a$ stands for streamflow from winter accumulation and $p$ for streamflow from precipitation.

The part of streamflow related to winter storage, $S^{(a)}$, can be obtained as:

$$\overline{Q_a^{(m)}} = \frac{S^{(a)}}{l^{(m)}} = \frac{\lambda_p^{(a)} \alpha^{(a)} l^{(a)} A^*}{l^{(m)} A}, \tag{6.5}$$

where $l^{(m)}$ is the length of melt season. The second equality comes from equation 6.2.

Snow-dominated catchments are typically saturated during the melting period, i.e. all precipitation events lead to streamflow; under this assumption, the average streamflow from precipitation during the melting period can be written as

$$\overline{Q_p^{(m)}} = \lambda_p^{(m)} \alpha^{(m)}, \tag{6.6}$$

where $\lambda_p^{(m)}$ is the precipitation frequency during the melt season and $\alpha^{(m)}$ the average amount of precipitation events.

Combining above equations (6.3) to (6.6) and solving for $\lambda^{(m)}$ yields:

$$\lambda^{(m)} = \lambda_p^{(m)} + \lambda_p^{(a)} \frac{\alpha^{(a)}}{\alpha^{(m)}} \frac{l^{(a)}}{l^{(m)}} \frac{A^*}{A}. \tag{6.7}$$

Thus the streamflow generating frequency during the melt period, $\lambda^{(m)}$, equals the precipitation frequency during the melt period, $\lambda_p^{(m)}$, plus a scaled version of the precipitation frequency during the accumulation season, $\lambda_p^{(a)}$. The scaling factor accounts for the ratio between precipitation amounts during the accumulation and the melt season ($\alpha^{(a)}/\alpha^{(m)}$), the ratio between the season lengths ($l^{(a)}/l^{(m)}$) and the ratio between the accumulation area during the accumulation period and the total catchment area ($A^*/A$). In the limiting case of no accumulation season ($l^{(a)} = 0$, $A^* = 0$), $\lambda^{(m)} = \lambda_p^{(m)}$. In all other cases, $\lambda_p^{(m)}$ is increased by an amount depending on the relative length of the accumulation period, the size of the accumulation area and the seasonality of average input amounts.

Following the above results, we can obtain two different estimates of $\lambda^{(m)}$. Upon appropriate season identification (section 6.2.2), we can estimate $\lambda^{(m)}$ either directly from observed average streamflow $Q^{(m)}$ and average precipitation input $\alpha^{(m)}$ during the melt season (Equation 6.3) or from the theoretical relationship of Equation 6.7 where $\lambda_p^{(a)}$, $\alpha^{(a)}$, $\alpha^{(m)}$, $l^{(a)}$, $l^{(m)}$ are calculated directly from observed data and $A^*$ is obtained from parameter estimation during the accumulation period (see section 6.2.3).

#### Incorporating effect of glaciers

Alpine glaciers are currently undergoing significant retreat (Fischer et al., 2015); corresponding mass loss represents a source of water for catchments with significant glacier coverage. In the context of this work, this additional water input is quantified from observed precipitation and streamflow data by closing the yearly water balance and the streamflow producing frequency $\lambda^{(m)}$ of Equation 6.7 becomes:

$$\lambda^{(m)} = \lambda_p^{(m)} + \lambda_p^{(a)} \frac{\alpha^{(a)}}{\alpha^{(m)}} \frac{l^{(a)}}{l^{(m)}} \frac{A^*}{A} + \frac{\Delta}{l^{(m)}\alpha^{(m)}} \tag{6.8}$$

The average yearly streamflow surplus, $\Delta$ is assumed to come from glacier mass loss and is added to carry-over from the accumulation season, $S^a$.

#### Effect of increasing $\lambda$ due to melt

The above extension to melting seasons assumes that all the contribution of the glacier and snow melt can be incorporated into the model by a proper increase of the streamflow producing frequency, $\lambda^{(m)}$. Increased water input during melting could also be split between both model parameters related to the water input, $\lambda^{(m)}$ and $\alpha^{(m)}$, the product of which has to be constant and equal to the equivalent precipitation (rainfall plus melt). An analysis of the moments of the streamflow distribution in the linear model case shows what would happen if $\alpha^{(m)}$ is increased (and consequently $\lambda^{(m)}$ decreased, to keep the equivalent precipitation constant). First, the expected value of the streamflow distribution ($\lambda^{(m)}\alpha^{(m)}$) is not affected by changes in the ratio between the two parameters. Given that $\lambda^{(m)}$ decreases with an increase of $\alpha^{(m)}$, the variance and the coefficient of skewness would both increase with an increase in $\alpha^{(m)}$. For the range of values studied in this chapter, this effect on the second and third moment is low ( Section 6.4).

### 6.2.2 Season identification

To apply a seasonal process-based model, we need to identify the seasons corresponding to the prevailing hydrological processes of snow accumulation and melt.

We assume that these processes are conditioned by the mean temperature over the catchment. The accumulation season is the period when precipitation occurs in form of snow and freezing conditions allow it to accumulate. It corresponds to the period when the mean temperature in the catchment is negative.

To define this accumulation period, we use a temperature model that represents the annual temperature cycles without daily fluctuations. Following the formulation proposed by Woods (2009), annual temperature cycles can be modeled as a sine curve defined by the time-averaged mean temperature, $\overline{T}$, a dimensionless seasonal amplitude, $\Delta_T$, and a phase shift, $s_T$:

$$T(t) = \overline{T} + \Delta_T \sin(2\pi(t - s_T)/d), \tag{6.9}$$

where $t$ is the time step, considered to be a day, and $d$ is the duration of the seasonal cycle, considered to be a year of 365 days. For the context of this study, we estimated the parameters of this model for a high number of meteorological stations across Switzerland (see 6.3 to obtain a relation between the parameters and elevation and to interpolate this temperature model to the mean elevation of all catchments. The length of the accumulation season can then be obtained analytically from the parameters $\overline{T}, \Delta_T$ and $s_T$ (for details see Woods, 2009).

There are many methods to calculate of the length of the melting season, such as based on water budgets or on snow melt models (e.g Woods, 2009). Although the melting season is usually shorter than the accumulation season, for the sake of simplicity, we decided to set the length of the melting season equal to the length of the accumulation season. Extensive tests showed that this convenient choice gives the best results for the analyzed case studies. If the accumulation and the melt seasons do not sum up to an entire year, there is and additional season when the streamflow producing mechanism is pluvial. To avoid too short seasons, we impose a minimum season length of 30 days. In case the third pluvial season becomes shorter than this minimum length, the duration of the melting season is increased accordingly. For catchments with significant glacier coverage (more than 20% of the area), the melting season is supposed to cover the entire year outside the accumulation season.

### 6.2.3 Parameter estimation

The parameters of the full model are listed in Table 6.1.

Table 6.1 – Summary of the model parameters. Superscripts indicate the season (accumulation $a$, melting $m$ or pluvial $p$). Subscripts differentiate different parameters.

| Parameter | Description |
|---|---|
| $\lambda_p^{(a)}$ | frequency of precipitation events during the accumulation season |
| $\lambda_p^{(m)}$ | frequency of precipitation events during the melting season |
| $\lambda_p^{(p)}$ | frequency of precipitation events during the pluvial season |
| $\alpha^{a}$ | mean depth of precipitation during the accumulation season |
| $\alpha^{(m)}$ | mean depth of precipitation during the melting season |
| $\alpha^{(p)}$ | mean depth of precipitation during the pluvial season |
| $l^{(a)}$ | mean length of the accumulation season |
| $l^{(m)}$ | mean length of the melting season |
| $A^{*}$ | non-responsive area of the catchments during the accumulation season |
| $\tau_D$ | residence time delay due to snow during the accumulation season |
| $k^{(m)}$ | linear recession parameter of the melting season |
| $k_n^{(p)}$ | nonlinear recession coefficient of the pluvial season |
| $a^{(p)}$ | nonlinear recession exponent of the pluvial season |
| $\lambda^{(m)}$ | frequency of streamflow producing events during the melting season |
| $\lambda^{(p)}$ | frequency of streamflow producing events during the pluvial season |

The precipitation parameters, $\lambda_p$ and $\alpha$, are obtained from the series of precipitation observations for each season after discounting interception, as explained in Section 3.2.1. Regarding $\lambda_p^{(a)}$ and $\alpha^{(a)}$, for the accumulation season, interception losses are considered to be 1 mm per rainfall event. For $\lambda_p^{(m)}$, $\alpha^{(m)}$, $\lambda_p^{(p)}$ and $\alpha^{(p)}$, interception losses are obtained from land use and the maximum interception is set to 4 mm for forests, 2 mm, for low vegetation, 1 mm for impervious areas and 0 mm for water bodies (Gerrits, 2010; Santos et al., 2018, 2019). The maximum interception for any season is considered to be at least 1 mm. Then, $\lambda_p$ is the frequency of the effective precipitation events during a season and $\alpha$ the mean depth of precipitation when it occurs. The frequency of streamflow producing events during the accumulation season is equal to the frequency of precipitation events, considering that evapotranspiration is negligible during this period. As discussed above, the frequency of streamflow producing events during the melting seasons is calculated in two ways, first from observed streamflows, $\lambda^{(m,o)}$ (Equation 6.3), and from the theoretical relationship of Equation 6.7 , $\lambda^{(m,t)}$.

The length of each season is defined by the seasons limits (see Subsection 6.2.2).

The non-responsive area is calculated by the optimization of the model performance indicator (the Kolmogorov-Smirnov distance, see 6.2.5) as described by Schaefli et al. (2013), but considering the accumulation season instead of the meteorological winter.

The linear recession parameter ($k^{(m)}$) is calculated by maximum likelihood estimation (MLE) for the melting season applied with the empiric $\lambda^{(m,o)}$ obtained from observed streamflows. The nonlinear recession parameters ($a^{(p)}$ and $k_n^{(p)}$) for the pluvial season are also calculated using MLE as done by Ceola et al. (2010); Santos et al. (2018, 2019).

The delay due to snow accumulation is estimated as as the mean duration of temperature excursion below freezing temperature, i.e. the mean duration of consecutive days with air temperature below 0°C, considering daily temperature observations, as done by (Schaefli et al., 2013). Here we use catchment-average temperature observations obtained from gridded data (see 6.3).

### 6.2.4 Annual distributions of daily streamflows

For practical purposes, it is more useful to obtain the distribution of daily streamflows for a complete year. This distribution is obtained by a weighted average of the underlying seasonal distributions, as proposed by Botter et al. (2008) and tested by Müller et al. (2014) for seasonally dry climates:

$$P_Y(q) = l^{(a)} P_Q^{(a)}(q) + l^{(m)} P_Q^{(m)}(q) + l^{(p)} P_Q^{(p)}(q), \tag{6.10}$$

When there is no pluvial season, such as for the glacier catchments, $l^{(p)}$ is zero and the annual distribution is based only on the distributions for the accumulation and melting seasons.

### 6.2.5 Evaluation criteria

We evaluate the quality of the results in two different ways: first comparing the values of the frequency of streamflow producing events calculated analytically ($\lambda^{(m,t)}$) with the empirical values of $\lambda^{(m,o)}$. Then, we assess the model performance for each season and for the year according to the Kolmogorov-Smirnov distance, $c^{\mathrm{KS}}$.

## 6.3 Case studies

In this chapter, we used 10 Swiss case studies affected by glacier and/or snow processes to verify the validity of the extension proposed to melting periods in mountainous catchments. The selected cases have areas ranging from 1.65 km$^2$ to 195 km$^2$ and mean elevations from 1252 m asl. to 2945 m asl. (Table 6.2, Figure 6.1). The selected streamflow gauging stations are run by the Swiss Federal Office for the Environment (FOEN, 2017), have unperturbed streamflows (i.e. minimal anthropogenic influence) and a single series of measured daily data from 1975 to 2014, the period used in our studies. Because the Dischmabach catchment presented measuring issues in the last decades, its data was considered only until the year 2000 (Schaefli et al., 2016).

Daily streamflow data for each catchment were provided by the Swiss Federal Office for the Environment (FOEN). Catchment scale precipitation (MeteoSwiss, 2011) and temperature (MeteoSwiss, 2014) are estimated as in the work of Santos et al. (2018) from

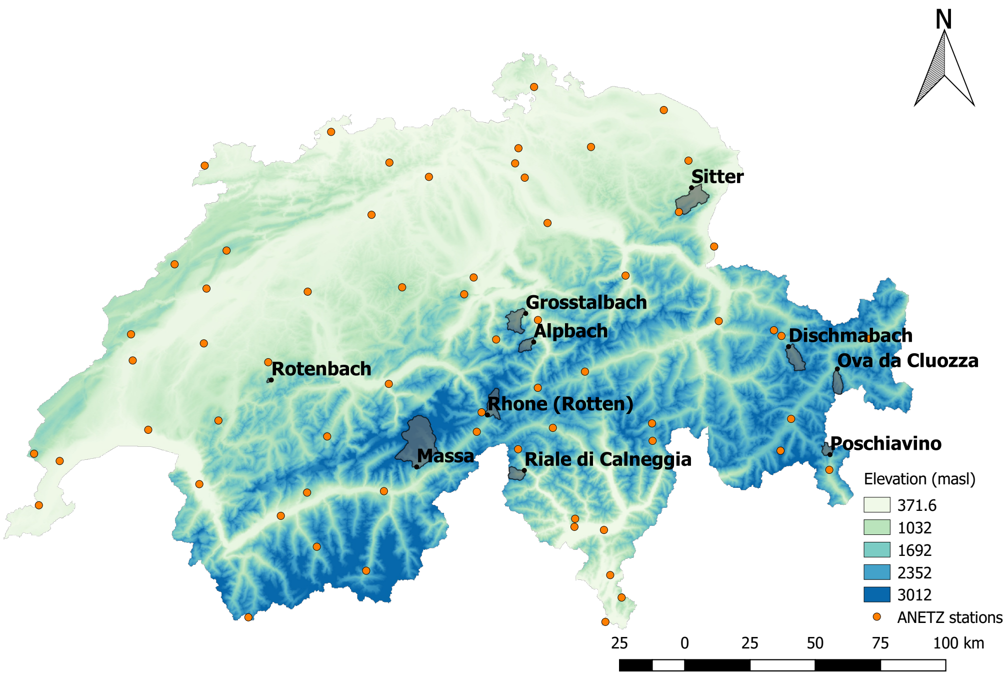


Figure 6.1 – Map of Switzerland showing the location of the 10 case studies and of the 64 meteorological stations. Source of the digital elevation model:(SwissTopo, 2005b)

gridded data. The same holds for the assessment of the land use characteristics used to estimate interception. To account for general gauge undercatch for the observation of solid precipitation, we adopted a catchment scale precipitation correction factor of 1.2 during the accumulation period (Magnusson et al., 2014).

Additionally, we used air temperature data from the 64 meteorological stations of to the Swiss automatic measurement network (formerly called ANETZ, now integrated into SwissMetNet) that have data since the 1980ies to develop the air temperature model (Woods, 2009). They have elevations that range from 203 m asl. to 3305 m asl.

## 6.4 Results

### 6.4.1 Temperature model and season identification

We applied the temperature model of Equation 6.9 to daily data of the 64 meteorological stations , resulting in 64 fitted sinusoidal curves. Figure 6.2 shows the values of the three curve parameters and their relation to the elevation of the meteorological stations. Due to the geographic characteristics of Switzerland, a relatively small country, with latitudes that go from 45$^{o}$49'N at Pedrinate to 47$^{o}$48'N at Oberbargen, the air temperature regime

Table 6.2 – Characteristics of the 10 case studies

| ID | Name | Code | Area $km^2$ | Station elevation m asl | Mean elevation m asl | Glaciation |
|---|---|---|---|---|---|---|
| 2327 | Dischmabach - Davos, Kriegsmatte | DIS | 43.3 | 1668 | 2372 | 2.1 % |
| 2112 | Sitter - Appenzell | SIT | 74.2 | 769 | 1252 | 0.08 % |
| 2251 | Rotenbach - Plaffeien, Schwyberg | ROT | 1.65 | 1275 | 1454 | 0 |
| 2299 | Alpbach - Erstfeld, Bodenberg | APB | 20.6 | 1022 | 2200 | 27.7 % |
| 2276 | Grosstalbach - Isenthal | GRO | 43.9 | 767 | 1820 | 9.3 % |
| 2268 | Rhône - Gletsch | RHG | 38.9 | 1761 | 2719 | 52.2 % |
| 2161 | Massa - Blatten bei Naters | MAS | 195 | 1446 | 2945 | 65.9 % |
| 2356 | Riale di Calneggia - Cavergno, Pontit | RDC | 24 | 890 | 1996 | 0 |
| 2366 | Poschiavino - La Rosa | POS | 14.1 | 1860 | 2283 | 0.35 % |
| 2319 | Ova da Cluozza - Zernez | OVA | 26.9 | 1509 | 2368 | 2.2 % |

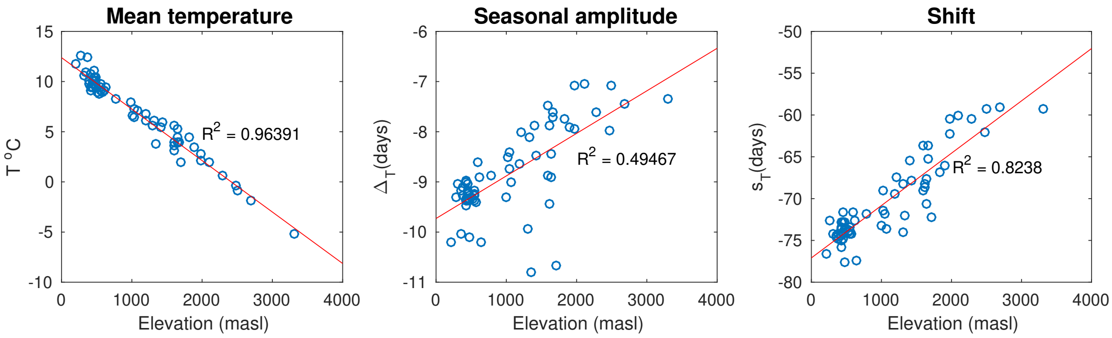


Figure 6.2 – Relation between the elevations of the meteorological stations and the temperature model parameters

essentially depends on elevation.

We then use the linear regression for each of these three parameters to interpolate the parameters to the mean elevation of each catchment and to obtain the accumulation season length for each catchment (6.3).

### 6.4.2 Mass balance

Table 6.4 summarizes the mass balance for each catchment in terms of annual precipitation ($\overline{P_y}$), annual streamflow ($\overline{Q_y}$) and losses due to interception and evapotranspiration ($\overline{L_y}$), obtained as the average over hydrological years (starting on 1 Oct in Switzerland). The losses are calculated as the sum of due to evaporation (i.e. interception, $\overline{I_y}$) and transpiration. Transpiration is obtained as the value that brings the mass balance to zero when $\overline{P_y} - \overline{Q_y} - \overline{I_y} > 0$ or at least 50 mm. It can be seen that for seven catchments we have that $\overline{P_y} < \overline{Q_y} + \overline{I_y}$. As discussed previously, for glacier catchments, this difference ($\Delta$) can a priori be assumed to come from glacier mass loss. For non glacier catchments, this points towards underestimation of area-average precipitation input from the available gridded precipitation product.

Table 6.3 – Lengths of accumulation season $l^{(a)}$, melting season $l^{(m)}$ and pluvial season $l^{(p)}$ for each case study. Differences between $l^{(a)}$ and $l^{(m)}$ occur if the pluvial season is incorporated into the melting season, see Section 6.2.2.

| Code | $l^{(a)}$ | $l^{(m)}$ | $l^{(p)}$ |
|---|---|---|---|
| DIS | 180 | 185 | 0 |
| SIT | 94 | 94 | 177 |
| ROT | 110 | 110 | 145 |
| APB | 166 | 199 | 0 |
| GRO | 137 | 137 | 91 |
| RHG | 206 | 159 | 0 |
| MAS | 227 | 138 | 0 |
| RDC | 151 | 151 | 63 |
| POS | 173 | 192 | 0 |
| OVA | 178 | 187 | 0 |

Table 6.4 – Main components of the mass balance for each catchment

| Code | $\overline{Q_y}$ (mm) | $\overline{P_y}$ (mm) | $\overline{L_y}$ (mm) | $\Delta$ (mm) |
|---|---|---|---|---|
| DIS | 1.260 | 991 | 197 | 466 |
| SIT | 1.479 | 1.899 | 420 | 0 |
| ROT | 1.684 | 1.771 | 233 | 146 |
| APB | 2.463 | 1.674 | 227 | 1.016 |
| GRO | 1.284 | 1.706 | 422 | 0 |
| RHG | 2.319 | 2.011 | 230 | 539 |
| MAS | 2.229 | 2.360 | 225 | 94 |
| RDC | 1.873 | 1.928 | 198 | 143 |
| POS | 1.243 | 1.455 | 212 | 0 |
| OVA | 926 | 930 | 183 | 179 |

Most of the values from out mass balance agree with those from Haller et al. (2004), but an exception to this is the Massa catchment. Fischer et al. (2015) estimated an annual mass loss around 700 mm to 800 mm for this catchment during the period from 1980 to 2010, which is not compatible with our budget (94 mm) and suggests that there is an underestimation of streamflows and/or an overestimation of precipitation.

### 6.4.3 Estimated parameters

The model was implemented for the selected case studies using the linear model for the accumulation and the melting season and, following the results of Santos et al. (2018) the nonlinear model for the pluvial season. The corresponding parameter values are given in Tables 6.5, 6.6 and 6.7 show the estimated parameters for the accumulation, melting and pluvial seasons. Overall, the mass balance-based theoretical streamflow producing frequency $\lambda^{(m,t)}$ reproduces the empirical frequency $\lambda^{(m,o)}$ very well (Figure 6.3).

For the estimation of recession parameters, we have chosen to calculate the recession parameters adopting the empiric frequency of streamflow production, $\lambda_{m,o}$, to avoid biases towards the theoretical frequency, $\lambda_{m,t}$.

Table 6.5 – Model parameters and performances for the accumulation season.

| Code | $\alpha^{(a)}$ | $\lambda_p^{(a)}$ | $\tau^{(m)}$ | $\tau_D$ | $A^*/A$ | $c^{\mathrm{KS},a}$ |
|---|---|---|---|---|---|---|
| | mm | 1/day | day | day | | |
| DIS | 6,1 | 0,32 | 4,3 | 24,5 | 0,50 | 0,06 |
| SIT | 10,0 | 0,45 | 3,8 | 6,4 | 0,58 | 0,15 |
| ROT | 10,6 | 0,42 | 1,7 | 6,1 | 0,58 | 0,12 |
| APB | 10,9 | 0,43 | 1,7 | 16,4 | 0,78 | 0,15 |
| GRO | 10,2 | 0,41 | 7,5 | 9,1 | 0,66 | 0,08 |
| RHG | 13,7 | 0,46 | 1,7 | 29,5 | 0,86 | 0,19 |
| MAS | 15,2 | 0,44 | 2,6 | 34,8 | 0,95 | 0,33 |
| RDC | 13,7 | 0,31 | 2,9 | 12,3 | 0,73 | 0,07 |
| POS | 12,1 | 0,29 | 5,0 | 24,7 | 0,62 | 0,07 |
| OVA | 7,3 | 0,26 | 4,6 | 51,5 | 0,61 | 0,10 |

Since many model parameters are related to catchment elevation (Santos et al. (2018); Schaefli et al. (2013)), we checked the relation of the frequency of streamflow producing events during the melting season with the mean catchment elevation (Figure 6.4). As expected, the frequency strongly increases with elevation, with the exception of the two case studies located in the Engadin region, POS and OVA; they have relatively low frequencies despite their high elevations. This region is in fact known to have a distinct climate and to be relatively dry (Begert et al., 2007).

Table 6.6 – Model parameters and performances for the melting season.

| Code | $\alpha^{(m)}$ mm | $\lambda_p^{(m)}$ 1/day | $\lambda^{m,o}$ 1/day | $\lambda^{m,t}$ 1/day | $k^{(m)}$ 1/day | $c^{\mathrm{KS},m}$ | $c^{\mathrm{KS},y}$ |
|---|---|---|---|---|---|---|---|
| DIS | 7,9 | 0,31 | 0,73 | 0,75 | 0,23 | 0,05 | 0,03 |
| SIT | 10,0 | 0,39 | 0,54 | 0,65 | 0,26 | 0,20 | 0,04 |
| ROT | 10,6 | 0,38 | 0,71 | 0,75 | 0,59 | 0,11 | 0,05 |
| APB | 9,5 | 0,44 | 1,20 | 1.30 | 0,58 | 0,07 | 0,07 |
| GRO | 10,9 | 0,42 | 0,53 | 0,67 | 0,13 | 0,23 | 0,08 |
| RHG | 9,9 | 0,49 | 1,34 | 1,54 | 0,59 | 0,10 | 0,11 |
| MAS | 13,0 | 0,53 | 1,14 | 1,40 | 0,38 | 0,13 | 0,20 |
| RDC | 15,1 | 0,34 | 0,57 | 0,61 | 0,35 | 0,10 | 0,04 |
| POS | 12,3 | 0,30 | 0,42 | 0,46 | 0,20 | 0,17 | 0,08 |
| OVA | 8,6 | 0,29 | 0,48 | 0,54 | 0,22 | 0,14 | 0,07 |

Table 6.7 – Model parameters and performances for the pluvial season

| Code | $\alpha^{(p)}$ mm | $\lambda_p^{(p)}$ 1/day | $\lambda^{(p,o)}$ 1/day | $k_n^{(p)}$ | $a^{(p)}$ | $c^{\mathrm{KS},p}$ |
|---|---|---|---|---|---|---|
| SIT | 11,8 | 0,40 | 0,34 | 0,13 | 1,82 | 0,03 |
| ROT | 12,1 | 0,34 | 0,30 | 0,18 | 1,88 | 0,04 |
| GRO | 11,0 | 0,35 | 0,28 | 0,04 | 1,97 | 0,03 |
| RDC | 21,1 | 0,31 | 0,28 | 0,06 | 1,99 | 0,04 |

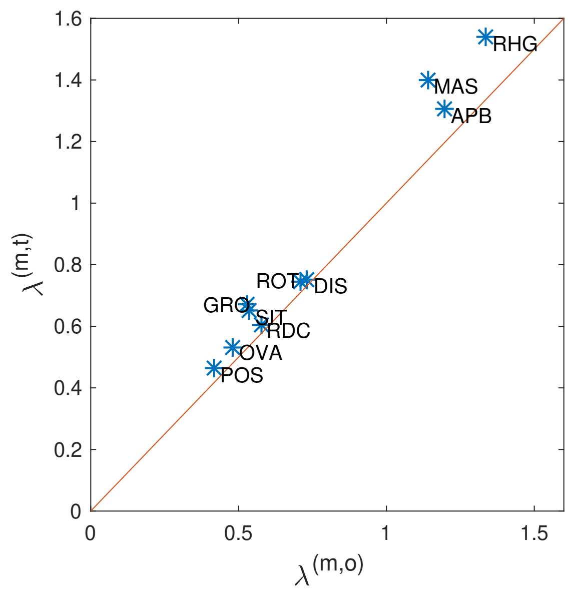


Figure 6.3 – Comparison between the values of observed and theoretical $\lambda_m$.

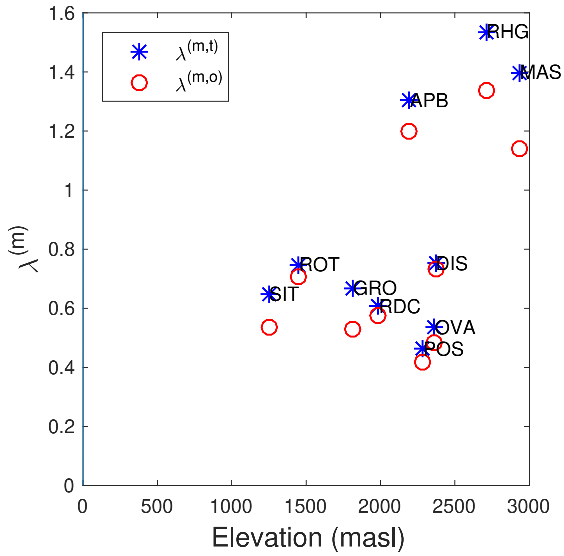


Figure 6.4 – Relation between the mean catchment elevation and the frequency of streamflow production.

### 6.4.4 Model performance

The model performance was assessed quantitatively according to the Kolmogorov-Smirnov distance: Tables 6.5, 6.6 and 6.7 show the values of this indicator for each season, Table 6.6 also shows the model performances for the year. Additionally, Figure 6.5 shows the cdfs for all the seasons in a snow dominated catchment, with three seasons (Riale di Calnegia) and in a glacier catchment with two seasons (Rhône). Figures for all catchments and seasons and for the year can be found in the Appendix D.

The results for the pluvial season tend to be very good since it is the season for which the model was initially developed and because of the use of MLE to obtain the recession parameters. The results for the accumulation season are mostly good, but since they are based on a linear model, they tend to be worse than the results for the nonlinear model. For the cases more influenced by glaciers, the model performance was impaired mostly by an overestimation of the recession timescale in a pattern observed by Santos et al. (2018) that can be seen in Figure 6.5 (accumulation season in Rhône). Regarding the melting season, the results are better if $\lambda^{(m,t)}$ is close to $\lambda^{(m,o)}$. When $\lambda^{(m,t)}$ is overestimated, the entire cdf is overestimated, as it happens in the Rhône catchment (see Figures 6.3 and 6.5).

Annual performances are coherent with the seasonal results. Low flows are generated mostly in the accumulation season and high flows in the melting season and the annual curves clearly mirror the characteristics of the seasonal curves in the corresponding streamflow range of the annual cdf. For the illustrated glacier case, for example, the accumulation curve has a small variability, which is repeated in the annual curve for low flows, while the good results for the melting seasons are also repeated for the high flows.

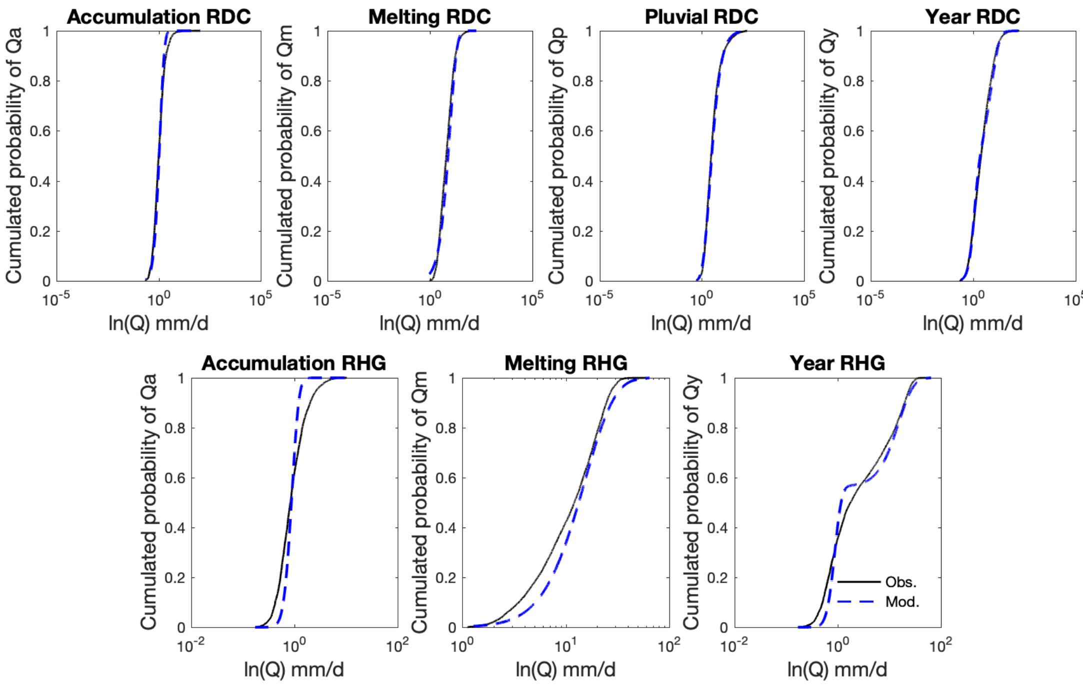


Figure 6.5 – Modeled cdfs for the two or three seasons and for the year for two selected catchments: Riale di Calnegia (snow-dominated) and Rhône (glacier).

The shapes of the curves, even when they show a step in the curve, are well represented by the model, in general. The annual performances of the model are mostly good, with annual values of $c^{\text{KS}}$ situated between the values for the seasonal curves (see Tables 6.5 to 6.7).

### 6.4.5 Effect of increasing precipitation frequency

We analysed numerically the effect of varying ratio between $\lambda^{(m)}$ and $\alpha^{(m)}$ on the model results. For this, we fixed the equivalent precipitation ($P_{eq} = \lambda\alpha$), varied the ratio between the parameters and calculated the pdfs for the different ratios. Here we present the results for one case, the Riale di Calnegia, in Figure 6.6.

First, it is important to notice that the change in the ratio between $\lambda^{(m)}$ and $\alpha^{(m)}$ also affects the results for the accumulation season, because of the used recession parameter estimation method, based on MLE. For this particular case, the linear recession parameter did not vary significantly, ranging from 0.30 for accounting of melting effects fully in $\alpha^{(m)}$ to 0.35 for accounting of melting fully in $\lambda^{(m)}$, which resulted in $c^{\text{KS},a}$ from 0.72 to 0.69 respectively. For this case, the best results for the melting season are the ones obtained with incorporating the complete contribution due to the carry-over effect in the value of $\lambda$ with the values of $c^{\text{KS},m}$ ranging from 0.24 to 0.07. Figure 6.6 confirms that the best values are obtained for the case where melting is fully incorporated in $\lambda^{(m)}$.

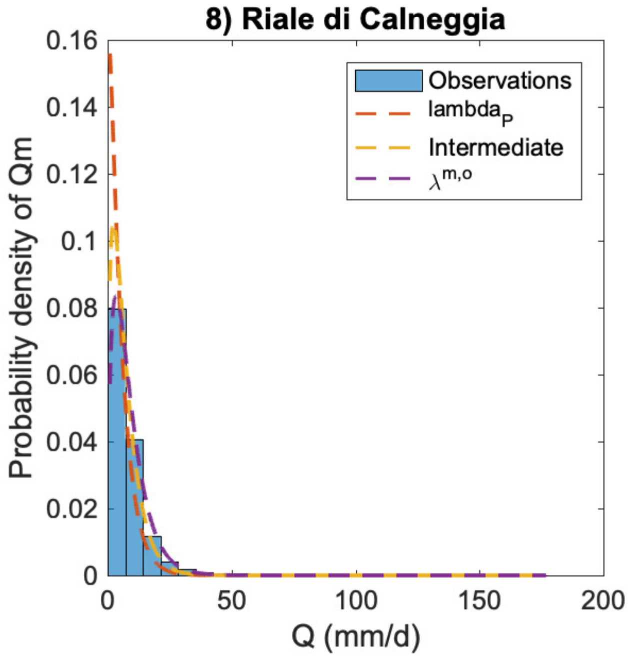


Figure 6.6 – Analysis of the variation of the ratio between $\lambda^{(m)}$ and $\alpha^{(m)}$ for a fixed equivalent precipitation for the catchment Riale di Calnegia

We also compared the coefficient of variation (CV) of the analytical distributions and to the CVs of the observed streamflow time series, as done by Botter et al. (2013) to verify the choice of how to account for melting effects. From a physical viewpoint, the snow-melting process corresponds more to a frequent additional supply of water (during melting conditions) than to an increase of the input pulse size ($\alpha$). As shown in Figure 6.7, the accommodation of the equivalent precipitation in $\alpha^{(m)}$ leads to a considerable increase in the CV and to strong deviations from the sample CVs. It would even lead to CVs higher than 1, which corresponds to exponential streamflow distributions, i.e. erratic streamflow regimes Botter et al. (2013), which are not observed in this hydroclimatic region. This analysis confirms that incorporating the effect of melting in the streamflow producing frequency $\lambda^{(m)}$ is more suitable in general in this region.

## 6.5 Discussion

In this study we extended the analytical streamflow distribution model proposed by Botter et al. (2007c) to periods of snow melt. The extension is based on three key previous results related to the model framework: i) the extension for winter in snow-dominated catchments (Schaefli et al., 2013) that allows the estimation of the amount of water stored during the accumulation season, ii) the extension of the model to seasonally dry catchments (Müller et al., 2014) that showed the robustness of the modelling framework

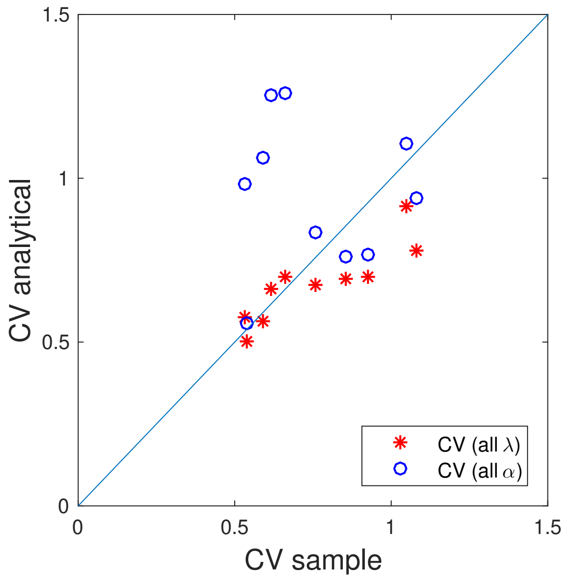


Figure 6.7 – Comparison between the CVs obtained for the sample and analytically for the complete consideration of the equivalent precipitation in $\lambda$ and in $\alpha$

for autocorrelated inputs, the importance of a careful definition of seasons when dealing with carry-over effects and iii) the finding of Santos et al. (2018) that the additional water from snow melt can be incorporated into the model for summer streamflow distributions by increasing the frequency of streamflow generating events, $\lambda$ The present chapter argues that this increase of $\lambda$ can be extended to the entire melting season to account for additional water input from melt and derives an analytical expression based on water balance considerations. The comparison of the resulting analytical coefficients of variation to the ones obtained from observed streamflow for the 10 case studies underlines the robustness of the resulting model for modelling melt-influenced streamflow distributions.

The good model performances show furthermore that the division of the year in two or three seasons is suitable for the studied hydrological regimes, which are typical for Alpine catchments.

The proposed season identification method based on a Swiss-wide elevation-dependent air temperature model overcomes an important limitation identified in previous work, where seasons were identified according to fixed calendar dates (Schaefli et al., 2013). They studied some of the same case studies as in the present chapter but due to their season identification, the results cannot be directly compared.

The model extension to snow-dominated catchments has an important limitation related to the strong dependence on reliable precipitation data for mountainous catchments. This is notoriously difficult at high elevations where the availability and the distribution of meteorological stations is generally insufficient and the precipitation gauging suffers from solid precipitation undercatch. The quality of streamflow data might potentially also be lower in high elevation catchments, especially during the accumulation season when streamflows may be very low and freezing can affect measuring instruments.

## 6.6 Conclusions

This Chapter extends the analytic streamflow distribution model framework discussed in Chapter 2 to warm seasons in catchments affected by significant glacier and snow processes. The extension was tested in ten Swiss catchments characterized by different elevations and climates, where streamflows present a strong seasonality due to the mentioned processes. The model reproduces observed daily streamflow distributions and coefficients of variation remarkably well.

The model extension is based on the definition of accumulation and melting seasons based on the elevation-dependent air temperature regime, and the incorporation of the increased water input during the melting season into the streamflow producing frequency.

The proposed model extension is argued to make the analytic streamflow distribution model suitable for annual streamflow in snow-dominated catchments.

# Conclusion Part III

# 7 Conclusions and perspectives

The present Thesis has suggested that the analytical streamflow distribution model of Botter et al. (2007c), originally developed for pluvial regimes, represents a reliable tool for water resources assessment in Alpine environments, where the hydrologic regimes show a spatial and seasonal transition from rainfall-dominated (pluvial), to snow- and glacier melt dominated. The required key extensions studied in this Thesis are the robust and transferable estimation of the model parameters and the incorporation of the effect of snow- and glacier melt during the ablation period.

In view of a robust parameter estimation, Chapter 3 studied the performance of the model framework for summer streamflow in 25 Swiss catchments representative of the range of hydro-climatological conditions typically encountered in Alpine environments. The chapter tested the pluvial model for a standard summer season between June and August. This work investigated the use of linear and nonlinear recession models, combined with different approaches to estimate recession parameters: the widely used recession analysis method (RAM) proposed by Brutsaert and Nieber (1977) and an inverse method based on maximum likelihood estimation (MLE). The detailed analysis of this conventional method underlined the need to study a broader range of RAMs.

The application of the model to a standard summer season in Chapter 3 showed that summer streamflow distributions in high elevation catchments can be explained by streamflow generating frequencies that exceed the frequency of rainfall inputs. This result underlined that high elevation summer streamflow is systematically influenced by melt processes, even in absence of a glacier cover that sustains summer streamflow.

The model was tested by adopting an increased frequency for streamflow producing events. Increasing the event generating frequency (with respect to rainfall input frequency) leads to an increase of the total available water during the summer, which is inline with the classical snow hydrology approach of estimating an equivalent precipitation input from rainfall and snow- and glacier melt. Importantly, this model represents a simple yet effective solution to incorporate snowmelt into the model framework during summer. In addition, this chapter clarified the need for defining better recession analysis methods. The detailed analysis for 25 catchments also allowed to find interesting correlations between model parameters (in particular the stream flow producing frequency) and the model performances with mean catchment elevation. In general, the nonlinear model performed better than the linear model, but the performance of the linear model improved with the mean catchment elevation, with very good results for catchments influenced by glacier and snow melt.

Because Chapter 3 strengthened the importance of robust recession parameter estimation, Chapter 4 studied the performance of different RAMs for the model framework. The focus was here on nonlinear recessions and annual streamflow distribution curves in catchments with pluvial regimes. For these conditions, the most suitable method resulted to be a combination of a strict recession extraction method and a ‘per event’ decorrelation parameter estimation method. The detailed analyses also showed that different RAMs can lead to very different parameter values and that in particular the choice of a recession extraction method strongly affects the recession parameters, especially for ‘per event’ parameter estimation.

The best RAMs had results very similar to the ones obtained by MLE, which raised the question whether MLE could become a reference method to calculate recession parameters. This approach was tested in detail and shown to be at least as performing as existing RAMs, with the advantage of eliminating the critical step of recession extraction.

While Chapter 4 focused on the study of annual nonlinear recessions, this Thesis aimed at more general situations. Accordingly, Chapter 4 presents additional results regarding RAMs in combination with linear recessions, which are more frequently used for the model framework. Again, results showed that the recession extraction method choice is fundamental for parameter estimation and that linear recession parameters are even more affected by methodological choices than nonlinear parameters. It was not possible to recommend a single best RAM for linear recessions, but it was observed that master curve methods yield lower parameter values, while ‘per event’ methods produce higher parameter values. Finally, the MLE approach had satisfactory results and could be used as a reference in future studies for ungauged catchments.

The extension of the model framework to the warm season in snow-dominated catchments and glacier catchments was the topic of Chapter 6. It studied the model framework under snow melting conditions, taking advantage of the extension to the snow accumulation (winter) season previously introduced by Schaefli et al. (2013). The new solution to account for snowmelt consisted of estimating the amount of water stored during snow accumulation and of estimating the increased frequency of streamflow producing events from the equivalent precipitation resulting from the sum of rainfall and winter accumulation. The consideration of snowmelt as an increased streamflow production frequency was a possibility raised by Chapter 3, but further testing was required, as well as a formal link between winter accumulation and water release during the melt period. In this context, the linear recession model was chosen because it allows better theoretical treatment of the problem. It is noteworthy that this solution was only possible after redefining the seasons and, instead of standard meteorological seasons, adopting an air temperature-based accumulation period. The obtained results were good for snow dominated and for glacier catchments, for seasonal as well as for ensuing annual streamflow distribution curves. The new frequency of streamflow producing events is strongly correlated with mean catchment elevation, which opens important perspectives for parameter regionalization.

Other promising perspectives for future work are:

- The identified robust recession parameter estimation methods should be further tested in view of applications of the model framework to ungauged catchments. The correlation observed between the model parameters and catchment elevation opens interesting perspectives for process-based parameter regionalization in Alpine catchments.
- The good MLE results for short series of streamflow observations make the model framework useful in situations with limited observed data. A parallel perspective is the possible use of the MLE approach to obtain recession parameters in other contexts, for example, using MLE with other simple hydrological models to estimate recession parameters or using the obtained parameters with other hydrological models.
- The streamflow distribution model provides a link between the FDC shape and climatic and geomorphological characteristics of a catchment and the results obtained from this Thesis were physically meaningful. Also, the model parameters are correlated to the mean catchment elevation (and consequently to the air temperatures in the catchment). The robustness of the model and the facility to obtain its parameters open another interesting perspective is related to the use of the model to predict the impact of climate change on the distribution of daily streamflows in regions affected by snow processes. The values of most of the model parameters could be estimated from climate change scenarios and mean catchment elevations; the only parameter that needs further study is the non-responsive area.
- This type of model is very simple, especially the nonlinear form that results in a gamma distribution. This simplicity makes it useful to be used as a framework to support comparative theoretical studies, such as the description of regimes done by Botter et al. (2013) and the ecological studies done by Ceola et al. (2014). The model extension based on the linear model provides new elements to support future studies related to snow-dominated and glacier catchments.

# A Supplementary material to Chapter 3

The supplementary material contains 3 tables, 2 figures and graphics showing the cdf model performance for all catchments including the linear and nonlinear model. Additional shape files with the catchments contour can also be found attached. The tables and figures show:

- Table A.1: Percentage of land use per catchment.
- Figure A.1: Interception per type of land use.
- Table A.2: Spatial data classes associated to FOEN land use classes.
- Figure A.2: Equivalence between the 16 discharge regimes from the Hydrological Atlas of Switzerland and the 3 types of regimes adopted.
- Table A.3: Precipitation grid cells per catchment.
- Table A.4: Summary of data sources.

Table A.1 – Percentage of land use per catchment. Data was obtained from the dataset associated to the “hydrological study area” (Aschwanden, 1996) except for the catchments: Areuse, Rhône-Gletch and Venoge, for which data was obtained from spatial data (Statistics, 2001), see Tab. A.2. Each column is identified by a letter that correspond to a type of land use, identified on Fig. A.1.

| Catchment | A | B | C | D | E | F | G | H | I | J | K | L | M | N | O |
|---|---|---|---|---|---|---|---|---|---|---|---|---|---|---|---|
| Rein da Sumvitg | 0,14 | 1,66 | 0,09 | 0,00 | 0,00 | 19,26 | 0,00 | 23,49 | 0,00 | 0,00 | 0,00 | 47,01 | 0,09 | 1,61 | 6,65 |
| Dischmabach | 2,38 | 1,87 | 0,23 | 0,00 | 0,46 | 37,80 | 0,00 | 20,89 | 0,05 | 0,00 | 0,28 | 33,50 | 0,13 | 0,35 | 2,06 |
| Goldach | 29,64 | 0,00 | 4,37 | 3,04 | 51,06 | 0,80 | 0,46 | 0,14 | 5,97 | 0,60 | 3,44 | 0,08 | 0,02 | 0,38 | 0,00 |
| Necker | 33,61 | 0,00 | 3,80 | 0,50 | 47,63 | 10,14 | 0,06 | 0,57 | 1,65 | 0,07 | 1,38 | 0,14 | 0,00 | 0,45 | 0,00 |
| Sitter | 25,13 | 0,13 | 2,94 | 0,05 | 24,08 | 31,84 | 0,04 | 4,99 | 1,30 | 0,03 | 1,16 | 7,24 | 0,19 | 0,80 | 0,08 |
| Murg | 30,58 | 0,00 | 2,87 | 3,83 | 51,62 | 0,82 | 0,26 | 0,00 | 4,64 | 0,71 | 4,07 | 0,24 | 0,13 | 0,23 | 0,00 |
| Scheulte | 47,75 | 0,00 | 3,97 | 1,00 | 26,59 | 17,81 | 0,07 | 0,14 | 1,31 | 0,00 | 1,17 | 0,07 | 0,00 | 0,12 | 0,00 |
| Gürbe | 21,95 | 0,28 | 2,55 | 2,69 | 53,84 | 7,75 | 0,11 | 2,00 | 3,69 | 0,28 | 2,40 | 1,43 | 0,28 | 0,75 | 0,00 |
| Rotenbach | 12,12 | 0,00 | 12,12 | 0,00 | 0,00 | 71,51 | 0,00 | 0,61 | 0,61 | 0,00 | 0,00 | 1,82 | 0,00 | 1,21 | 0,00 |
| Sense | 32,34 | 0,06 | 3,65 | 1,17 | 36,38 | 17,94 | 0,07 | 2,07 | 1,84 | 0,10 | 1,51 | 1,56 | 0,14 | 1,17 | 0,00 |
| Areuse | 44,02 | 0,00 | 4,04 | 0,14 | 26,51 | 20,15 | 0,16 | 0,25 | 0,67 | 2,07 | 0,17 | 0,17 | 1,53 | 0,13 | 0,00 |
| Ilfis | 44,27 | 0,14 | 4,45 | 0,55 | 31,46 | 14,07 | 0,06 | 0,87 | 1,21 | 0,09 | 1,26 | 0,71 | 0,00 | 0,86 | 0,00 |
| Sellenbodenbach | 10,66 | 0,00 | 3,52 | 5,14 | 72,69 | 0,00 | 0,19 | 0,00 | 4,47 | 0,29 | 3,04 | 0,00 | 0,00 | 0,00 | 0,00 |
| Alpbach | 1,51 | 6,56 | 0,15 | 0,00 | 0,00 | 5,73 | 0,00 | 10,20 | 0,00 | 0,00 | 0,00 | 46,97 | 0,22 | 0,99 | 27,67 |
| Grosstalbach | 17,89 | 1,48 | 2,71 | 0,00 | 4,73 | 25,26 | 0,00 | 9,55 | 0,23 | 0,05 | 0,09 | 28,01 | 0,00 | 0,75 | 9,25 |
| Alp | 48,51 | 0,00 | 3,62 | 0,00 | 30,56 | 9,94 | 0,19 | 1,29 | 2,59 | 0,41 | 1,36 | 0,84 | 0,00 | 0,69 | 0,00 |
| Rhone | 0,00 | 2,81 | 0,13 | 0,00 | 0,00 | 8,79 | 0,00 | 0,51 | 9,42 | 0,03 | 0,00 | 29,69 | 0,43 | 0,05 | 48,15 |
| Massa | 0,68 | 0,03 | 0,15 | 0,00 | 0,00 | 2,87 | 0,00 | 3,52 | 0,00 | 0,00 | 0,00 | 26,74 | 0,01 | 0,07 | 65,93 |
| Venoge | 31,04 | 0,00 | 1,88 | 1,74 | 54,20 | 2,30 | 0,83 | 0,16 | 0,18 | 4,17 | 0,28 | 0,09 | 3,12 | 0,02 | 0,00 |
| Melera | 86,27 | 0,00 | 0,99 | 0,00 | 0,00 | 10,78 | 0,00 | 1,96 | 0,00 | 0,00 | 0,00 | 0,00 | 0,00 | 0,00 | 0,00 |
| Verzasca | 28,78 | 12,67 | 3,31 | 0,00 | 0,80 | 8,02 | 0,02 | 25,04 | 0,30 | 0,01 | 0,10 | 18,95 | 0,06 | 1,94 | 0,00 |
| Riale di Calneggia | 6,87 | 6,71 | 3,94 | 0,00 | 0,05 | 8,93 | 0,00 | 18,23 | 0,04 | 0,00 | 0,00 | 52,51 | 1,40 | 1,32 | 0,00 |
| Krummbach | 0,25 | 0,00 | 1,01 | 0,00 | 0,00 | 55,89 | 0,00 | 12,15 | 0,05 | 0,00 | 0,66 | 25,25 | 0,50 | 1,21 | 3,03 |
| Poschiavino | 6,35 | 1,07 | 2,14 | 0,00 | 0,00 | 48,50 | 0,00 | 12,62 | 0,30 | 0,00 | 1,85 | 25,18 | 0,10 | 1,54 | 0,35 |
| Ova da Cluozza | 5,07 | 12,78 | 0,60 | 0,00 | 0,00 | 0,00 | 0,00 | 12,07 | 0,00 | 0,00 | 0,00 | 66,91 | 0,01 | 0,33 | 2,23 |

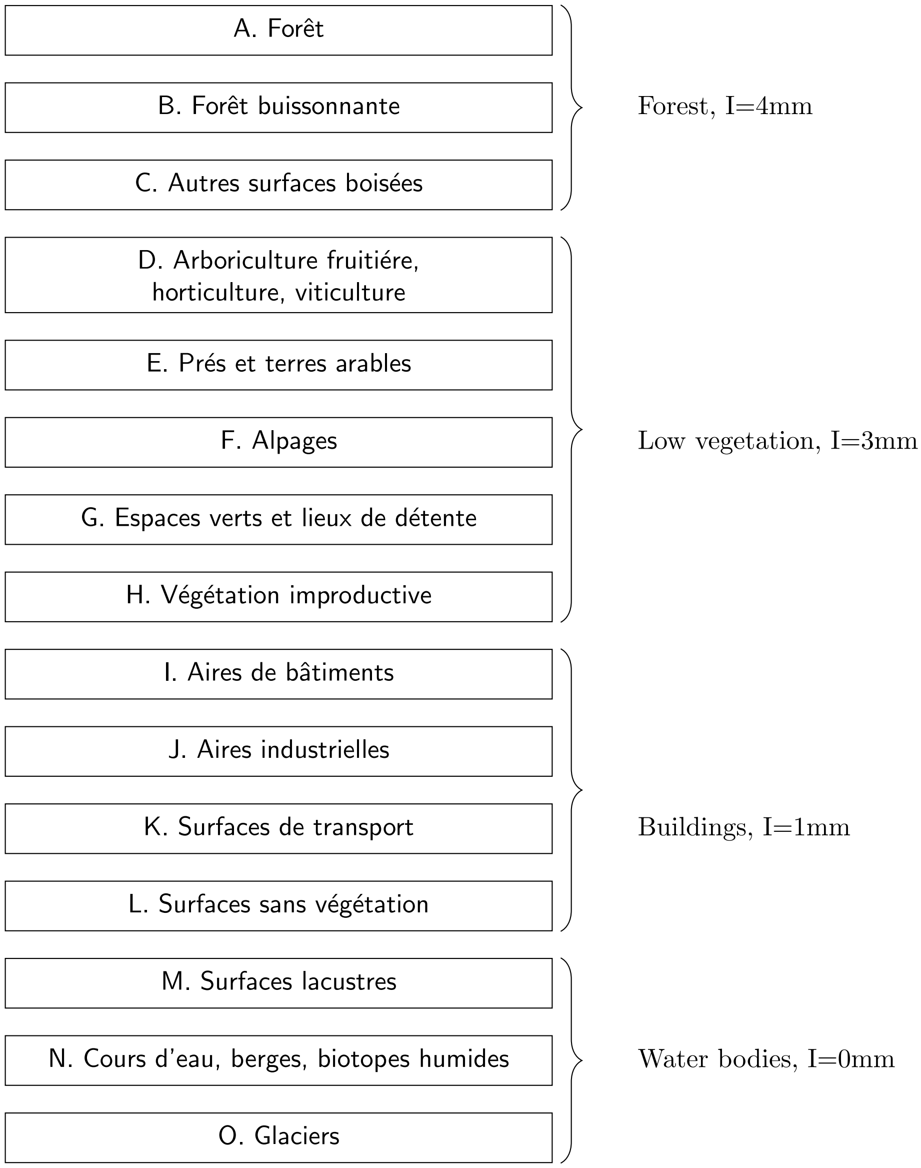


Figure A.1 – Equivalence between the land use categories proposed by the FOEN and the ones adopted to calculate interception, followed by the value of interception for each category.

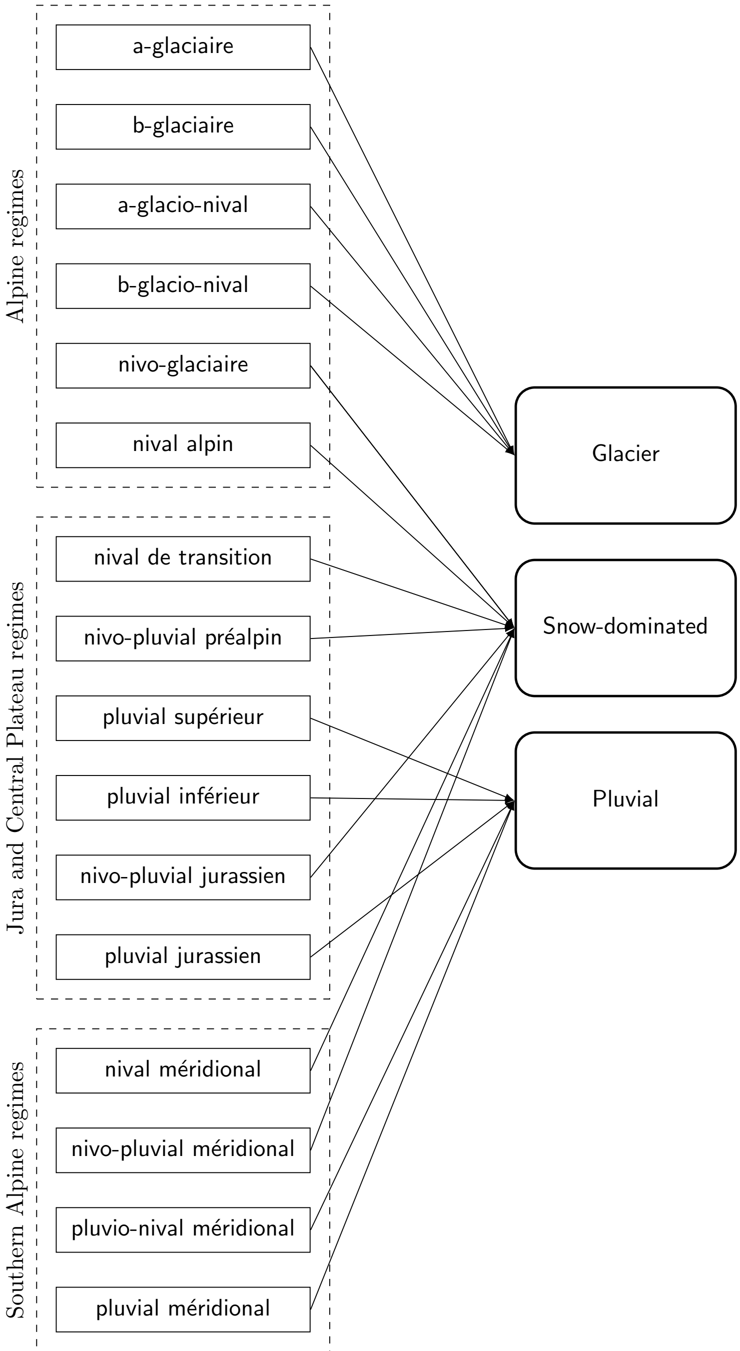


Figure A.2 – Equivalence between the 16 discharge regimes from the Hydrological Atlas of Switzerland and the simplified classification in 3 types of regimes adopted in this work.

Table A.2 – Spatial data classes (FSO, 2001) associated to FOEN land use classes (Aschwanden, 1996).

| ID own | FOEN land use hydrological study areas | Geostat1997 classes associated to this FOEN class |
|---|---|---|
| A | Forêt | 9, 10, 11, 12, 13, 14 |
| B | Forêt buissonnante | 15 |
| C | Autres surfaces boisées | 17, 18, 19 |
| D | Arboriculture fruitière, horticulture, viticulture | 71, 72, 75, 76, 77, 78 |
| E | Prés et terres arables | 73, 81, 82, 83, 84 |
| F | Alpages | 85, 86, 87, 88, 89 |
| G | Végétation improductive | 16, 95, 96, 97, 98 |
| H | Aires de bâtiments | 25,26, 27, 28, 29, 45, 46, 47, 48, 49 |
| I | Aires industrielles | 21, 41 |
| J | Espaces verts et lieux de détente | 23, 51, 52, 53, 54, 56, 59 |
| K | Surfaces de transport | 31, 32, 33, 34, 35, 36, 37, 38, 68, 67 |
| L | Surfaces lacustres | 91 |
| M | Cours d'eau, berges, biotopes humides | 92, 93, 69 |
| N | Surfaces sans végétation | 99 |
| O | Glaciers | 90 |

Table A.3 – Selected precipitation grid cells of the MeteoSwiss RhiresD (MeteoSwiss, 2014a) per catchment.

| Catchment | Cells |
|---|---|
| Rein da Sumvitg | 15923; 16026; 16128; 16129; 16231; 16232; 16233 |
| Dischmabach | 20448; 20449; 20551; 20552; 20553; 20655; 20657; 20759; 20760 |
| Goldach | 18150; 18252; 18253; 18254; 18355; 18356; 18357; 18358; 18459; 18460; 18461; 18562; 18563; 18564; 18666 |
| Necker | 16712; 16713; 16816; 16817; 16818; 16919; 16920; 16921; 17022; 17023; 17024; 17025; 17125; 17126; 17127; 17128; 17228; 17229; 17230; 17231; 17331; 17333; 17334; 17437 |
| Sitter | 17745; 17746; 17848; 17849; 17850; 17951; 17952; 17953; 18054; 18055; 18156; 18157; 18158; 18258; 18259; 18260; 18361; 18362; 18363; 18465; 18466 |
| Murg | 15679; 15782; 15783; 15882; 15883; 15884; 15885; 15886; 15887; 15984; 15985; 15986; 15987; 15988; 15989; 16088; 16089; 16090; 16091; 16191; 16193; 16294; 16396 |
| Scheulte | 8370; 8371; 8472; 8473; 8474; 8575; 8576; 8577; 8678; 8679; 8680; 8681; 8781; 8782; 8783; 8885; 8886; 8988; 8989 |
| Gürbe | 8502; 8503; 8598; 8599; 8600; 8601; 8602; 8604; 8605; 8606; 8701; 8702; 8703; 8704; 8705; 8706; 8707; 8708; 8709; 8805; 8806; 8807; 8808; 8809; 8810; 8811; 8812; 8909; 8911; 8912; 8913; 8914; 8915 |
| Rotenbach | 7577 |
| Sense | 7475; 7476; 7477; 7574; 7575; 7576; 7577; 7578; 7579; 7676; 7677; 7678; 7679; 7680; 7681; 7682; 7776; 7777; 7778; 7779; 7780; 7781; 7782; 7783; 7784; 7877; 7878; 7879; 7880; 7881; 7882; 7883; 7884; 7885; 7886; 7887; 7980; 7981; 7982; 7983; 7984; 7985; 7986; 7987; 7988; 7989; 7990; 8082; 8083; 8084; 8085; 8086; 8087; 8088; 8089; 8090; 8091; 8092; 8185; 8186; 8187; 8188; 8189; 8190; 8191; 8192; 8193; 8194; 8195; 8391; 8392; 8393; 8394; 8395; 8396; 8397; 8398; 8399; 8400; 8495; 8496; 8497; 8498; 8499; 8500; 8501; 8603 |
| Areuse | 3346; 3348; 3445; 3451; 3452; 3451; 3452; 3453; 3454; 3455; 3651; 3652; 3653; 3657; 3753; 3754; 3757; 3758; 3856; 3857; 3858; 3859; 3860; 3861; 3959; 3960; 3961; 3962; 3963; 3964; 4061; 4062; 4063; 4064; 4065; 4066; 4164; 4165; 4166; 4167; 4168; 4169; 4267; 4268; 4269; 4270; 4271; 4272; 4369; 4370; 4371; 4372; 4373; 4374; 4471; 4472; 4473; 4474; 4475; 4476; 4477; 4574; 4575; 4576; 4577; 4578; 4579; 4677; 4678; 4679; 4680; 4681; 4681; 4780; 4781; 4782; 4783; 4784; 4883; 4884; 4885; 4886; 4887; 4986; 4987; 4988; 4989; 4990; 5089; 5090; 5091; 5092; 5191; 5192; 5195; 5294; 5298; 5396; 5397 |
| Ilfis | 10241; 10242; 10243; 10244; 10343; 10344; 10345; 10346; 10347; 10348; 10447; 10448; 10449; 10450; 10451; 10549; 10550; 10551; 10552; 10553; 10554; 10555; 10556; 10557; 10652; 10653; 10654; 10655; 10656; 10657; 10658; 10659; 10660; 10755; 10756; 10757; 10758; 10759; 10760; 10761; 10762; 10763; 10858; 10859; 10863; 10864; 10865; 10866; 10966; 10967; 10968; 11070; 11071 |
| Sellenbodenbach | 12090; 12192; 12193 |
| Alpbach | 13854; 13855; 13957; 13958; 14060; 14061 |
| Grosstalbach | 13541; 13542; 13644; 13645; 13646; 13746; 13747; 13748; 13749; 13849; 13852 |
| Alp | 14564; 14664; 14665; 14666; 14667; 14766; 14767; 14768; 14769; 14770; 14868; 14869 |
| Rhone | 13039; 13040; 13041; 13042; 13141; 13142; 13143; 13144; 13145; 13244; 13245; 13248 |
| Massa | 10783; 10882; 10885; 10886; 10985; 10986; 10987; 10988; 10989; 11086; 11087; 11088; 11089; 11090; 11091; 11092; 11189; 11190; 11191; 11192; 11193; 11194; 11195; 11196; 11292; 11293; 11294; 11295; 11296; 11297; 11298; 11299; 11395; 11396; 11397; 11398; 11399; 11400; 11401; 11402; 11498; 11499; 11500; 11501; 11502; 11503; 11504; 11603; 11604; 11605; 11606; 1709 |
| Venoge | 2844; 2946; 2947; 2948; 3048; 3049; 3050; 3051; 3150; 3152; 3153; 3154; 3253; 3254; 3255; 3256; 3355; 3356; 3357; 3358; 3458; 3459; 3460; 3461; 3561; 3562; 3563; 3564; 3565; 3665; 3666; 3667; 3668; 3669; 3670; 3768; 3769; 3770; 3771; 3772; 3773; 3871; 3872; 3873; 3874; 3875; 3979; 3974; 3975; 3976; 3977; 3978; 3979; 4077; 4078; 4079; 4080; 4082 |
| Melera | 16562 |
| Verzasca | 14701; 14702; 14803; 14804; 14805; 14904; 14905; 14906; 14907; 14908; 14909; 15007; 15008; 15009; 15010; 15011; 15012; 15111; 15112; 15113; 15114; 15115; 15116; 15117; 15214; 15215; 15216; 15217; 15218; 15219; 15220; 15318; 15319; 15320; 15321; 15322; 15323; 15423; 15424; 15425; 15526; 15527; 15528; 15529; 15630; 15631; 15632; 15735 |
| Riale di Calneggia | 13566; 13567; 13669; 13670; 13773; 13876 |
| Krummbach | 11203; 11204; 11205; 11306; 11307 |
| Poschiavino | 21288; 21289; 21392 |
| Ova da Cluozza | 21586; 21587; 21588; 21689; 21690; 21691 |

Table A.4 – Sources of the data used in this work.

| Type of data | All catchments | Source |
|---|---|---|
| Daily discharge | All catchments | FOEN (on demand) |
| Daily precipitation | All catchments | MeteoSwiss (Rhires D) (www.meteoswiss.admin.ch- requires contract) |
| Daily temperature | All catchments | MeteoSwiss (Tabs D) (www.meteoswiss.admin.ch- requires contract) |
| Elevations of catchments | All catchments | FOEN (www.hydrodaten.admin.ch) |
| Land use | Study areas | Aschwanden, 1996 |
| | Other catchments | FSO, 2001 |
| Regimes | Study areas | Aschwanden, 1996 |
| | Other catchments | FOEN (map.geo.admin.ch) |

## Results for all catchments for the linear model

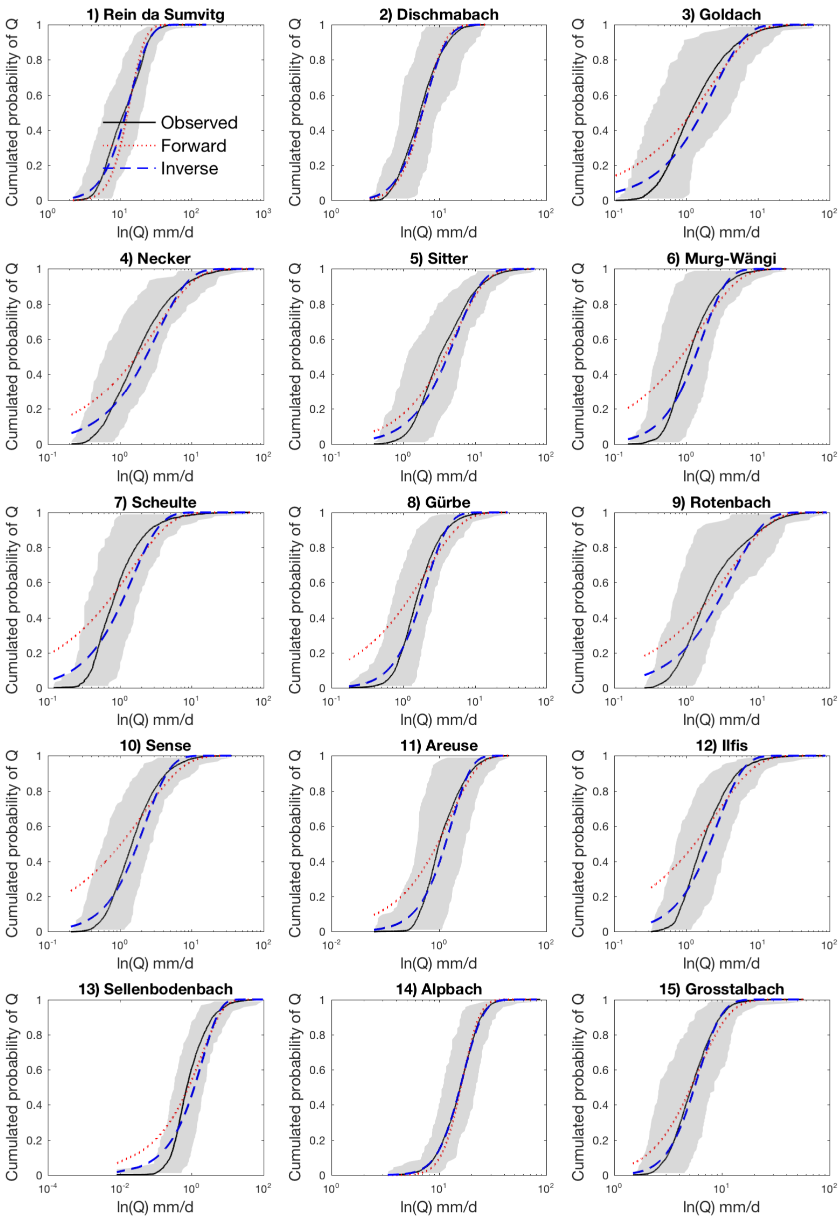

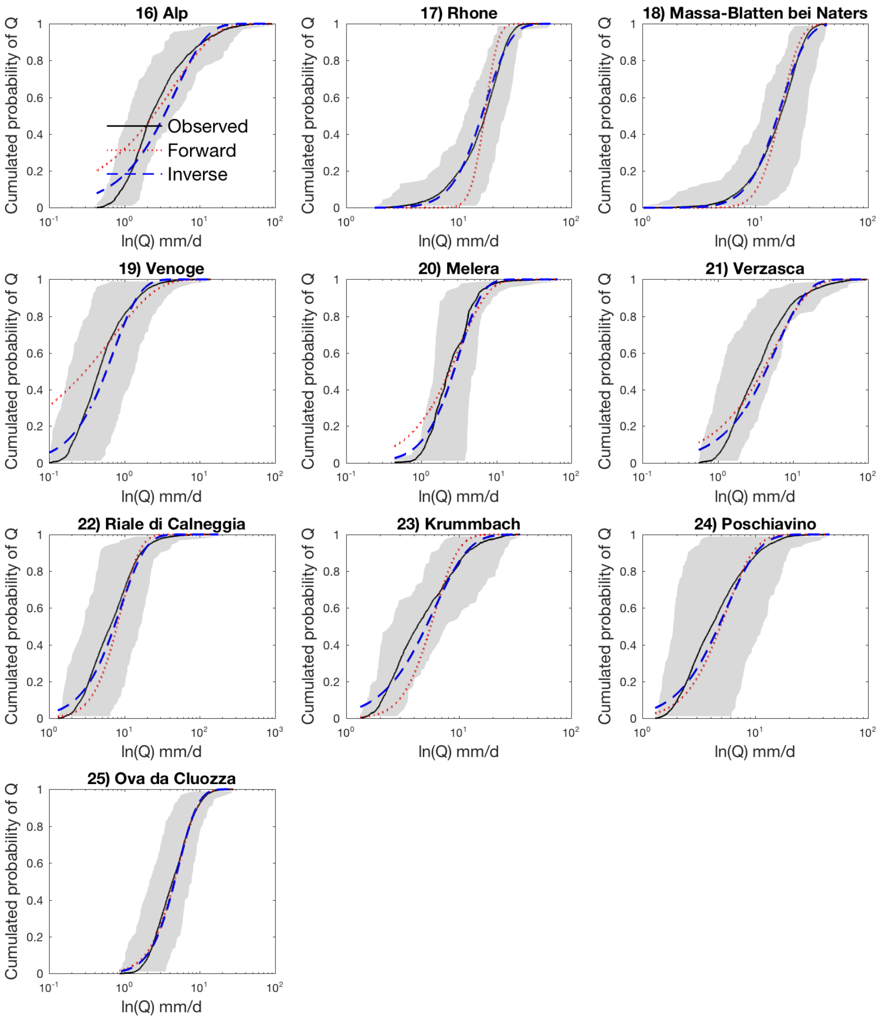

16) Alp
17) Rhone
18) Massa-Blatten bei Naters
19) Venoge
20) Melera
21) Verzasca
22) Riale di Calneggia
23) Krummbach
24) Poschiavino
25) Ova da Cluozza
Observed
Forward
Inverse
Cumulated probability of Q
ln(Q) mm/d

## Results for all catchments for the nonlinear model

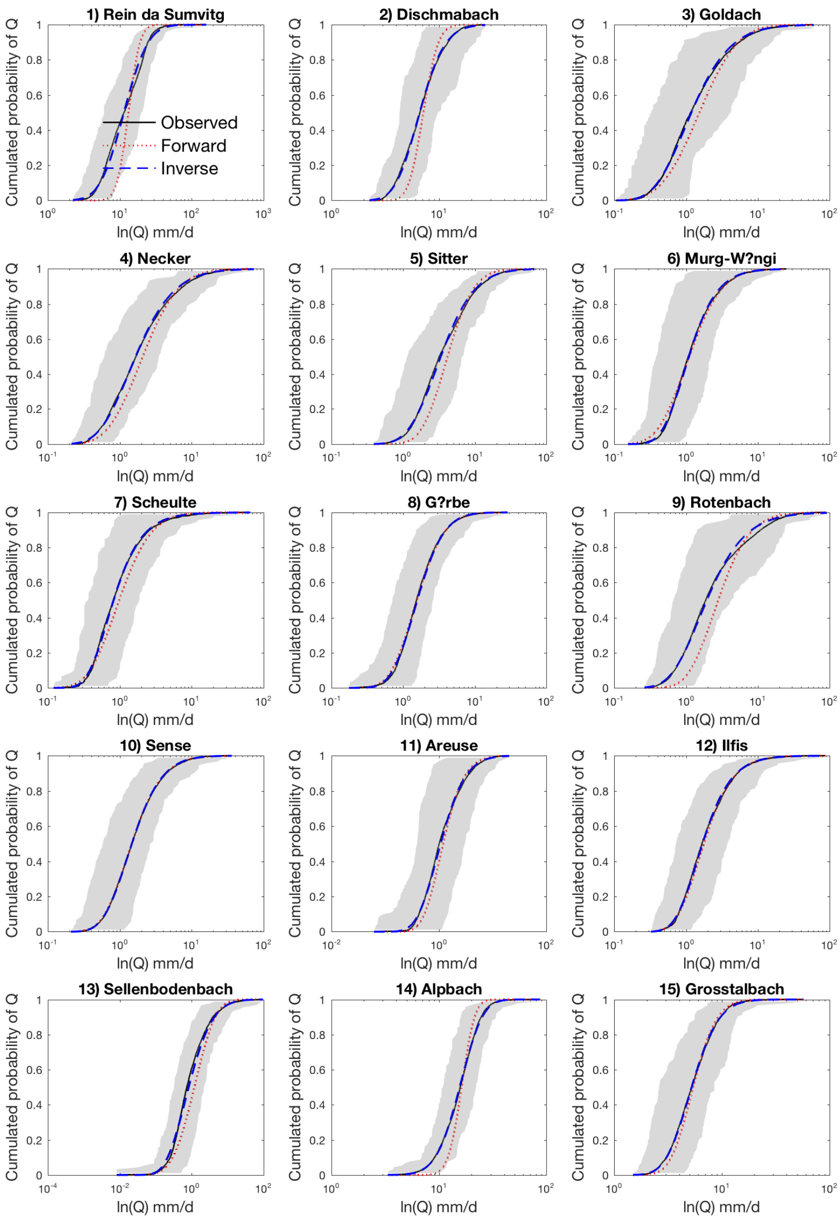

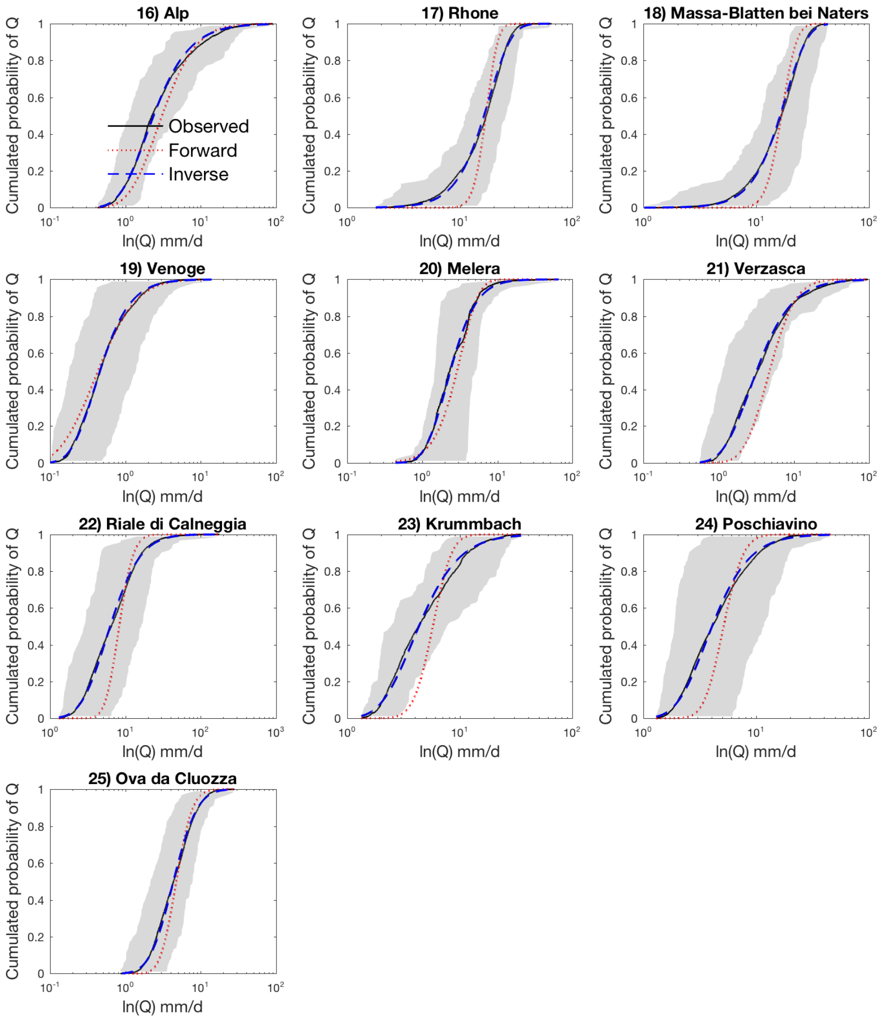
16) Alp
17) Rhone
18) Massa-Blatten bei Naters
19) Venoge
20) Melera
21) Verzasca
22) Riale di Calneggia
23) Krummbach
24) Poschiavino
25) Ova da Cluozza
Cumulated probability of Q
ln(Q) mm/d
Observed
Forward
Inverse

# B Supplementary material to Chapter 4

The supplementary material contains 3 figures and a Matlab code with the implementation of the MLE parameter estimation. The figures show:

- Figure 1: Annual variation of model parameters .
- Figure 2: Histograms of the inter-arrival times of the streamflow generating events.
- Figure 3: Histograms of the recharge depths.

## B.1 Figures

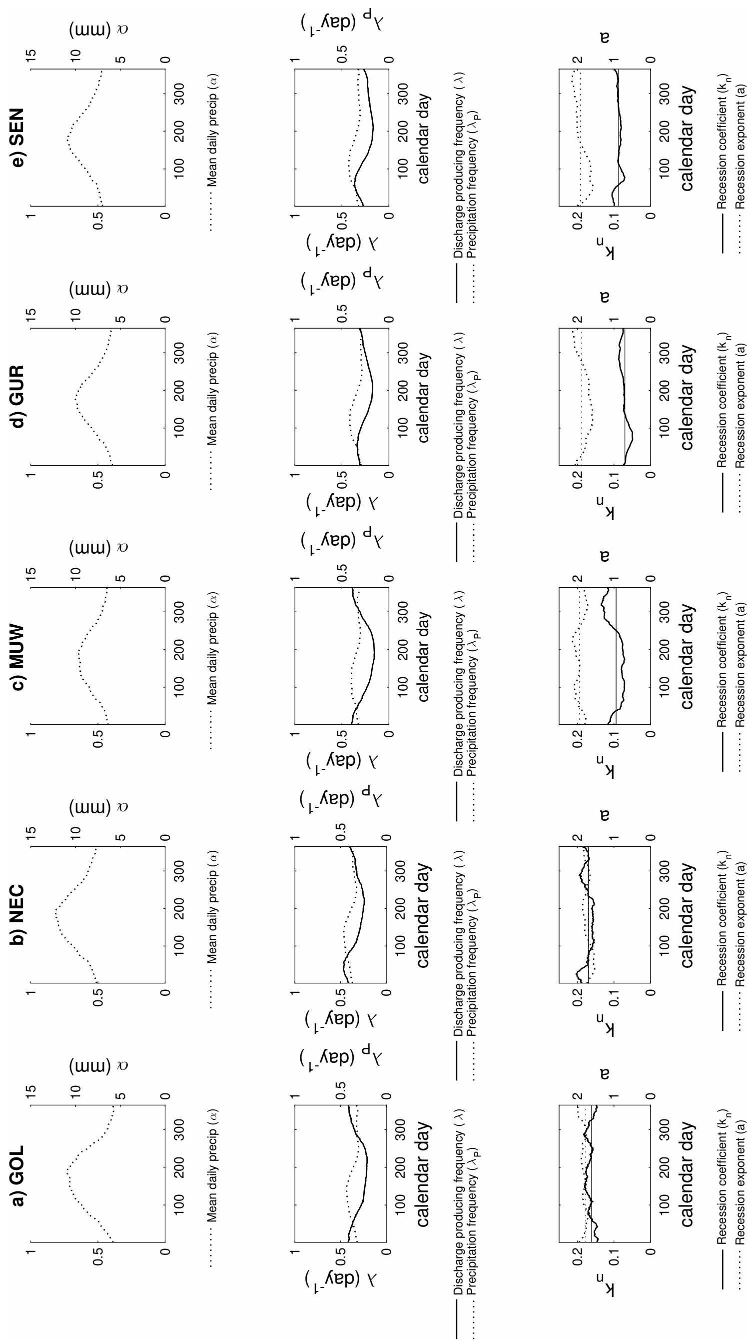

Figure B.1 – Annual variation of model parameters (mean precipitation depth, $\alpha$, discharge producing frequency, $\lambda$, precipitation frequency, $\lambda_p$, and recession parameters $a$ and $k_n$) for each case study. The parameters presented in the figure were calculated for overlapping intervals of three months centered on the dates of a civil year. Recession parameters are obtained by MLE.

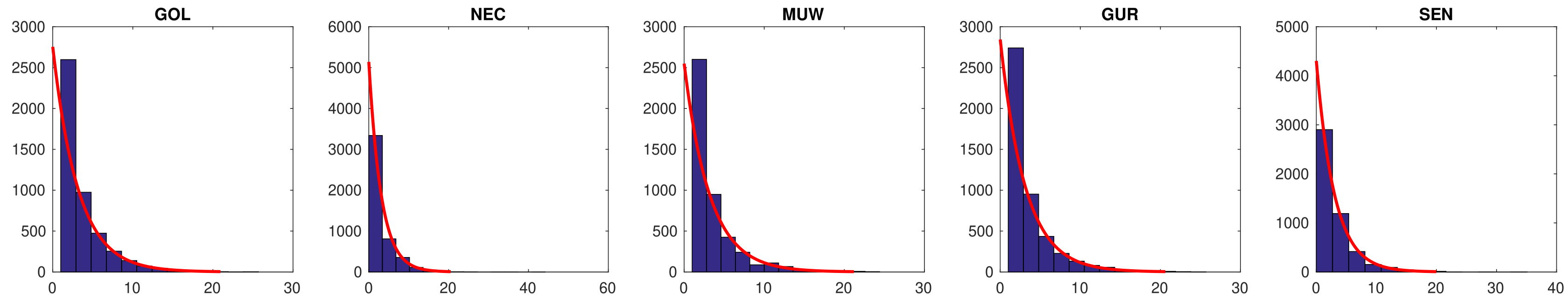


Figure B.2 – Histograms of the inter-arrival times of the streamflow generating events and an exponential distribution.

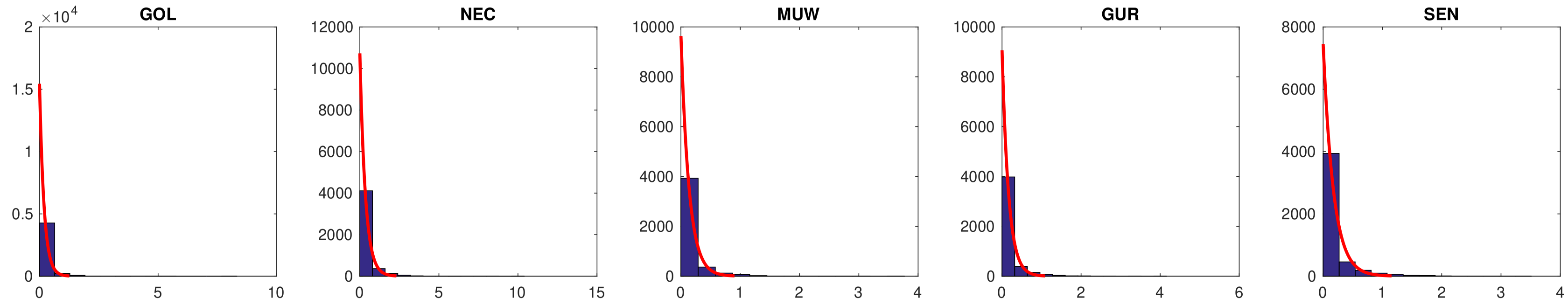


Figure B.3 – Histograms of the recharge depths and an exponential distribution. The power exponents estimated via MLE for each catchment are close to 2, so it is possible to compute storage increments by approximating it with a polynomial.

## B.2 Matlab code

```

clear all; close all

% prepare a daily discharge series in mm/day, format n x 1, call it Q

% for illustration purposes, we use a random process obtained by first
  generating a marked Poisson process (to emulate the precipitation series)
  and then simply filtering it to emulate a discharge series 0) set the
  state of the random number generator
rng(123456); % can choose any value 1) generate a marked Poisson process
lambdaP=0.5; % frequency of the Poisson process
alpha=3; % mean precipitation on days with precipitation
N=3000; % number of precip events to generate
precip_times = cumsum(random('Poisson',1/lambdaP, [N,1]));
precip_times(precip_times<1)=[]; % remove precipitation times smaller than 1
N=length(precip_times); % update the length of the series
precip_amounts = random('Exp',alpha,N,1);
precip=accumarray(precip_times, precip_amounts); % Matlab function to build
  arrays of values
% check frequency of generated series: sum(precip>0)/length(precip)
% compute actual mean precip on precip days
% alphaObs=mean(precip(precip>0))

% 2) now compute pseudo discharge Q by simple linear filtering
windowSize=20;% not too large window size, otherwise MLE cannot find a
  solution
Q = filter(ones(1,windowSize)/windowSize,1,precip); % Q in mm/day
Q(Q==0)=0.1; % add a small value since zeros yield NaN values in pdf
  evaluation

% compute the discharge generating frequency lambda<lambdaP,
lambda=mean(Q)/alpha; % equation 6 of the paper

% 3) define the pdf function of equation 5 of the paper with input k and a
% first define the not normalized part of the function
pdfNotNorm=@(Q,a,k) Q.^(-a).*exp(-Q.^(2-a)/(alpha*k*(2-a))+lambda*Q.^(1-a)/(
  k*(1-a)));

% We can now write the pdf as function of the normalization constant C
% custompdf=@(Q,a,k) C*pdfNotNorm(Q,a,k);
% where the normalizing constant is obtained as
% C=1/integral(@(Q) pdfNotNorm(Q,a,k),0,inf,'AbsTol',1e-5);

% for MLE, write above in a single function
custompdf=@(Q,a,k) 1/integral(@(Q) pdfNotNorm(Q,a,k),0,inf,'AbsTol',1e-5)*
  pdfNotNorm(Q,a,k);

% 4) MLE estimation
% define lower and upper bounds for MLE estimation for parameter a and k
  these bounds need to be adjusted to the problem at hand; depending on the
  above random process realization, the used bounds might not work
lowerbd=[1.1,0.05]; % lower bounds a, k
upperbd=[2.5,5];% upper bounds a, k
startval=[1.8,1]; % initial value

% find the optimal values of a and k with the Matlab function MLE or any
% other optimisation function
```

```
optimle=mle(Q,'pdf',custompdf,'start',startval,'lowerbound',lowerbd,'
  upperbound',upperbd);
opta=optimle(1); %MLE value for k
optk=optimle(2); %MLE value for a

% 5) plot the results
% first estimate the empirical distribution via histogram function
[freq,bins]=hist(Q,20);
% estimate the normalization constant
binWidth=bins(2)-bins(1);
normalization=sum(freq)*binWidth;
figure(1)
plot(bins,freq/normalization,'o')
sQ=sort(Q); % sorted Q
hold on
plot(sQ,custompdf(sQ,opta,optk))
xlabel('Discharge')
ylabel('pdf')
```

# C Supplementary material to Chapter 5

The supplementary material contains 5 tables with the following results for each catchment and time interval:

- Linear recession parameter ($k$, Table C.2)
- Linear model performance considering the estimated parameters ($c_l^{KS}$, Table C.3)
- Nonlinear recession exponent ($a$, Table C.4)
- Nonlinear recession coefficient ($k_n$, Table C.5)
- Nonlinear model performance considering the estimated parameters ($c_n^{KS}$, Table C.6)

The studied methods are summarized in Table C.1:

Table C.1 – Synthesis of the adopted RAMs

| Symbol | Description | References |
|---|---|---|
| E1 | Permissive recession extraction | Santos et al. (2019); Schaefli et al. (2013) |
| E2 | Intermediate recession extraction | Vogel and Kroll (1992) |
| E3 | Recession extraction with concavity criteria | Dralle et al. (2017b) |
| PL1 | Linear parameter estimation based on master recession curve | Brutsaert and Nieber (1977) |
| PL2 | Linear parameter estimation per event | |
| PN1 | Nonlinear parameter estimation based on master recession curve | Brutsaert and Nieber (1977) |
| PN2 | Nonlinear parameter estimation with linear least square method per event | Basso et al. (2015b); Mutzner et al. (2013) |
| PN3 | Decorrelation nonlinear parameter estimation per event | Dralle et al. (2015) |

Table C.2 – Linear recession parameters ($k$) for each case

| | | E1 | | E2 | | E3 | |
|---|---|---|---|---|---|---|---|
| Case | MLE | PL1 | PL2 | PL1 | PL2 | PL1 | PL2 |
| GOL | | | | | | | |
| Spring | 0,43 | 0,11 | 0,19 | 0,10 | 0,22 | 0,12 | 0,37 |
| Summer | 0,40 | 0,15 | 0,28 | 0,09 | 0,20 | 0,16 | 0,57 |
| Autumn | 0,35 | 0,12 | 0,24 | 0,10 | 0,20 | 0,15 | 0,52 |
| Winter | 0,43 | 0,08 | 0,17 | 0,07 | 0,19 | 0,11 | 0,36 |
| Year C | 0,41 | 0,11 | 0,22 | 0,09 | 0,20 | 0,14 | 0,48 |
| Year S | 0,40 | 0,12 | 0,22 | 0,09 | 0,20 | 0,14 | 0,45 |
| NEC | | | | | | | |
| Spring | 0,29 | 0,10 | 0,20 | 0,09 | 0,18 | 0,12 | 0,44 |
| Summer | 0,26 | 0,14 | 0,31 | 0,12 | 0,21 | 0,15 | 0,62 |
| Autumn | 0,23 | 0,10 | 0,25 | 0,09 | 0,20 | 0,12 | 0,54 |
| Winter | 0,28 | 0,08 | 0,18 | 0,07 | 0,18 | 0,10 | 0,47 |
| Year C | 0,27 | 0,10 | 0,23 | 0,09 | 0,19 | 0,13 | 0,53 |
| Year S | 0,27 | 0,10 | 0,23 | 0,09 | 0,19 | 0,12 | 0,52 |
| MUW | | | | | | | |
| Spring | 0,17 | 0,06 | 0,13 | 0,05 | 0,15 | 0,07 | 0,25 |
| Summer | 0,11 | 0,09 | 0,16 | 0,06 | 0,18 | 0,11 | 0,35 |
| Autumn | 0,13 | 0,07 | 0,13 | 0,06 | 0,17 | 0,10 | 0,39 |
| Winter | 0,21 | 0,04 | 0,13 | 0,04 | 0,14 | 0,06 | 0,26 |
| Year C | 0,16 | 0,06 | 0,13 | 0,05 | 0,16 | 0,09 | 0,31 |
| Year S | 0,16 | 0,06 | 0,14 | 0,05 | 0,16 | 0,09 | 0,31 |
| GUR | | | | | | | |
| Spring | 0,08 | 0,05 | 0,11 | 0,03 | 0,17 | 0,05 | 0,25 |
| Summer | 0,07 | 0,07 | 0,15 | 0,06 | 0,15 | 0,08 | 0,36 |
| Autumn | 0,07 | 0,05 | 0,10 | 0,05 | 0,12 | 0,08 | 0,36 |
| Winter | 0,10 | 0,04 | 0,09 | 0,03 | 0,12 | 0,06 | 0,26 |
| Year C | 0,09 | 0,05 | 0,11 | 0,04 | 0,14 | 0,07 | 0,32 |
| Year S | 0,08 | 0,05 | 0,11 | 0,04 | 0,14 | 0,07 | 0,31 |
| SEN | | | | | | | |
| Spring | 0,04 | 0,05 | 0,15 | 0,04 | 0,09 | 0,06 | 0,36 |
| Summer | 0,03 | 0,08 | 0,19 | 0,06 | 0,15 | 0,09 | 0,52 |
| Autumn | 0,03 | 0,07 | 0,15 | 0,06 | 0,14 | 0,10 | 0,44 |
| Winter | 0,03 | 0,06 | 0,13 | 0,05 | 0,15 | 0,08 | 0,40 |
| Year C | 0,04 | 0,06 | 0,16 | 0,05 | 0,14 | 0,09 | 0,45 |
| Year S | 0,03 | 0,06 | 0,16 | 0,05 | 0,13 | 0,08 | 0,43 |
| ARE | | | | | | | |
| Spring | 0,07 | 0,06 | 0,16 | 0,05 | 0,14 | 0,08 | 0,28 |
| Summer | 0,03 | 0,08 | 0,15 | 0,07 | 0,15 | 0,11 | 0,38 |
| Autumn | 0,04 | 0,07 | 0,20 | 0,06 | 0,15 | 0,10 | 0,39 |
| Winter | 0,06 | 0,05 | 0,20 | 0,05 | 0,17 | 0,07 | 0,33 |
| Year C | 0,06 | 0,07 | 0,18 | 0,06 | 0,15 | 0,09 | 0,35 |
| Year S | 0,05 | 0,07 | 0,18 | 0,06 | 0,15 | 0,09 | 0,34 |

Table C.3 – Linear model performances ($c_l^{KS}$) for each case

| | | E1 | | E2 | | E3 | |
|---|---|---|---|---|---|---|---|
| Case | MLE | PL1 | PL2 | PL1 | PL2 | PL1 | PL2 |
| GOL | | | | | | | |
| Spring | 0,09 | 0,31 | 0,21 | 0,32 | 0,19 | 0,29 | 0,11 |
| Summer | 0,13 | 0,30 | 0,19 | 0,38 | 0,25 | 0,29 | 0,16 |
| Autumn | 0,13 | 0,31 | 0,19 | 0,34 | 0,22 | 0,27 | 0,18 |
| Winter | 0,12 | 0,38 | 0,26 | 0,41 | 0,25 | 0,33 | 0,14 |
| Year C | 0,11 | 0,32 | 0,21 | 0,37 | 0,23 | 0,29 | 0,10 |
| Year S | 0,12 | 0,34 | 0,23 | 0,38 | 0,25 | 0,33 | 0,13 |
| NEC | | | | | | | |
| Spring | 0,07 | 0,23 | 0,11 | 0,24 | 0,12 | 0,19 | 0,10 |
| Summer | 0,13 | 0,23 | 0,11 | 0,25 | 0,16 | 0,21 | 0,28 |
| Autumn | 0,10 | 0,25 | 0,09 | 0,27 | 0,12 | 0,21 | 0,28 |
| Winter | 0,12 | 0,31 | 0,17 | 0,33 | 0,17 | 0,27 | 0,18 |
| Year C | 0,09 | 0,26 | 0,12 | 0,29 | 0,14 | 0,21 | 0,20 |
| Year S | 0,10 | 0,26 | 0,12 | 0,25 | 0,16 | 0,27 | 0,19 |
| MUW | | | | | | | |
| Spring | 0,10 | 0,26 | 0,14 | 0,28 | 0,12 | 0,22 | 0,14 |
| Summer | 0,12 | 0,16 | 0,15 | 0,21 | 0,19 | 0,12 | 0,33 |
| Autumn | 0,13 | 0,22 | 0,13 | 0,25 | 0,14 | 0,16 | 0,34 |
| Winter | 0,09 | 0,35 | 0,18 | 0,37 | 0,16 | 0,30 | 0,10 |
| Year C | 0,10 | 0,24 | 0,13 | 0,29 | 0,11 | 0,19 | 0,20 |
| Year S | 0,10 | 0,26 | 0,14 | 0,27 | 0,11 | 0,23 | 0,19 |
| GUR | | | | | | | |
| Spring | 0,07 | 0,15 | 0,10 | 0,20 | 0,18 | 0,15 | 0,26 |
| Summer | 0,09 | 0,11 | 0,20 | 0,14 | 0,19 | 0,10 | 0,40 |
| Autumn | 0,12 | 0,17 | 0,15 | 0,18 | 0,20 | 0,12 | 0,44 |
| Winter | 0,11 | 0,27 | 0,14 | 0,28 | 0,13 | 0,20 | 0,28 |
| Year C | 0,08 | 0,16 | 0,11 | 0,18 | 0,14 | 0,11 | 0,33 |
| Year S | 0,09 | 0,16 | 0,09 | 0,21 | 0,15 | 0,19 | 0,30 |
| SEN | | | | | | | |
| Spring | 0,05 | 0,10 | 0,32 | 0,05 | 0,20 | 0,14 | 0,51 |
| Summer | 0,10 | 0,27 | 0,49 | 0,21 | 0,42 | 0,29 | 0,70 |
| Autumn | 0,13 | 0,29 | 0,48 | 0,25 | 0,46 | 0,39 | 0,71 |
| Winter | 0,11 | 0,20 | 0,40 | 0,18 | 0,43 | 0,27 | 0,64 |
| Year C | 0,08 | 0,18 | 0,41 | 0,15 | 0,38 | 0,27 | 0,64 |
| Year S | 0,10 | 0,18 | 0,38 | 0,13 | 0,34 | 0,22 | 0,62 |
| ARE | | | | | | | |
| Spring | 0,05 | 0,06 | 0,20 | 0,09 | 0,17 | 0,06 | 0,35 |
| Summer | 0,12 | 0,31 | 0,45 | 0,27 | 0,45 | 0,36 | 0,66 |
| Autumn | 0,12 | 0,20 | 0,45 | 0,17 | 0,38 | 0,27 | 0,62 |
| Winter | 0,11 | 0,13 | 0,33 | 0,14 | 0,29 | 0,09 | 0,46 |
| Year C | 0,09 | 0,09 | 0,32 | 0,09 | 0,28 | 0,16 | 0,50 |
| Year S | 0,09 | 0,09 | 0,31 | 0,08 | 0,27 | 0,14 | 0,49 |

Table C.4 – Nonlinear recession exponent ($a$) for each case

| | | | E1 | | | E2 | | | E3 | |
|---|---|---|---|---|---|---|---|---|---|---|
| Case | MLE | PN1 | PN2 | PN3 | PN1 | PN2 | PN3 | PN1 | PN2 | PN3 |
| GOL | | | | | | | | | | |
| Spring | 1,67 | 1,52 | 2,32 | 2,21 | 1,59 | 1,77 | 1,78 | 1,63 | 2,02 | 1,73 |
| Summer | 1,81 | 1,55 | 2,30 | 2,19 | 1,55 | 2,30 | 2,32 | 1,62 | 1,89 | 1,68 |
| Autumn | 1,86 | 1,76 | 2,44 | 2,23 | 2,10 | 2,48 | 2,32 | 1,76 | 1,97 | 1,74 |
| Winter | 1,94 | 1,70 | 2,50 | 2,42 | 1,70 | 2,30 | 2,53 | 1,64 | 2,18 | 1,88 |
| Year C | 1,76 | 1,57 | 2,38 | 2,28 | 1,70 | 2,29 | 2,29 | 1,64 | 2,02 | 1,74 |
| Year S | 1,82 | 1,63 | 2,39 | 2,26 | 1,73 | 2,21 | 2,24 | 1,66 | 2,01 | 1,76 |
| NEC | | | | | | | | | | |
| Spring | 1,53 | 1,42 | 2,56 | 2,39 | 1,26 | 1,73 | 2,27 | 1,54 | 2,23 | 1,88 |
| Summer | 1,81 | 1,73 | 2,40 | 2,31 | 1,97 | 2,21 | 2,16 | 1,71 | 1,90 | 1,68 |
| Autumn | 1,75 | 1,84 | 2,43 | 2,28 | 1,99 | 2,32 | 2,25 | 1,83 | 2,02 | 1,78 |
| Winter | 1,87 | 1,76 | 2,38 | 2,27 | 1,77 | 1,87 | 2,39 | 1,80 | 2,04 | 1,77 |
| Year C | 1,68 | 1,65 | 2,44 | 2,31 | 1,64 | 2,17 | 2,27 | 1,68 | 2,01 | 1,76 |
| Year S | 1,74 | 1,69 | 2,44 | 2,31 | 1,74 | 2,03 | 2,27 | 1,72 | 2,05 | 1,78 |
| MUW | | | | | | | | | | |
| Spring | 2,04 | 1,82 | 2,78 | 2,62 | 1,95 | 2,53 | 2,39 | 1,88 | 2,49 | 2,30 |
| Summer | 2,00 | 1,86 | 3,17 | 3,03 | 2,01 | 2,89 | 2,50 | 1,79 | 2,21 | 1,94 |
| Autumn | 2,17 | 1,99 | 3,16 | 2,84 | 2,20 | 2,95 | 2,83 | 1,89 | 2,46 | 2,18 |
| Winter | 2,08 | 2,02 | 2,79 | 2,65 | 2,10 | 2,64 | 2,51 | 1,93 | 2,50 | 2,34 |
| Year C | 1,94 | 1,80 | 2,95 | 2,78 | 1,95 | 2,68 | 2,54 | 1,79 | 2,46 | 2,22 |
| Year S | 2,07 | 1,92 | 2,98 | 2,78 | 2,06 | 2,75 | 2,56 | 1,87 | 2,42 | 2,19 |
| GUR | | | | | | | | | | |
| Spring | 1,76 | 1,68 | 4,07 | 3,87 | 2,07 | 2,73 | 2,42 | 2,17 | 3,41 | 3,11 |
| Summer | 1,78 | 1,75 | 3,67 | 3,52 | 1,75 | 3,19 | 3,48 | 1,99 | 2,81 | 2,30 |
| Autumn | 2,26 | 2,13 | 4,19 | 3,57 | 2,12 | 3,38 | 3,14 | 2,10 | 2,88 | 2,42 |
| Winter | 2,41 | 2,31 | 3,79 | 3,65 | 2,40 | 3,05 | 3,14 | 2,13 | 2,94 | 2,49 |
| Year C | 1,89 | 1,91 | 3,96 | 3,63 | 2,04 | 3,15 | 3,14 | 2,01 | 2,96 | 2,49 |
| Year S | 2,05 | 1,97 | 3,93 | 3,65 | 2,09 | 3,09 | 3,04 | 2,10 | 3,01 | 2,58 |
| SEN | | | | | | | | | | |
| Spring | 1,65 | 1,78 | 3,78 | 3,38 | 2,09 | 2,83 | 2,62 | 2,01 | 3,05 | 2,43 |
| Summer | 1,93 | 2,02 | 3,64 | 3,27 | 2,02 | 3,17 | 2,83 | 2,10 | 2,51 | 2,05 |
| Autumn | 2,26 | 2,36 | 3,66 | 3,16 | 2,48 | 3,36 | 3,10 | 2,09 | 2,52 | 2,07 |
| Winter | 2,36 | 2,18 | 3,32 | 2,94 | 2,20 | 2,66 | 2,65 | 2,11 | 2,71 | 2,19 |
| Year C | 1,91 | 1,99 | 3,60 | 3,19 | 2,23 | 3,13 | 2,85 | 2,01 | 2,63 | 2,13 |
| Year S | 2,05 | 2,08 | 3,60 | 3,19 | 2,19 | 3,00 | 2,80 | 2,08 | 2,70 | 2,19 |
| ARE | | | | | | | | | | |
| Spring | 1,35 | 1,56 | 2,84 | 2,48 | 1,64 | 2,22 | 2,15 | 1,65 | 2,50 | 2,08 |
| Summer | 1,77 | 1,88 | 3,66 | 3,17 | 1,97 | 2,90 | 2,86 | 1,83 | 2,29 | 1,78 |
| Autumn | 1,85 | 1,94 | 2,91 | 2,55 | 1,99 | 2,86 | 2,59 | 1,81 | 2,20 | 1,87 |
| Winter | 1,77 | 1,91 | 2,67 | 2,50 | 1,90 | 2,40 | 2,46 | 1,81 | 2,25 | 1,89 |
| Year C | 1,62 | 1,72 | 2,94 | 2,64 | 1,80 | 2,49 | 2,48 | 1,71 | 2,31 | 1,88 |
| Year S | 1,68 | 1,82 | 3,02 | 2,67 | 1,87 | 2,59 | 2,51 | 1,78 | 2,31 | 1,90 |

Table C.5 – Nonlinear recession coefficient ($k_n$) for each case

| | | E1 | | | E2 | | | E3 | | |
|---|---|---|---|---|---|---|---|---|---|---|
| Case | MLE | PN1 | PN2 | PN3 | PN1 | PN2 | PN3 | PN1 | PN2 | PN3 |
| GOL | | | | | | | | | | |
| Spring | 0,19 | 0,11 | 0,08 | 0,12 | 0,09 | 0,08 | 0,09 | 0,13 | 0,09 | 0,13 |
| Summer | 0,19 | 0,15 | 0,15 | 0,22 | 0,10 | 0,11 | 0,13 | 0,16 | 0,13 | 0,17 |
| Autumn | 0,17 | 0,12 | 0,12 | 0,17 | 0,09 | 0,11 | 0,15 | 0,15 | 0,13 | 0,17 |
| Winter | 0,17 | 0,08 | 0,07 | 0,09 | 0,07 | 0,07 | 0,07 | 0,11 | 0,07 | 0,11 |
| Year C | 0,19 | 0,11 | 0,10 | 0,15 | 0,08 | 0,08 | 0,11 | 0,14 | 0,11 | 0,15 |
| Year S | 0,18 | 0,12 | 0,10 | 0,15 | 0,09 | 0,09 | 0,11 | 0,14 | 0,10 | 0,15 |
| NEC | | | | | | | | | | |
| Spring | 0,17 | 0,09 | 0,03 | 0,08 | 0,09 | 0,08 | 0,13 | 0,12 | 0,05 | 0,12 |
| Summer | 0,15 | 0,13 | 0,11 | 0,17 | 0,12 | 0,13 | 0,16 | 0,15 | 0,13 | 0,15 |
| Autumn | 0,16 | 0,10 | 0,09 | 0,14 | 0,09 | 0,10 | 0,13 | 0,12 | 0,11 | 0,14 |
| Winter | 0,17 | 0,08 | 0,06 | 0,08 | 0,07 | 0,07 | 0,07 | 0,10 | 0,08 | 0,10 |
| Year C | 0,17 | 0,10 | 0,07 | 0,12 | 0,08 | 0,09 | 0,12 | 0,13 | 0,10 | 0,14 |
| Year S | 0,16 | 0,10 | 0,07 | 0,12 | 0,09 | 0,09 | 0,12 | 0,12 | 0,09 | 0,13 |
| MUW | | | | | | | | | | |
| Spring | 0,08 | 0,06 | 0,04 | 0,05 | 0,05 | 0,04 | 0,05 | 0,07 | 0,04 | 0,05 |
| Summer | 0,08 | 0,09 | 0,09 | 0,14 | 0,06 | 0,05 | 0,09 | 0,11 | 0,09 | 0,12 |
| Autumn | 0,09 | 0,07 | 0,06 | 0,08 | 0,06 | 0,05 | 0,06 | 0,10 | 0,07 | 0,09 |
| Winter | 0,10 | 0,04 | 0,03 | 0,04 | 0,04 | 0,03 | 0,04 | 0,06 | 0,03 | 0,04 |
| Year C | 0,10 | 0,06 | 0,05 | 0,07 | 0,05 | 0,04 | 0,05 | 0,09 | 0,05 | 0,07 |
| Year S | 0,08 | 0,06 | 0,05 | 0,08 | 0,05 | 0,04 | 0,06 | 0,09 | 0,06 | 0,08 |
| GUR | | | | | | | | | | |
| Spring | 0,06 | 0,05 | 0,01 | 0,02 | 0,03 | 0,02 | 0,03 | 0,05 | 0,01 | 0,03 |
| Summer | 0,06 | 0,07 | 0,04 | 0,07 | 0,05 | 0,03 | 0,04 | 0,08 | 0,04 | 0,07 |
| Autumn | 0,07 | 0,05 | 0,05 | 0,06 | 0,05 | 0,04 | 0,05 | 0,08 | 0,04 | 0,07 |
| Winter | 0,08 | 0,04 | 0,03 | 0,04 | 0,03 | 0,03 | 0,04 | 0,06 | 0,03 | 0,05 |
| Year C | 0,07 | 0,05 | 0,03 | 0,05 | 0,04 | 0,03 | 0,04 | 0,07 | 0,03 | 0,05 |
| Year S | 0,07 | 0,05 | 0,03 | 0,05 | 0,04 | 0,03 | 0,04 | 0,07 | 0,03 | 0,06 |
| SEN | | | | | | | | | | |
| Spring | 0,05 | 0,05 | 0,01 | 0,04 | 0,03 | 0,04 | 0,06 | 0,06 | 0,03 | 0,06 |
| Summer | 0,07 | 0,08 | 0,07 | 0,14 | 0,06 | 0,05 | 0,09 | 0,09 | 0,07 | 0,12 |
| Autumn | 0,11 | 0,07 | 0,07 | 0,13 | 0,05 | 0,06 | 0,11 | 0,10 | 0,08 | 0,12 |
| Winter | 0,14 | 0,06 | 0,05 | 0,07 | 0,05 | 0,05 | 0,06 | 0,08 | 0,04 | 0,09 |
| Year C | 0,08 | 0,06 | 0,04 | 0,09 | 0,05 | 0,05 | 0,08 | 0,09 | 0,06 | 0,10 |
| Year S | 0,08 | 0,06 | 0,05 | 0,09 | 0,05 | 0,05 | 0,08 | 0,08 | 0,06 | 0,10 |
| ARE | | | | | | | | | | |
| Spring | 0,08 | 0,06 | 0,02 | 0,06 | 0,05 | 0,04 | 0,07 | 0,08 | 0,03 | 0,06 |
| Summer | 0,09 | 0,08 | 0,12 | 0,16 | 0,07 | 0,08 | 0,13 | 0,11 | 0,07 | 0,13 |
| Autumn | 0,12 | 0,07 | 0,07 | 0,12 | 0,06 | 0,06 | 0,11 | 0,10 | 0,07 | 0,12 |
| Winter | 0,11 | 0,05 | 0,03 | 0,05 | 0,05 | 0,04 | 0,05 | 0,07 | 0,04 | 0,08 |
| Year C | 0,10 | 0,07 | 0,05 | 0,09 | 0,06 | 0,05 | 0,09 | 0,09 | 0,05 | 0,09 |
| Year S | 0,10 | 0,07 | 0,06 | 0,10 | 0,06 | 0,06 | 0,09 | 0,09 | 0,05 | 0,09 |

Table C.6 – Nonlinear model performances ($c_n^{KS}$) for each case

| | | E1 | | | E2 | | | E3 | | |
|---|---|---|---|---|---|---|---|---|---|---|
| Case | MLE | PN1 | PN2 | PN3 | PN1 | PN2 | PN3 | PN1 | PN2 | PN3 |
| GOL | | | | | | | | | | |
| Spring | 0,03 | 0,19 | 0,10 | 0,13 | 0,21 | 0,19 | 0,16 | 0,13 | 0,12 | 0,10 |
| Summer | 0,02 | 0,16 | 0,13 | 0,16 | 0,25 | 0,08 | 0,11 | 0,12 | 0,10 | 0,09 |
| Autumn | 0,03 | 0,15 | 0,12 | 0,13 | 0,13 | 0,12 | 0,12 | 0,09 | 0,07 | 0,06 |
| Winter | 0,03 | 0,26 | 0,11 | 0,08 | 0,30 | 0,16 | 0,09 | 0,21 | 0,18 | 0,15 |
| Year C | 0,02 | 0,19 | 0,11 | 0,13 | 0,23 | 0,11 | 0,10 | 0,13 | 0,09 | 0,08 |
| Year S | 0,03 | 0,21 | 0,09 | 0,10 | 0,23 | 0,12 | 0,09 | 0,15 | 0,14 | 0,11 |
| NEC | | | | | | | | | | |
| Spring | 0,02 | 0,14 | 0,14 | 0,16 | 0,19 | 0,11 | 0,21 | 0,07 | 0,13 | 0,06 |
| Summer | 0,02 | 0,07 | 0,12 | 0,18 | 0,06 | 0,09 | 0,12 | 0,04 | 0,05 | 0,05 |
| Autumn | 0,03 | 0,15 | 0,12 | 0,12 | 0,15 | 0,11 | 0,11 | 0,09 | 0,11 | 0,06 |
| Winter | 0,02 | 0,22 | 0,20 | 0,15 | 0,25 | 0,23 | 0,15 | 0,15 | 0,18 | 0,15 |
| Year C | 0,02 | 0,15 | 0,13 | 0,12 | 0,19 | 0,11 | 0,12 | 0,09 | 0,11 | 0,05 |
| Year S | 0,03 | 0,16 | 0,17 | 0,10 | 0,17 | 0,13 | 0,10 | 0,11 | 0,16 | 0,09 |
| MUW | | | | | | | | | | |
| Spring | 0,03 | 0,12 | 0,10 | 0,09 | 0,14 | 0,10 | 0,08 | 0,06 | 0,10 | 0,08 |
| Summer | 0,04 | 0,04 | 0,20 | 0,26 | 0,10 | 0,09 | 0,10 | 0,10 | 0,04 | 0,12 |
| Autumn | 0,04 | 0,11 | 0,14 | 0,13 | 0,14 | 0,10 | 0,09 | 0,05 | 0,07 | 0,04 |
| Winter | 0,03 | 0,22 | 0,17 | 0,13 | 0,24 | 0,21 | 0,17 | 0,16 | 0,20 | 0,16 |
| Year C | 0,02 | 0,13 | 0,12 | 0,13 | 0,17 | 0,16 | 0,11 | 0,06 | 0,13 | 0,07 |
| Year S | 0,06 | 0,15 | 0,12 | 0,11 | 0,18 | 0,15 | 0,11 | 0,09 | 0,14 | 0,10 |
| GUR | | | | | | | | | | |
| Spring | 0,02 | 0,07 | 0,17 | 0,19 | 0,11 | 0,17 | 0,07 | 0,03 | 0,15 | 0,12 |
| Summer | 0,03 | 0,04 | 0,17 | 0,23 | 0,06 | 0,11 | 0,15 | 0,08 | 0,08 | 0,08 |
| Autumn | 0,03 | 0,09 | 0,17 | 0,13 | 0,11 | 0,18 | 0,10 | 0,04 | 0,13 | 0,04 |
| Winter | 0,04 | 0,21 | 0,24 | 0,17 | 0,23 | 0,25 | 0,19 | 0,13 | 0,25 | 0,12 |
| Year C | 0,01 | 0,09 | 0,19 | 0,18 | 0,12 | 0,16 | 0,11 | 0,02 | 0,14 | 0,05 |
| Year S | 0,02 | 0,09 | 0,21 | 0,16 | 0,14 | 0,19 | 0,13 | 0,04 | 0,19 | 0,07 |
| SEN | | | | | | | | | | |
| Spring | 0,01 | 0,02 | 0,39 | 0,22 | 0,12 | 0,17 | 0,08 | 0,05 | 0,25 | 0,08 |
| Summer | 0,02 | 0,03 | 0,34 | 0,19 | 0,09 | 0,31 | 0,19 | 0,04 | 0,16 | 0,11 |
| Autumn | 0,04 | 0,18 | 0,43 | 0,25 | 0,25 | 0,39 | 0,26 | 0,05 | 0,17 | 0,09 |
| Winter | 0,04 | 0,22 | 0,42 | 0,31 | 0,24 | 0,33 | 0,29 | 0,13 | 0,36 | 0,11 |
| Year C | 0,03 | 0,10 | 0,39 | 0,26 | 0,19 | 0,32 | 0,23 | 0,04 | 0,24 | 0,06 |
| Year S | 0,07 | 0,13 | 0,43 | 0,29 | 0,21 | 0,32 | 0,23 | 0,08 | 0,29 | 0,08 |
| ARE | | | | | | | | | | |
| Spring | 0,02 | 0,11 | 0,34 | 0,21 | 0,15 | 0,23 | 0,16 | 0,08 | 0,29 | 0,18 |
| Summer | 0,04 | 0,06 | 0,43 | 0,29 | 0,14 | 0,35 | 0,25 | 0,04 | 0,22 | 0,10 |
| Autumn | 0,04 | 0,17 | 0,38 | 0,23 | 0,22 | 0,39 | 0,25 | 0,07 | 0,24 | 0,04 |
| Winter | 0,03 | 0,21 | 0,37 | 0,28 | 0,22 | 0,31 | 0,27 | 0,12 | 0,29 | 0,13 |
| Year C | 0,02 | 0,15 | 0,39 | 0,26 | 0,20 | 0,32 | 0,25 | 0,07 | 0,31 | 0,11 |
| Year S | 0,06 | 0,18 | 0,42 | 0,30 | 0,22 | 0,35 | 0,27 | 0,11 | 0,32 | 0,14 |

# D Supplementary material to Chapter 6

The supplementary material contains 3 figures showing the seasonal and annual cdfs for each snow-dominated catchment.

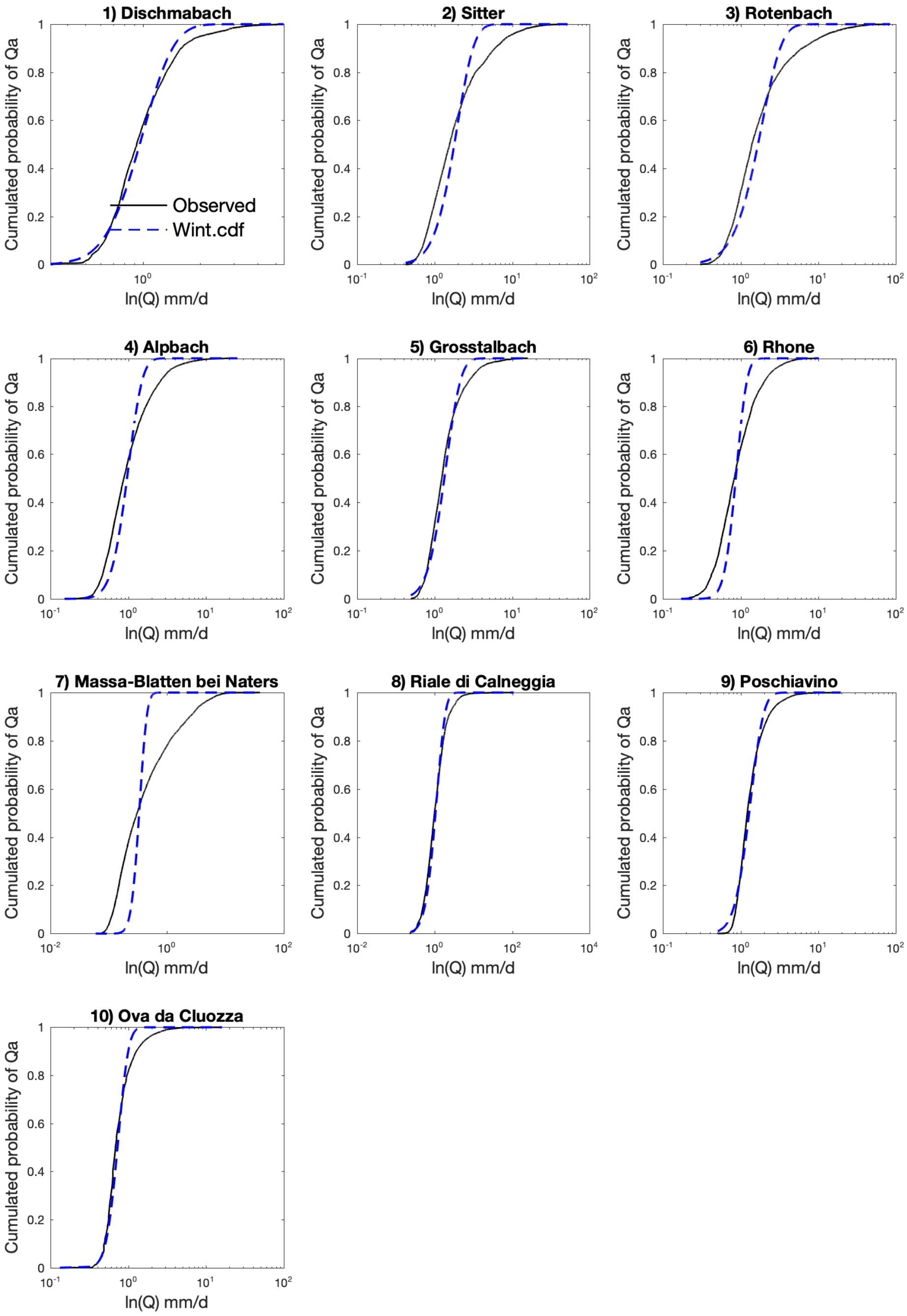


Figure D.1 – Modeled cdfs for all catchments during the accumulation season.

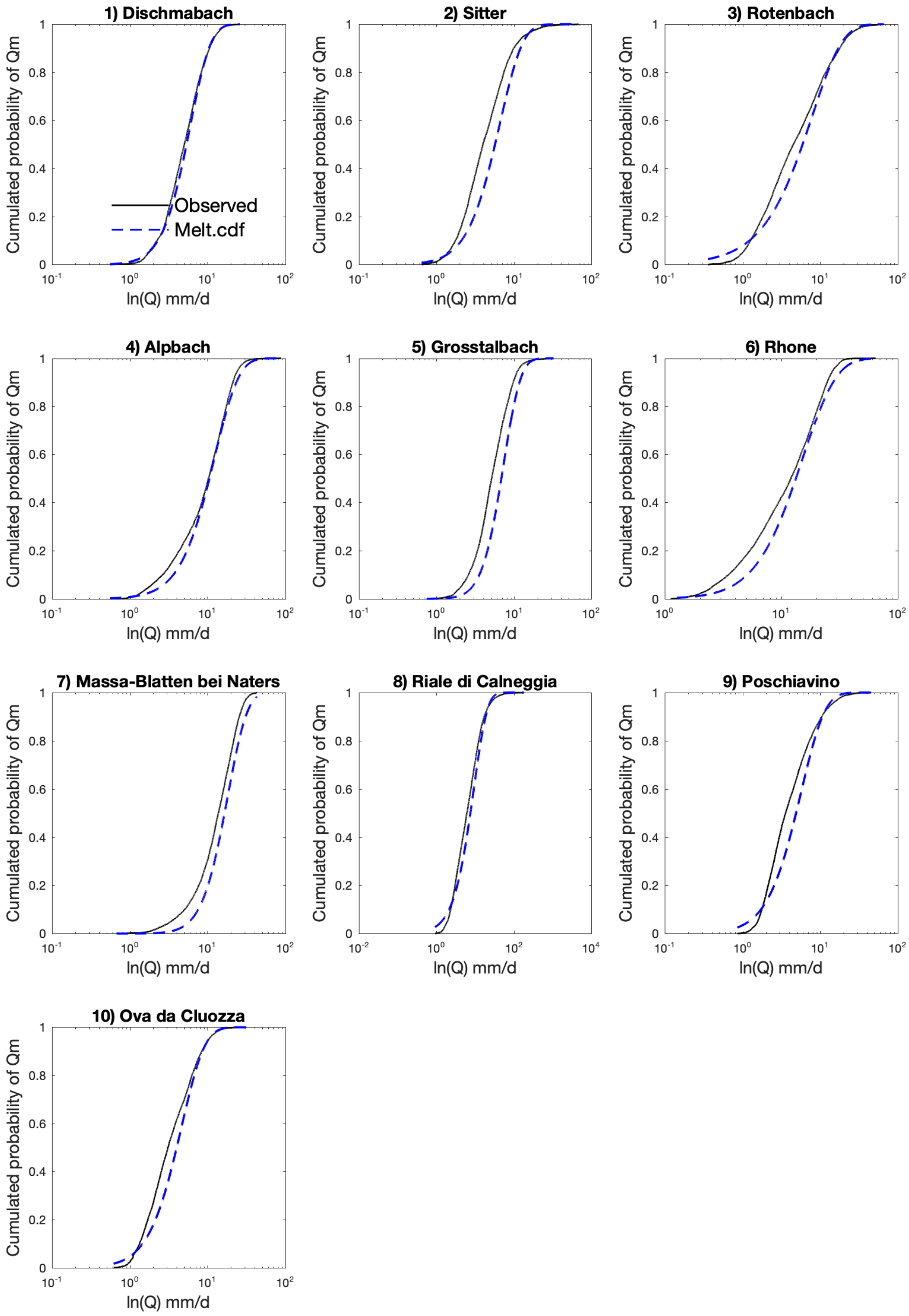


Figure D.2 – Modeled cdfs for all catchments during the melting season.

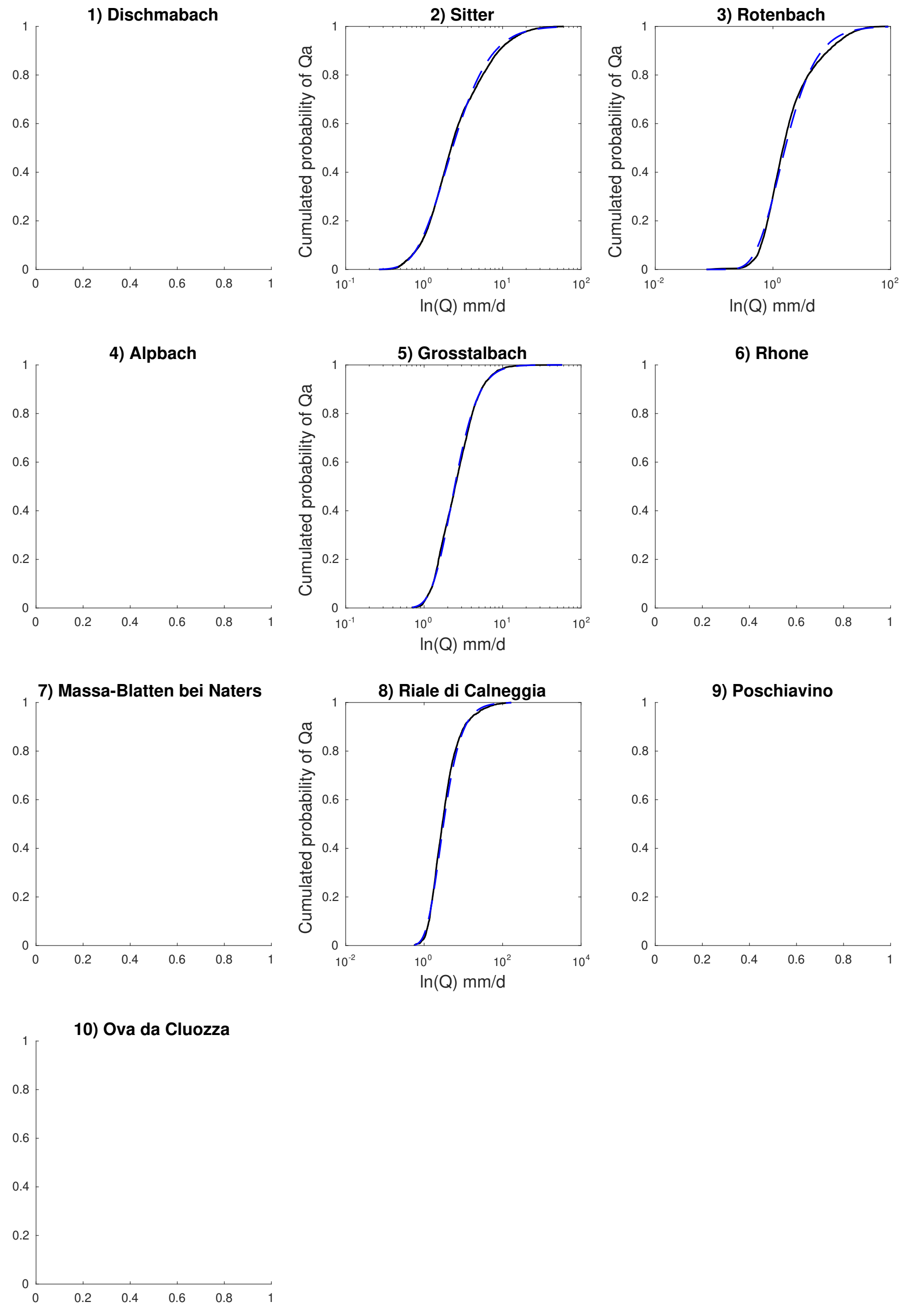


Figure D.3 – Modeled cdfs for all catchments during the pluvial season.

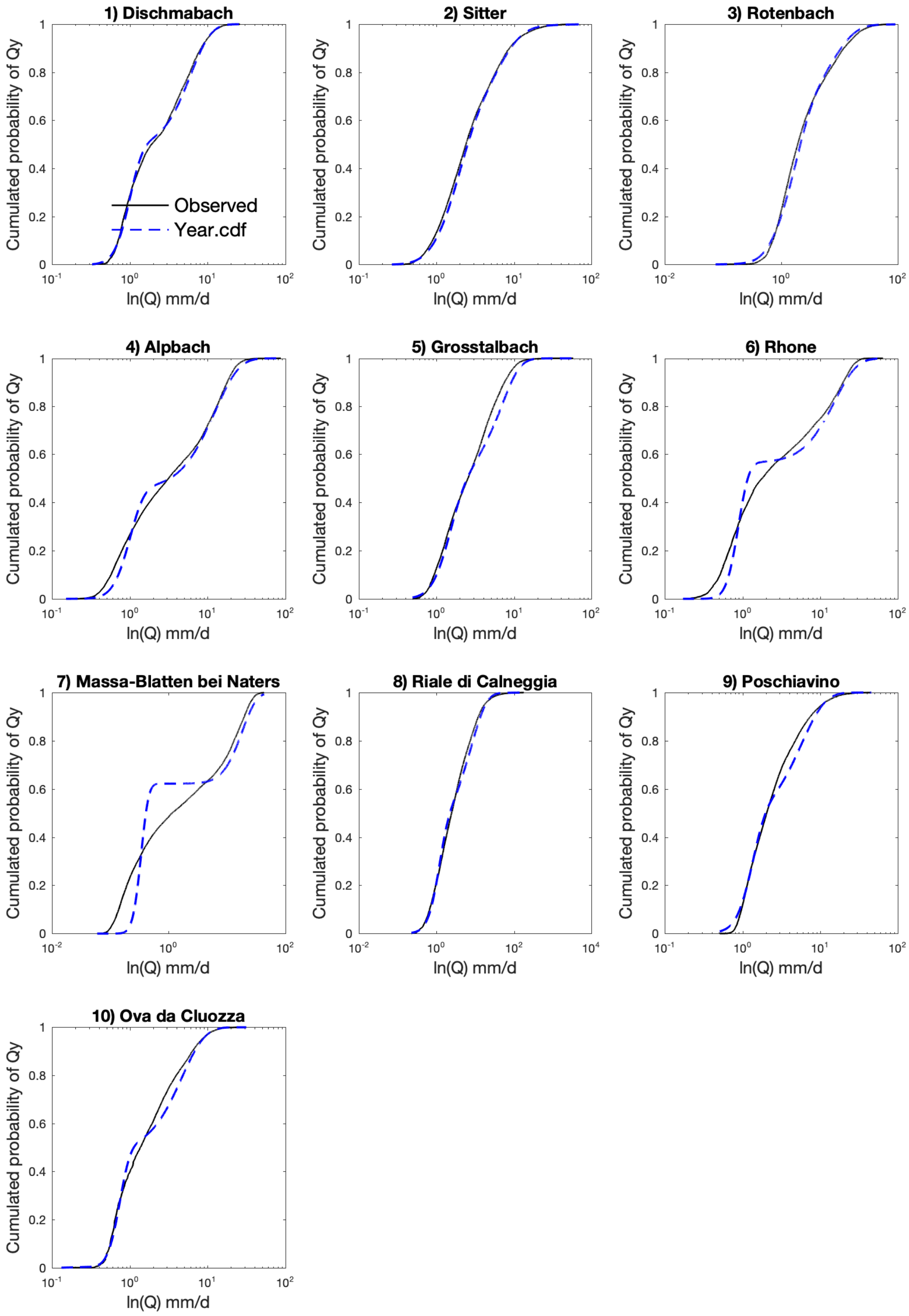


Figure D.4 – Modeled cdfs for all catchments during the complete year.

# Bibliography

Addor, N. and Fischer, E. M. (2015). The influence of natural variability and interpolation errors on bias characterization in rcm simulations. *Journal of Geophysical Research: Atmospheres*, 120(19).

Aksoy, H. and Wittenberg, H. (2011). Nonlinear baseflow recession analysis in watersheds with intermittent streamflow. *Hydrological Sciences Journal*, 56(2):226–237.

Archfield, S. A. and Vogel, R. M. (2010). Map correlation method: Selection of a reference streamgage to estimate daily streamflow at ungaged catchments. *Water Resources Research*, 46(10).

Arciniega-Esparza, S., Breña-Naranjo, J. A., Pedrozo-Acuña, A., and Appendini, C. M. (2017). HYDRORECESSION: A matlab toolbox for streamflow recession analysis. *Computers & Geosciences*, 98:87–92.

Aschwanden, A. (1996). Caractéristiques physiographiques des bassins de recherches hydrologiques en suisse.

Bako, M. D. and Hunt, D. N. (1988). Derivation of baseflow recession constant using computer and numerical analysis. *Hydrological Sciences Journal*, 33(4):357–367.

Basso, S. and Botter, G. (2012). Streamflow variability and optimal capacity of run-of-river hydropower plants. *Water Resources Research*, 48(10).

Basso, S., Frascati, A., Marani, M., Schirmer, M., and Botter, G. (2015a). Climatic and landscape controls on effective discharge. *Geophysical Research Letters*, 42(20):8441–8447.

Basso, S., Schirmer, M., and Botter, G. (2015b). On the emergence of heavy-tailed streamflow distributions. *Advances in Water Resources*, 82:98–105.

Begert, M., Seiz, G., Foppa, N., Schlegel, T., Appenzeller, C., and Muller, G. (2007). Die uberfuhrung der klimatologischen referenzstationen der schweiz in das swiss national basic climatological network (swiss nbcn), arbeitsbericht meteoschweiz nr. 215. Klimaregionen der Schweiz, climate regions, hydroclimatic regions, MeteoSchweiz, meteoswiss, nach Gensler Schuepp.

Bernet, D. B., Prasuhn, V., and Weingartner, R. (2017). Surface water floods in switzerland: what insurance claim records tell us about the damage in space and time. *Natural Hazards and Earth System Sciences*, 17(9):1659–1682.

Betterle, A., Schirmer, M., and Botter, G. (2017). Characterizing the spatial correlation of daily streamflows. *Water Resources Research*, 53(2):1646–1663.

Biswal, B. (2016). Dynamic hydrologic modeling using the zero-parameter budyko model with instantaneous dryness index. *Geophysical Research Letters*, 43(18):9696–9703.

Biswal, B. and Marani, M. (2010). Geomorphological origin of recession curves. *Geophysical Research Letters*, 37(24).

Biswal, B. and Nagesh, D. K. (2014). Study of dynamic behaviour of recession curves. *Hydrological Processes*, 28(3):784–792.

Blanc, P. and Schädler, B. (2013). Water in switzerland - an overview, available in english on http://www.naturalsciences.ch/topics/water/ (accessed 18.08.2015). Technical report.

Blöschl, G. and Sivapalan, M.and Wagener, T. (2013). *Runoff prediction in ungauged basins: synthesis across processes, places and scales*. Cambridge University Press.

Bogaart, P. W., Van Der Velde, Y., Lyon, S. W., and Dekker, S. C. (2016). Streamflow recession patterns can help unravel the role of climate and humans in landscape co-evolution. *Hydrology and Earth System Sciences*, 20(4):1413–1432.

Booker, D. and Snelder, T. (2012). Comparing methods for estimating flow duration curves at ungauged sites. *Journal of Hydrology*, 434:78–94.

Botter, G. (2010). Stochastic recession rates and the probabilistic structure of stream flows. *Water Resources Research*, 46(12):n/a–n/a.

Botter, G. (2014). Flow regime shifts in the little piney creek (us). *Advances in water resources*, 71:44–54.

Botter, G., Basso, S., Porporato, A., Rodriguez-Iturbe, I., and Rinaldo, A. (2010). Natural streamflow regime alterations: Damming of the piave river basin (italy). *Water Resources Research*, 46(6).

Botter, G., Basso, S., Rodriguez-Iturbe, I., and Rinaldo, A. (2013). Resilience of river flow regimes. *Proceedings of the National Academy of Sciences*, 110(32):12925–12930.

Botter, G., Peratoner, F., Porporato, A., Rodriguez-Iturbe, I., and Rinaldo, A. (2007a). Signatures of large-scale soil moisture dynamics on streamflow statistics across u.s. climate regimes. *Water Resources Research*, 43(11).

Botter, G., Porporato, A., Daly, E., Rodriguez-Iturbe, I., and Rinaldo, A. (2007b). Probabilistic characterization of base flows in river basins: Roles of soil, vegetation, and geomorphology. *Water Resources Research*, 43(6).

Botter, G., Porporato, A., Rodriguez-Iturbe, I., and Rinaldo, A. (2007c). Basin-scale soil moisture dynamics and the probabilistic characterization of carrier hydrologic flows: Slow, leaching-prone components of the hydrologic response. *Water Resources Research*, 43(2). W02417.

Botter, G., Porporato, A., Rodriguez-Iturbe, I., and Rinaldo, A. (2009). Nonlinear storage-discharge relations and catchment streamflow regimes. *Water Resources Research*, 45(10).

Botter, G., Zanardo, S., Porporato, A., Rodriguez-Iturbe, I., and Rinaldo, A. (2008). Ecohydrological model of flow duration curves and annual minima. *Water Resources Research*, 44(8).

Botter, M., Burlando, P., and Fatichi, S. (2019). Anthropogenic and catchment characteristic signatures in the water quality of swiss rivers: a quantitative assessment. *Hydrology and Earth System Sciences*, 23(4):1885–1904.

Boussinesq, J. (1904). Recherches théoriques sur l'écoulement des nappes d'eau infiltrées dans le sol et sur le débit des sources. *Journal de mathématiques pures et appliquées*, 10:5–78.

Brutsaert, W. (2008). Long-term groundwater storage trends estimated from streamflow records: Climatic perspective. *Water Resources Research*, 44(2).

Brutsaert, W. and Nieber, J. L. (1977). Regionalized drought flow hydrographs from a mature glaciated plateau. *Water Resources Research*, 13(3):637–643.

Burnham, K. P. and Anderson, D. R., editors (2004). *Model Selection and Multimodel Inference*. Springer New York.

Castellarin, A., Botter, G., Hughes, D. A., Liu, S., Ouarda, T. B. M. J., Parajka, J., Post, D. A., Sivapalan, M., Spence, C., Viglione, A., et al. (2013). Prediction of flow duration curves in ungauged basins. *Runoff prediction in ungauged basins: Synthesis across processes, places and scales*, pages 135–162.

Castellarin, A., Galeati, G., Brandimarte, L., Montanari, A., and Brath, A. (2004a). Regional flow-duration curves: reliability for ungauged basins. *Advances in Water Resources*, 27(10):953–965.

Castellarin, A., Vogel, R. M., and Brath, A. (2004b). A stochastic index flow model of flow duration curves. *Water Resources Research*, 40(3).

Castiglioni, S., Castellarin, A., and Montanari, A. (2009). Prediction of low-flow indices in ungauged basins through physiographical space-based interpolation. *Journal of hydrology*, 378(3):272–280.

Ceola, S., Bertuzzo, E., Singer, G., Battin, T. J., Montanari, A., and Rinaldo, A. (2014). Hydrologic controls on basin-scale distribution of benthic invertebrates. *Water Resources Research*, 50(4):2903–2920.

Ceola, S., Botter, G., Bertuzzo, E., Porporato, A., Rodriguez-Iturbe, I., and Rinaldo, A. (2010). Comparative study of ecohydrological streamflow probability distributions. *Water Resources Research*, 46(9).

Ceola, S., Hödl, I., Adlboller, M., Singer, G., Bertuzzo, E., Mari, L., Botter, G., Waringer, J., Battin, T., and Rinaldo, A. (2013). Hydrologic variability affects invertebrate grazing on phototrophic biofilms in stream microcosms. *PloS one*, 8(4):e60629.

Chen, B. and Krajewski, W. (2016). Analysing individual recession events: sensitivity of parameter determination to the calculation procedure. *Hydrological Sciences Journal*, 61(16):2887–2901.

Cox, D. and Miller, H. (1987). *The theory of stochastic processes*. Science paperbacks. Chapman and Hall, London, repr. edition.

Deal, E., Braun, J., and Botter, G. (2018). Understanding the role of rainfall and hydrology in determining fluvial erosion efficiency. *Journal of Geophysical Research: Earth Surface*, 123(4):744–778.

Doulatyari, B., Basso, S., Schirmer, M., and Botter, G. (2014). River flow regimes and vegetation dynamics along a river transect. *Advances in Water Resources*, 73:30–43.

Doulatyari, B., Betterle, A., Basso, S., B., Schirmer, M., and Botter, G. (2015). Predicting streamflow distributions and flow duration curves from landscape and climate. *Advances in Water Resources*, 83:285–298.

Doulatyari, B., Betterle, A., D.Radny, Celegon, E. A., Fanton, P., Schirmer, M., and Botter, G. (2017). Patterns of streamflow regimes along the river network: The case of the thur river. *Environmental Modelling & Software*, 93:42–58.

Dralle, D., Karst, N., Müller, M., Vico, G., and Thompson, S. E. (2017a). Stochastic modeling of interannual variation of hydrologic variables. *Geophysical Research Letters*, 44(14):7285–7294.

Dralle, D., Karst, N., and Thompson, S. E. (2015). a, b careful: The challenge of scale invariance for comparative analyses in power law models of the streamflow recession. *Geophysical Research Letters*, 42(21):9285–9293.

Dralle, D., Karst, N. J., Charalampous, K., Veenstra, A., and Thompson, S. E. (2017b). Event-scale power law recession analysis: quantifying methodological uncertainty. *Hydrology and Earth System Sciences*, 21(1):65–81.

Dralle, D. N., Karst, N. J., and Thompson, S. E. (2016). Dry season streamflow persistence in seasonal climates. *Water Resources Research*, 52(1):90–107.

Estoppey, R., Kiefer, B., Kummer, M., Lagger, S., and Aschwanden, H. (2000). Débits résiduels convenables - comment les déterminer?

Fabris, L.and Lazzaro, G. B. W. B., Botter, G., and Soulsby, C. (2018). A general analytical approach for assessing the effects of hydroclimatic variability on fish habitat. *Journal of hydrology*, 566:520–530.

Fischer, M., Huss, M., and Hoelzle, M. (2015). Surface elevation and mass changes of all swiss glaciers 1980–2010. *The Cryosphere*, 9(2):525–540.

Floriancic, M. G., van Meerveld, I., Smoorenburg, M., Margreth, M., Naef, F., Kirchner, J. W., and Molnar, P. (2018). Spatio-temporal variability in contributions to low flows in the high alpine poschiavino catchment. *Hydrological Processes*, 32(26):3938–3953.

FOEN (2004). Biogeographical regions of switzerland (ch) , https://opendata.swiss/en/dataset/biogeographische-regionen-der-schweiz-ch (last accessed: 15 december 2017).

FOEN (2013). Dataset mq-gwn-ch, modeled natural annual and monthly streamflow means (mq) and streamflow regime types for the swiss (ch) river network (gwn). Formelery referenced as Pfaundler and Schoneberger.

FOEN (2017). Swiss federal office for the environment: Hydrological data and forecasts.

FOEN (2018). Energy strategy 2050 once the new energy act is in force.

FOS (2015). Swiss federal statistical office: Statistique de la superficie du sol selon nomenclature 2004, utilisation du sol (land use).

Foster, H. A. (1934). Duration curves. *Transactions of the American Society of Civil Engineers*, 99(1):1213–1235.

Froidurot, S., Zin, I., Hingray, B., and Gautheron, A. (2014). Sensitivity of precipitation phase over the swiss alps to different meteorological variables. *Journal of Hydrometeorology*, 15(2):685–696.

Gabella, M., Speirs, P., Hamann, U., Germann, U., and Berne, A. (2017). Measurement of precipitation in the alps using dual-polarization c-band ground-based radars, the gpm spaceborne ku-band radar, and rain gauges. *Remote sensing*, 9(11):1147.

Ganora, D., Claps, P., Laio, F., and Viglione, A. (2009). An approach to estimate nonparametric flow duration curves in ungauged basins. *Water Resources Research*, 45(10).

Gerrits, A. M. J. (2010). *The role of interception in the hydrological cycle.* TU Delft, Delft University of Technology.

Gottschalk, L., Tallaksen, L. M., and Perzyna, G. (1997). Derivation of low flow distribution functions using recession curves. *Journal of Hydrology*, 194(1-4):239–262.

Haller, T., Hauser, F., and Weingartner, R. (2004). Atlas hydrologique de la suisse. *Office Fédéral de l'Environnement (OFEV), Berne.*

Hänggi, P. and Weingartner, R. (2012). Variations in discharge volumes for hydropower generation in switzerland. *Water resources management*, 26(5):1231–1252.

Harlin, J. (1991). Development of a process oriented calibration scheme for the hbv hydrological model. *Hydrology Research*, 22(1):15–36.

Harman, C., Sivapalan, M., and Kumar, P. (2009). Power law catchment-scale recessions arising from heterogeneous linear small-scale dynamics. *Water Resources Research*, 45(9).

Harpold, A. A., Kaplan, M. L., Klos, P. Z., Link, T., McNamara, J. P., Rajagopal, S., Schumer, R., and Steele, C. M. (2017). Rain or snow: hydrologic processes, observations, prediction, and research needs. *Hydrology and Earth System Sciences*, 21(1):1–22.

Helbling, A. (2016). Topographical catchments of the foen gauging stations. geodataset ezg hydrometrische stationen.

Hingray, B., Dedieu, J., Lebel, T., Obled, C., Sicart, J., Six, D., Vincent, C., Wagnon, P., and Zin, I. (2012). Observations glaciologiques et hydrométéorologiques en zone de montagne : quelques problématiques et perspectives actuelles. *La Houille Blanche*, (2):5–11.

Horton, R. E. (1941). An approach toward a physical interpretation of infiltration-capacity. *Soil Science Society of America Journal*, 5(C):399–417.

Jovanovic, T., Sun, F.and Mahjabin, T., and Mejia, A. (2018). Disentangling the effects of climate and urban growth on streamflow for sustainable urban development: A stochastic approach to flow regime attribution. *Landscape and urban planning*, 177:160–170.

Kirchner, J. W. (2009). Catchments as simple dynamical systems: Catchment characterization, rainfall-runoff modeling, and doing hydrology backward. *Water Resources Research*, 45(2).

Kirnbauer, R. (1992). An analysis of snow cover patterns in a small alpine catchment. *Hydrological Processes*, 6(1):99–109.

Klemeš, V. (1986). Operational testing of hydrological simulation models. *Hydrological Sciences Journal*, 31(1):13–24.

Kottegoda, N. T. and Rosso, R. (1997). Probability, statistics, and reliability for civil and environmental engineers.

Laio, F., Baldassarre, G. D., and Montanari, A. (2009). Model selection techniques for the frequency analysis of hydrological extremes. *Water Resources Research*, 45(7).

Lazzaro, G. and Botter, G. (2015). Run-of-river power plants in alpine regions: Whither optimal capacity? *Water Resources Research*, 51(7):5658–5676.

LEaux, L. f. d. l. C. S. (1991). Loi fédérale sur la protection des eaux 840.20. *L'Assemblée fédérale de la Confédération Suisse*.

Magnusson, J., Gustafsson, D., Hüsler, F., and Jonas, T. (2014). Assimilation of point swe data into a distributed snow cover model comparing two contrasting methods. *Water resources research*, 50(10):7816–7835.

Mays, L. W. (2010). *Water resources engineering*. John Wiley & Sons.

McMillan, H., Westerberg, I., and Branger, F. (2017). Five guidelines for selecting hydrological signatures. *Hydrological Processes*, 31(26):4757–4761.

Mejía, A., Daly, E., Rossel, F., Jovanovic, T., and Gironás, J. (2014). A stochastic model of streamflow for urbanized basins. *Water Resources Research*, 50(3):1984–2001.

MeteoSwiss (2011). Documentation of meteoswiss grid-data products: Daily precipitation (final analysis): Rhiresd.

MeteoSwiss (2014). Daily temperature (final analysis): Tabsd.

Milano, M., Reynard, E., Köplin, N., and Weingartner, R. (2015). Climatic and anthropogenic changes in western switzerland: Impacts on water stress. *Science of the total environment*, 536:12–24.

Montanari, R. (2003). Criteria for the economic planning of a low power hydroelectric plant. *Renewable energy*, 28(13):2129–2145.

Müller, M. F., Dralle, D. N., and Thompson, S. E. (2014). Analytical model for flow duration curves in seasonally dry climates. *Water Resources Research*, 50(7):5510–5531.

Müller, M. F. and Thompson, S. E. (2016). Comparing statistical and process-based flow duration curve models in ungauged basins and changing rain regimes. *Hydrology and Earth System Sciences*, 20(2):669–683.

Muneepeerakul, R., Azaele, S., Botter, G., Rinaldo, A., and Rodriguez-Iturbe, I. (2010). Daily streamflow analysis based on a two-scaled gamma pulse model. *Water Resources Research*, 46(11).

Musy, A. and Higy, C. (2010). *Hydrology: a science of nature.* CRC Press.

Musy, A., Hingray, B., and Picouet, C. (2014). *Hydrology: a science for engineers.* CRC Press.

Mutzner, R., Bertuzzo, E., Tarolli, P., Weijs, S. V., Nicotina, L., Ceola, S., Tomasic, N., Rodriguez-Iturbe, I., Parlange, M. B., and Rinaldo, A. (2013). Geomorphic signatures on brutsaert base flow recession analysis. *Water Resources Research*, 49(9):5462–5472.

Nag, A. and Biswal, B. (2019). Can a calibration-free dynamic rainfall–runoff model predict fdcs in data-scarce regions? comparing the idw model with the dynamic budyko model in south india. *Hydrology*, 6(2):32.

Naghettini, M. (2016). Fundamentals of statistical hydrology.

Nathan, R. and McMahon, T. (1992). Estimating low flow characteristics in ungauged catchments. *Water Resources Management*, 6(2):85–100.

Paschalis, A., Fatichi, S., Molnar, P., Rimkus, S., and Burlando, P. (2014). On the effects of small scale space–time variability of rainfall on basin flood response. *Journal of Hydrology*, 514:313–327.

Patnaik, S., Biswal, B., Kumar, D. N., and Sivakumar, B. (2018). Regional variation of recession flow power-law exponent. *Hydrological Processes*, 32(7):866–872.

Penche, C. (1998). Layman's handbook on how to develop a small hydro site. *ESHA, European Commission.*

Petts, G. E. (1996). Water allocation to protect river ecosystems. *Regulated rivers: research & management*, 12(4-5):353–365.

Poff, N. L., Allan, J. D., Bain, M. B., Karr, J. R., Prestegaard, K. L., Richter, B. D., Sparks, R. E., and Stromberg, J. C. (1997). The natural flow regime. *BioScience*, 47(11):769–784.

Polubarinova-Koch, P. I. (2015). *Theory of ground water movement.* Princeton University Press.

Pumo, D. and Noto, L. V.and Viola, F. (2013). Ecohydrological modelling of flow duration curve in mediterranean river basins. *Advances in water resources*, 52:314–327.

Rodriguez-Iturbe, I., Porporato, A., Ridolfi, L., Isham, V., and Coxi, D. R. (1999). Probabilistic modelling of water balance at a point: the role of climate, soil and vegetation. *Proceedings of the Royal Society A: Mathematical, Physical and Engineering Sciences*, 455(1990):3789–3805.

Roques, C., Rupp, D., and Selker, J. S. (2017). Improved streamflow recession parameter estimation with attention to calculation of dq/dt. *Advances in Water Resources*, 108(Supplement C):29 – 43.

Rorabaugh, M. (1964). Estimating changes in bank storage and ground-water contribution to streamflow. *International Association of Scientific Hydrology*, 63(1):432–441.

Rupp, D. E. and Woods, R. A. (2008). Increased flexibility in base flow modelling using a power law transmissivity profile. *Hydrological Processes*, 22(14):2667–2671.

Santolin, A., Cavazzini, G., Pavesi, G., Ardizzon, G., and Rossetti, A. (2011). Techno-economical method for the capacity sizing of a small hydropower plant. *Energy Conversion and Management*, 52(7):2533–2541.

Santos, A., Portela, M., Rinaldo, A., and Schaefli, B. (2019). Estimation of streamflow recession parameters: New insights from an analytic streamflow distribution model. *Hydrological Processes*.

Santos, A. C., Portela, M. M., Rinaldo, A., and Schaefli, B. (2018). Analytical flow duration curves for summer streamflow in switzerland. *Hydrology and Earth System Sciences*, 22(4):2377–2389.

Sawaske, S. R. and Freyberg, D. L. (2014). An analysis of trends in baseflow recession and low-flows in rain-dominated coastal streams of the pacific coast. *Journal of Hydrology*, 519:599 – 610.

Sawicz, K., Wagener, T., Sivapalan, M., Troch, P. A., and Carrillo, G. (2011). Catchment classification: empirical analysis of hydrologic similarity based on catchment function in the eastern usa. *Hydrology and Earth System Sciences*, 15(9):2895–2911.

Schaefli, B., Ceperley, N., Brauchli, T., Lehning, M., Jonas, T., and Zappa, M. (2016). The dischma river mystery: why does my snow hydrological model not work here ? geophysical research abstracts vol. 18, egu2016-1624, 2016, egu general assembly 2016, vienna.

Schaefli, B., Hingray, B., Niggli, M., and Musy, A. (2005). A conceptual glacio-hydrological model for high mountainous catchments. *Hydrology and Earth System Sciences*, 9:95 – 109.

Schaefli, B., Manso, P., Fischer, M., Huss, M., and Farinotti, D. (2019). The role of glacier retreat for swiss hydropower production. *Renewable energy*, 132:615–627.

Schaefli, B., Rinaldo, A., and Botter, G. (2013). Analytic probability distributions for snow-dominated streamflow. *Water Resources Research*, 49(5):2701–2713.

Searcy, J. K. (1959). *Flow-duration curves.* US Government Printing Office.

Smakhtin, V. (2001). Low flow hydrology: a review. *Journal of hydrology*, 240(3):147–186.

Spreafico, M. and Weingartner, R. (2005). *The hydrology of Switzerland: selected aspects and results*. Bundesamt für Wasser und Geologie.

Staudinger, M.and Stoelzle, M., Seeger, S., Seibert, J., Weiler, M., and Stahl, K. (2017). Catchment water storage variation with elevation. *Hydrological Processes*, 31(11):2000–2015.

Stoelzle, M., Stahl, K., and Weiler, M. (2013). Are streamflow recession characteristics really characteristic? *Hydrology and Earth System Sciences*, 17(2):817–828.

Sturges, H. A. (1926). The choice of a class interval. *Journal of the American Statistical Association*, 21(153):65–66.

Sugiyama, H. (1996). Analysis and extraction of low flow recession characteristics. *JAWRA Journal of the American Water Resources Association*, 32(3):491–497.

Suweis, S., Bertuzzo, E., Botter, G., Porporato, A., Rodriguez-Iturbe, I., and Rinaldo, A. (2010). Impact of stochastic fluctuations in storage-discharge relations on streamflow distributions. *Water Resources Research*, 46(3).

Swain, J.B.and Patra, K. (2017). Streamflow estimation in ungauged catchments using regional flow duration curve: comparative study. *Journal of Hydrologic Engineering*, 22(7):04017010.

SwissTopo (2005a). Dhm25- the digital height model of switzerland.

SwissTopo (2005b). Dhm25- the digital height model of switzerland dhm25, product information. Technical report.

Tallaksen, L. (1995). A review of baseflow recession analysis. *Journal of hydrology*, 165(1-4):349–370.

Tobin, C.and Schaefli, B., Nicótina, L., Simoni, S.and Barrenetxea, G., Smith, R., Parlange, M., and Rinaldo, A. (2013). Improving the degree-day method for sub-daily melt simulations with physically-based diurnal variations. *Advances in water resources*, 55:149–164.

Viviroli, D. and Weingartner, R. (2004). The hydrological significance of mountains: from regional to global scale. *Hydrology and Earth System Sciences Discussions*, 8(6):1017–1030.

Vogel, R. M. and Fennessey, N. M. (1994). Flow-duration curves i: New interpretation and confidence intervals. *Journal of Water Resources Planning and Management*, 120(4):485–504.

Vogel, R. M. and Fennessey, N. M. (1995). Flow duration curves ii: a review of the applications in water resources planning. *Journal of the American Water Resources Association*, 31(6):1029–1039.

Vogel, R. M. and Kroll, C. N. (1992). Regional geohydrologic-geomorphic relationships for the estimation of low-flow statistics. *Water Resources Research*, 28(9):2451–2458.

Von Sperling, M. (2007). *Wastewater characteristics, treatment and disposal.* IWA publishing London:.

Wagener, T. and Wheater, H. S. (2006). Parameter estimation and regionalization for continuous rainfall-runoff models including uncertainty. *Journal of Hydrology*, 320(1):132–154.

Wagner, H. and Mathur, J. (2011). *Introduction to hydro energy systems: basics, technology and operation.* Springer Science & Business Media.

Weingartner, R. and Aschwanden, H. (1992). Discharge regime–the basis for the estimation of average flows. *Hydrological Atlas of Switzerland, Plate*, 5:26.

Weingartner, R. and Aschwanden, H. (1994). Quantification des débits des cours d'eau des alpes suisses et des influences anthropiques qui les affectent. *Révue de Géographie alpine*, 82(2):45–57.

Westerberg, I.K.and McMillan, H. (2015). Uncertainty in hydrological signatures. *Hydrology and Earth System Sciences*, 19(9):39–51.

Westerberg, I., Guerrero, J.-L., Younger, P., Beven, K., Seibert, J., Halldin, S., Freer, J., and Xu, C.-Y. (2011). Calibration of hydrological models using flow-duration curves. *Hydrology and Earth System Sciences*, 15(7):2205–2227.

Woods, R. A. (2009). Analytical model of seasonal climate impacts on snow hydrology: Continuous snowpacks. *Advances in Water Resources*, 32(10):1465–1481.

Ye, S., Li, H., Huang, M., Ali, M., Leng, G., Leung, L. R., Wang, S., and Sivapalan, M. (2014). Regionalization of subsurface stormflow parameters of hydrologic models: Derivation from regional analysis of streamflow recession curves. *Journal of hydrology*, 519:670–682.

Rua Cruz da Carreira, 35
1150-118, Lisbon, Portugal
(+351) 913407467
anaclarapbs@gmail.com
Nationality: Brazilian
Birth: 3 April 1985

# Ana Clara Santos

## Education

2014-2019 **Ph.D. candidate**, *École polytechnique fédérale de Lausanne and Instituto Superior Técnico de Lisboa*, Supervisors: Prof. Andrea Rinaldo and Prof. Maria Manuela Portela.
Thesis: On flow duration curve modelling in Alpine catchments

2010 **Specialization in Project Management**, *Fundação Dom Cabral.*, Brazil.

2008-2010 **M.Sc. Water resources engineering**, *Programa de pós graduação em saneamento, meio ambiente e recursos hídricos – UFMG*, Brazil, Supervisor: Prof. Márcio Baptista.
Dissertation: A new approach to evaluate the state of alteration of streams

2006 **Academic exchange**, *École nationale des ponts et chaussées*, France.

2003-2007 **Civil engineering**, *Universidade Federal de Mnas Gerais*, Brazil.

## Experience

### Teaching Experience

2013-2014 **Lecturer**, *Departamento de Engenharia Hidráulica e Recursos Hídricos da Universidade Federal de Minas Gerais.*

2013-2014 **Lecturer**, *Faculdade Pitágoras*, Courses: Hydraulics and Fluid Mechanics.

### Work Experience

2010-2012 **Full engineer**, *Vale SA*, Project risk management.

2008-2009 **Engineer**, *Participant in the working group that prepared the "Laudo técnico pericial para valoração do impacto ambiental na Mina do Quéias – Brumadinho (MG)" – Evaluation of the hydrology and fluvial system.*

### Internships

2007 **Intern**, *Banco de Desenvolvimento de Minas Gerais (BDMG)*, Infra-structure and urban development department.

2005-2006 **Intern**, *UFMG - Sanitation and environmental engineering department*, Brazil, Supervisor: Prof. Raphael Barros.
Research project on garden waste management on the UFMG campus

2004-2005 **Intern**, *UFMG - Materials and construction department*, Brazil, Supervisor: Prof. Maria Tereza Paulino Aguilar.
Research project on construction waste management in Belo Horizonte

## Languages

| | | |
|---|---|---|
| Portuguese | Mother tongue | |
| English | Advanced - C1 | *CAE – Certificate in Advanced English* |
| French | Advanced - C1 | *DALF C1- Diplôme approfondi de langue française* |
| Spanish | Intermediate | |

## Publications

### Journal articles


- Moura, P. ; Cardoso, A.S. ; Santos, A. C. P. B. ; Baptista, M. B. . Avaliação ambiental para restauração hidrológica e fluvial em áreas degradadas por atividades de mineração. REGA. Revista de Gestão de Águas da América Latina, v. 11, p. 5-19, 2014.
- Santos A.C., Portela M.M., Rinaldo A., Schaefli B. Analytical flow duration curves for summer streamflow in Switzerland. Hydrology and Earth System Sciences, v.22, p. 2377-2389,2018
- Santos, A.C., Portela, M.M., Rinaldo, A., and Schaefli, B. Estimation of streamflow recession parameters: New insights from an analytic streamflow distribution model. Hydrological Processes, mar 2019. doi: 10.1002/hyp.13425. URL https://doi.org/10.1002/hyp.13425.


### Conferences


- Moura, P. M. ; Cardoso, A. S. ; Santos, A. C. P. B. ; Quick, F. ; Baptista, M. B. . Metodologia para avaliação do potencial de recuperação de cursos de água em áreas de mineração. In: XXIV Congreso Latinoamericano de Hidráulica, 2010, Punta del Este. Anais do XXIV Congreso Latinoamericano de Hidráulica, 2010.
- Santos, A.C.; Schaefli, B.; Manso, P.; Schleiss, A.; Portela,M.M.; Rinaldo, A. Tapping hidden hydropower potential in Swiss Alpine catchments in the context of the planned nuclear power phase out. In: European Geophysical Union General Assembly, 2015, Viena, Áustria. EGU Geophysical Research Abstracts. Viena: EGU, 2015. v. 17.
- Santos, A.C.; Schaefli, B.; Manso,P.; Portela,M.M.; Rinaldo, A.; Schleiss, A. Flow duration curves for water resources quantification in Alpine environments. In: Poster session presented at the Swiss Competence Center on Supply for Electricity Annual Conference 2015, Neuchâtel, Switzerland.
- Santos A.C.; Schaefli B.; Portela M.M.; Manso P.; Schleiss A.; Rinaldo A. Characterization of flow duration curves in Switzerland. In: Abstract Volume 13th Swiss Geoscience Meeting, 2015, Basel, Switzerland.
- Santos, A.C.; Schaefli, B.; Manso, P.; Portela,M.M.; Rinaldo, A.; Schleiss, A. An analytical model to quantify water resources in Alpine environments. In: Poster session presented at the Swiss Competence Center on Supply for Electricity Annual Conference 2016, Sion, Switzerland.
- Portela, M. M. ; Silva, A. T. ; Santos, A. C.; Schaefli, B. Generation of daily synthetic flows for Switzerland. In: 10th World Congress of EWRA, 2017, Atenas.

- Portela, M. M. ; Zeleňákpva, M. ; Silva, A. T. ; Santos, A. C. Obtenção de séries sintéticas de escoamentos diários por desagregação direta de escoamentos anuais. In: 13o Simpósio de Hidráulica e Recursos Hídricos dos Países de Língua Portuguesa, 2017, Porto.
- Santos A.C., Portela M.M., Schaefli B. Application of an analytical model to obtain daily flow duration curves in Portugal. In: 14o Congresso da água, 2018, Évora, 2018.
- Santos A.C., Schaefli B., Rinaldo A., Portela M.M., Analytical flow duration curves to understand discharge regimes across elevation gradients in Alpine environments. In: EGU General Assembly 2018, Vienna. Geophysical Research Abstracts, 2018, v.20
- Santos A.C., Portela M.M., Schaefli B. Application of an analytical model to obtain daily flow duration curves for different hydrological regimes. 10th International Perspective on Water Resources and the Environment Conference, December 4-7, 2018, Cartagena

Ce document a été imprimé au Centre d’impression EPFL,
imprimerie climatiquement neutre, certifiée myClimate.